Breaker Model for Coastal Structures

Probability of Wave Impacts on Vertical Walls

January 2002

Magchiel van Os

Technische Universiteit Delft

Facultaty of Civil Engineering and Geosciences
Subfaculty Civil Engineering
Hydraulic and Offshore Engineering division

Breaker Model for Coastal Structures

Probability of Wave Impacts on Vertical Walls

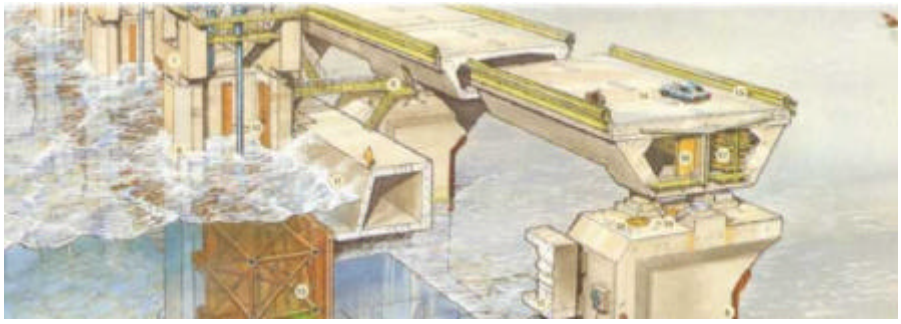

Delft, Januari 2002

Master thesis of: M. van Os

Examiner committee:

Prof.drs.ir. J.K. Vrijling (chairman)	(TU Delft)
Prof.dr.ir. J.A. Battjes	(TU Delft)
Dr. ir. M.R.A. van Gent	(WL/Delft Hydraulics)
Ir. H.G. Voortman	(TU Delft)

Come quickly to my help. Fill your channels with water from the springs, replenish all your mountain streams, raise a great surge and send it down, seething with logs and boulders, so that we may stop this savage who is carrying all before him.
He thinks himself a match for the gods; but I am determined not to let his strength or beauty save him now, nor shall that splendid armour.

The Iliad, Homer

PREFACE

This study was carried out as the final thesis of M. van Os. This master's thesis was a part of my study Civil Engineering and Geotechnics at Delft University of Technology.

Finalising this report, I would like to thank a few people, because they were a big help during this study. First I would like to thank Yvonne for her support and Mark for his help. Then my friends and colleagues at the Technical University Delft. Also I want to thank my examiner committee starting with ir. H.G.Voortman, who teached me more than this thesis could contain, prof.dr.ir. H.Vrijling for his enthusiastic piloting as well as the other members: dr.ir. M.R.A. van Gent and prof.dr.ir. J.A.Battjes for their critical reviews.

Delft, Januari 2002

Magchiel van Os

Table of Contents

LIST OF FIGURES

LIST OF TABLES

NOTATIONS

Symbol	Description	Unit
c	Wave celerity	[m/s]
c_g	Wave group celerity	[m/s]
d	Depth above caisson berm / mound	[m]
f	Frequency	[s^{-1}]
$f_{\underline{H}}$	Wave height probability density function (pdf)	[m^{-1}]
$F_{\underline{H}}$	Wave height cumulative density function (cdf)	[-]
F	Force	[$kg.m.s^{-2}$]
γ	Breaker index	[-]
h	Water depth (commonly used)	[m]
h_s	Water depth in front of caisson foundation/berm	[m]
h_b	Berm height	[m]
H	Wave height	[m]
H_0	Deep water wave height	[m]
H_b	Wave height breakers criterion (breaker height)	[m]
H_i	Incoming non-reflected wave height	[m]
H_s	Significant wave height	[m]
H_{si}	Incoming unreflected significant wave height	[m]
H_{rms}	Root-Mean-Square wave height	[m]
k	Wave number (=2ð/L)	[m^{-1}]
K_{refr}	Refraction coefficient	[-]
Kr	Reflection coefficient	[-]
K_s	Shoaling coefficient	[-]
m	Berm slope	[-]
η	Water surface elevation	[m]
NAP	Dutch chart datum	[-]
P	Wave energy flux	[W/m]
p_{max}	Maximum wave pressure	[kN/m^2]
p_0	Atmospheric pressure	[kN/m^2]
P_{br}	Probability of occurrence of breaking waves	[-]
Q_{br}	Prob. of occurrence of breaking waves used for p.d.f. truncation	[-]
S_{xx}	Radiation stress tensor for component x	[kN/m]
s	Wave steepness	[-]
Ur	Ursell or Stokes parameter	[-]
ω	Wave motion frequency	[rad/s]
ξ	Surf-similarity parameter or Irribarren parameter	[-]
ξ_c	Plunging breaker criterion for Irribarren parameter	[-]

N.B. All references to authors written as [...] refer to a known reference listed at the end of this report (see chapter References). When written as (...) only the reference between (...) is known

ABSTRACT

The reasons why caisson structures or vertical walls are built vary widely. Because of new perspectives on Coastal Engineering and harbour developments a certain shift from breakwater design to vertical wall structures like caissons has occurred in the last decennia. Caisson structures require less maintenance, need less time to be placed and result in lower costs than rubble-mound or berm breakwaters when constructed in larger depths.

The hydraulic conditions to which the caisson structures are exposed are a result of atmospheric pressures, tidal motions of ocean water and wind fields. As a result the structure responds to the exerted pressures induced by flows, waves and (changing) water levels.

The aim of this report is to give an overview of research done on the subject of wave impacts and to develop a breaker model to calculate the probabilities of breaking and impact waves. This is done by showing the formulae and theories which are used to calculate the dynamic behaviour of (wind) waves and design formulae wich are used for calculating different types of wave impact loads of waves impinging on a vertical wall.

Chapter 2 introduces regular periodic progressive waves. It describes the analytical theories for non-breaking waves, such as linear wave theory and non-linear wave theories. A list of wave deformations due to changing environmental influences is given and the phenomenon of breaking waves in introduced.

Chapter 3 explains the way wind wave height prediction is carried out (the spectral analysis and level crossing probability theory on which this prescription is based are explained briefly).

The different types of hydraulic forces exerted on the structure and the way these coastal structures respond to these forces can vary widely. Besides the quasi-static wave loads, two types of impact wave loads can be distinguished; severe wave impact pressures due to very small wave pressure rise times and pulsating loads or oscillation of (a component of) the structure due to resonance or air compression.

The first type of impact wave load gives the most severe wave impact pressures. The second type often causes a second wave pressure peak. This is called a double peaked pressure type. Many researchers try to understand the phenomenon of breaking wave impacts by focussing on the maximum wave impact pressures and hence maximum horizontal and vertical forces.

In chapter 4 wave pressures on a vertical wall due to non-breaking and breaking waves are described. Design formulae are also outlined.

Chapter 5 demonstrates some results of prototype measurements of wave impact pressures. Examples shown are the storm-surge barrier Oosterschelde, the caisson breakwater at Dieppe breakwater and Ship hulls.

In the last part of this study, changing the perspective from the wave forces to the breaking wave probabilities and the wave impact probabilities should give more insight in the way these phenomena demonstrate themselves in nature.

Three models, based on the probability of occurrence of wave heights together with a set of breaker criteria, have been developed: the simple reflection model, the truncated distribution model and the random wave reflection model. The models are validated with data of hydraulic model tests for random waves done by Oumeraci [1995] and McConnel and Kortenhaus [1996].

After calculating the optimal reflection coefficients for all models and their corresponding accuracy, one model shows the largest accuracy. This is the normal reflection model with the McCowan breaker function. When the data set is sorted by relative berm heights, this model gives only for larger relative berm heights the largest accuracy. For smaller relative berm heights the normal reflection model gives the most accuracy.

This model can be used to predict the probability of occurrence of impact waves as a rule of thumb. The scatter around the model results is large. The optimal reflection coefficient expressed by the relative berm height can not be presented by a function, which is consistence for both the data sets.

1 INTRODUCTION

1.1 Why build vertical wall structures?

This chapter introduces the caisson type breakwater. Twofold is the origin of breakwaters in a global sense. Because of harbour planning caisson type breakwaters introduce new possibilities for commodity exchange and maintenance procedures. Also for defending a harbour, coastal inlets and polders or other types of land, the necessity to construct such breakwater types arises. In the next two sections these necessities are explained. Section 1.2 describes different breakwater types.

1.1.1 Harbour planning

The first ports ever built were located in fjords and rivers; the Vikings in Scandinavia built some of the most magnificent of these. Four to five thousand years ago the Phoenicians attempted and succeeded in establishing a port on the open-sea coast at Tyre. The Romans built the famous naval port on the Tiber River at Ostia. Medieval ports such as London, Rotterdam, and Hamburg were all located on rivers, estuaries, bays, or sounds. The same was true of the first American ports – New York, Boston, Baltimore, Washington (Georgetown), and New Orleans.
The primary port function is to accommodate vessels. For most ports the geographic position (e.g. between sea and river) dictates the market position of such a port. In the last few centuries the dimensions of ships and therefore the dimensions of ports are growing continuously. As a result cargo-handling facilities have to follow the implicit demands made by shipping companies. Most ports have grown towards and beyond maximum sizes and have also grown towards the sea.
An important downtime cause with cargo handling was the influence of wave forces on ships and also on quays and terminals. In order to minimise this and guarantee safety to moored ships, breakwaters were designed and constructed. Wind waves now had a decreased influence in the harbour bay area.

1.1.2 Floods

To place some hydraulic coastal structures in the proper context it is necessary to highlight some typical problems concerning the battle against the sea of the Netherlands.

Over half of the Netherlands lies below sea level. Just how vulnerable this country is to floods was demonstrated on 1 February 1953. A combination of a spring tide and a persistent, violent north-westerly storm created, on a particularly large scale, an event that happened many times over the centuries. A major part of Zealand, the southern part of South Holland and the western part of North Brabant were flooded.

The Delta Project was the outcome of the determination that such a catastrophe should never happen again. To improve the safety of the south-west Netherlands the shoreline was to be reinforced with hydraulic engineering projects. In the Delta law criteria for exceedance frequencies were defined, as can be seen in Figure 1-3a. An overview of closure structures is shown in Figure 1-3b. The Delta Project resulted in fresh water lakes as a result of closing some inlets and estuaries, reinforcement of the dykes, construction

of new dykes and the construction of coastal structures like the Haringvliet, the Brouwersdam and the Storm-surge Barrier Oosterschelde.

Figure 1-1: Storm-surge barrier New Waterway

Figure 1-2: Storm-surge barrier Cappelle aan de IJssel

Also extreme river discharges can result in severe floods. During the period 1993-1995 the Netherlands, Belgium, Luxembourg, Germany and France experienced heavy floods. Large parts of land surrounding the riverbed (uiterwaarden) were flooded together with some polders due to failure of river dikes. Because prediction of these water levels is entirely different than prediction of water levels at sea where also the influence of (wind) waves is important, river floods are not outlined any further.

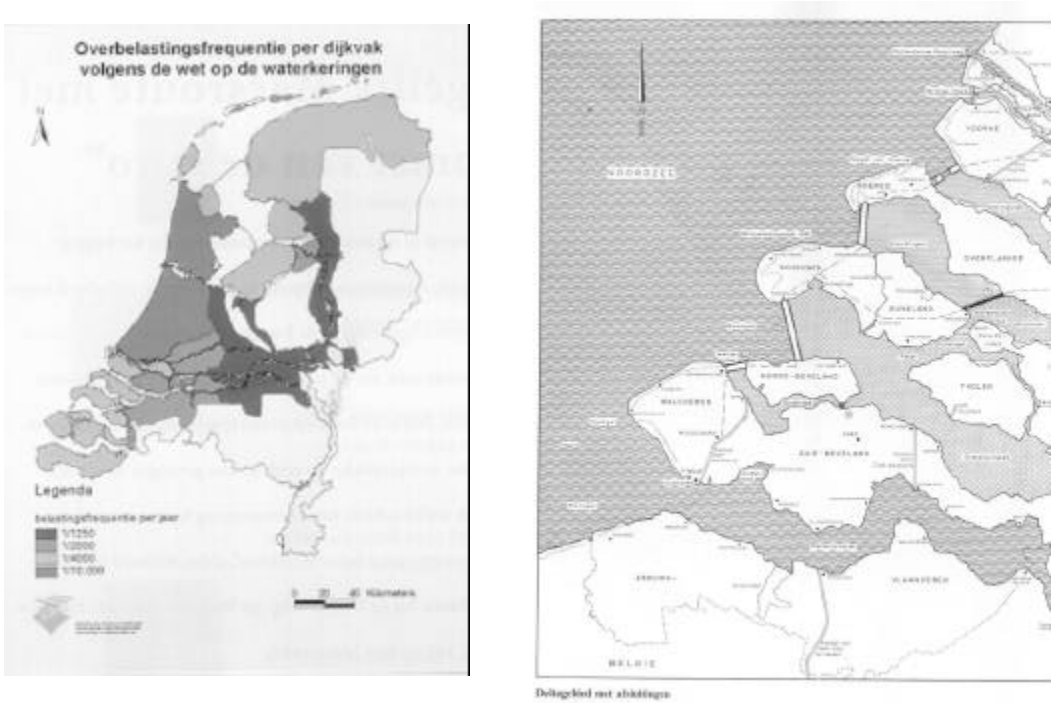

Figure 1-3a,b: Exceedance frequencies (Delta Law) and Delta area

1.2 Breakwater types

Breakwaters are primarily built to give protection against wave attack on ship moorings, manoeuvring areas, port facilities and adjoining areas of land. They can also reduce the amount of dredging required in a harbour entrance by guiding currents in entrance channels. With a single breakwater, the Phoenicians built their famous open coast port at Tyre using rectangular blocks tied together to form a vertical wall. Similar vertical designs were common in the nineteenth and in the beginning of the twentieth century [Bruun 1989].

Basically there are two main types of breakwaters: the vertical (or almost vertical) wall type (monolithic, or caisson type) and the sloping mound type which may be built of rock, concrete or of rock/concrete/asphalt mixtures also called rubble mound structures.

The sloping mound type breakwater (see Figure 1-4) consisted normally of quarry stone, armoured with one or more layers of heavy rock gradings. Because the rock volume is proportional to the square of the depth, construction time of rock placements in great depths is large and maintenance is very difficult.

Some special breakwater types are developed for reducing hydraulic forces due to their shape. Examples are (non-gravity) types like curtain wall breakwaters, steel pile breakwaters, horizontal plate breakwaters, floating breakwaters, pneumatic breakwaters, hydraulic breakwaters. Some of these special breakwater types are still being employed but next to extra maintenance costs and extra material costs their uses are mostly limited to special conditions [Takahashi, 1996].

1.2.1 Rubble-mound breakwater

The rubble-mound breakwaters, also called sloping type breakwater, are subject to all types of waves, always in some way breaking on the slope. Because of the slope the

breakwater itself can withstand the extra pressure if it is build not too small or instable. The problem is the erosion of the armour rock layer. The most fundamental sloping type breakwater is one with randomly placed stones. To decrease material costs the core of the breakwater is constructed with quarry-run. The stability of the (multi-layered) armour layer can be strengthened using shape designed concrete blocks, while wave transmission can be reduced using a superstructure (see Figure 1-4c), which can also be used as an access road for maintenance or transport road.

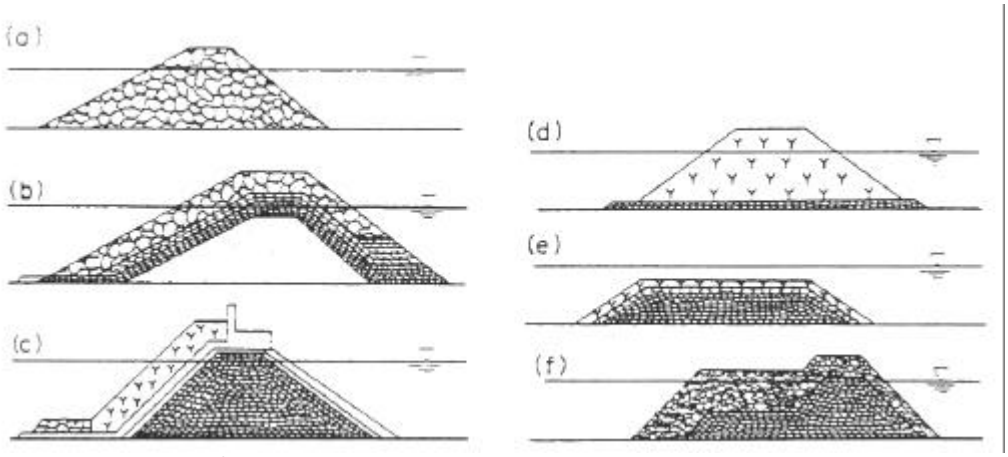

Figure 1-4: Examples of sloping type rubble-mound breakwaters [Takahashi 1996]

All these considerations can be viewed in Figure 1-4. Low-mound, high-mound and berm-breakwaters form the major part of rubble-mound breakwaters.

1.2.2 Caisson type breakwater

Figure 1-5 shows some vertical type breakwater with different foundation heights. The first is called a basic (caisson) breakwater while the others are called composite breakwaters being constructed of both a caisson type structure and a (rubble-mound) foundation. These caissons may be built of natural rock, masonry, wood, steel or concrete. Commonly observed are the increased occurrences of impulsive wave pressures due to wave breaking for higher foundation mound heights (Figure 1-5c,d).

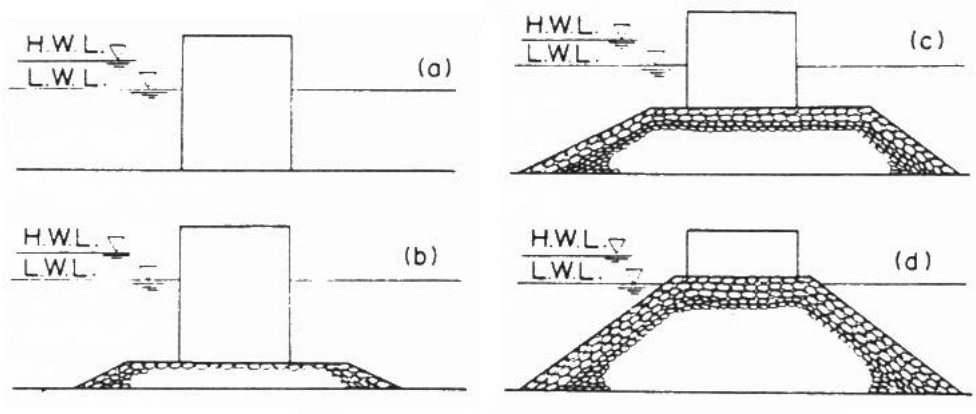

Figure 1-5: Examples of vertical type breakwaters [Takahashi 1996]

Sometimes a combination of a caisson type (super-) structure, a rubble-mound foundation and a berm in front of the caisson is being built to decrease the reflection and create a buffer for storm erosion (see Figure 1-6). Although this combination looks favourable in some ways, the large horizontal pressure due to the berm weight is an important unfavourable design aspect.

1.3 Failures of vertical breakwaters

The vertical breakwater type, in the thirties commonly built in Japan, became more favourable after a series of failures of rubble-mound breakwaters, and development and research was increased on this subject. Nowadays many vertical breakwaters have been built all over the world. Though the phenomenon of wave impacts and the stability against hydraulic forces are better understood, more and more research is needed to minimise the failures of this type of coastal structure.

1.3.1 Breakwater failures

The following table emphasises the necessity of research on this subject because of the large number of failed vertical breakwaters. Also in the next two figures two examples are shown being simplifications of the armoured and non-armoured type vertical breakwaters in which the vertical breakwater failures are classified.

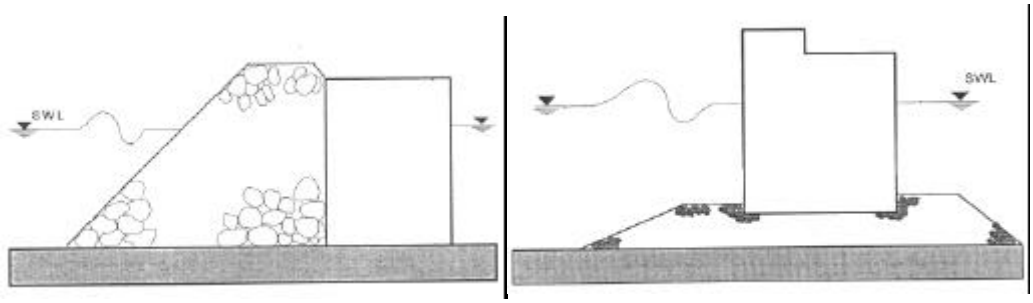

Figure 1-6: Armoured and non-armoured vertical breakwater [after Oumeraci, 1994]

Breakwater	Country	Year	depth [m]	design[1]	Actual[2]	Reason[3]
Madras	India	1881	22	-	-	O/Sc
Bizerta	Tunisia	1915	17	-	-	O/Er
Valencia	Spain	1926	12	-	7/15	O/Ex/Sc
Antofa-G	Chilli	1928	30	6/8	9/15	Ex
Catania	Italy	1930	17.5	6/7	7/9	O/Ex
Genoa	Italy	1955	17.5	5.5/7	7/12	Ex
Algiers	Algeria	1930	20	5/7.4	9.5/11	Er/Ex/Sc
Niigata	Japan	1976	17	7/13	7/13.5	O
Bari	Italy	1974	15.5	-	-	Er/Ex
Palermo	Italy	1973	36	5.5/7	6.1/11.3	Er/Ex
Naples	Italy	1987	19	-	5/-	-
Mishike	Japan		7	5.5/10	6.6/12	O/Ex
Fukaura	Japan		15	7.6/11	6.3/13	O/Er
Sakata	Japan		7	3.3/8.8	5.5/13	Ex
Onahama	Japan		16	6.1/14	6.1/14	Er
Niigata	Japan		18	7.5/13.5	7.5/11	O/Er
Niigata	Japan		15	7/13	7.1/13.5	O

Table 1-1: Vertical breakwater failures [Oumeraci, 1994]

[1] H_{design} [m] / T_{design} [s]
[2] H_{actual} [m] / T_{actual} [s]
[3] Overtopping/sea bed SCour/Exceedance design wave/Erosion rubble mound foundation/Settlement

Breakwater	Country	depth [m]	design[1]	actual[2]	Weight [T]	Reason[2]
Ventotene	Italy	5	-	-	12	Er
Rumoi	Japan	18	8.9/13	6.8/10	45	Er
Ishikari	Japan	8	5.6/11	3.8/75	20	Er/Sc
Oshidomari	Japan	14.6	5/11	5.8/9.5	16	Er/Settl
Miyako	Japan	11.5	4.4/10	4.6/11	12.5	Er/O

Table 1-2: Damaged armoured vertical breakwater [Oumeraci, 1994]

1.3.2 Reasons of Instability

Except for the well-known reasons like wave overtopping, impact wave loads and purely geotechnical failures, some important reasons for failure of vertical breakwaters are given:

Non-monolithicity of the structure
Shoreward sliding of the superstructure caused by impacts of breaking waves and collapse of superstructure caused by difference in settlement are two principal modes of failure. A very wide breach in the breakwater and a gap between the settled single blocks and the superstructure could develop and undermine the breakwater.

Low structure and high toe berm
By examining the structures which failed and which were built as “vertical breakwater”, it can be seen that most of them had too high a toe berm. Waves then are reflected by the wall when the water level is high, but break against the wall or the rock fill slope when the water level is low [PIANC, 1976].

Exceedance of design wave conditions
An exceedance of the design wave conditions by about 40% to 80% in terms of the wave height and 40% to 100% in terms of wave period occurred for vertical breakwaters, built before 1940. The maximum design wave height in the range of H=5-6m were often easily exceeded by waves with heights in the range of H=7-10m.

Design and failure modes
Over the last 70 years experiments were done to create understanding about interaction between hydrodynamic forces and (concrete) structures. Many mishaps proved the weakness in old vertical wall designs. Collapses were caused partly by waves breaking directly onto the structure and partly by bottom scour in front of the wall, causing it to overturn.
In the thirties a series of catastrophic failures by vertical breakwaters was experienced. Examples are the breakwater at Niigata West Port in Japan (1930), 700 meters of the breakwater at Catania (1933) and the Mustapha breakwater in Algiers (1934) with four hundred meters of overturned breakwater. These breakwaters consisted of a vertical wall of superimposed blocks based on a rubble stone foundation. Why these breakwaters failed was not clear.

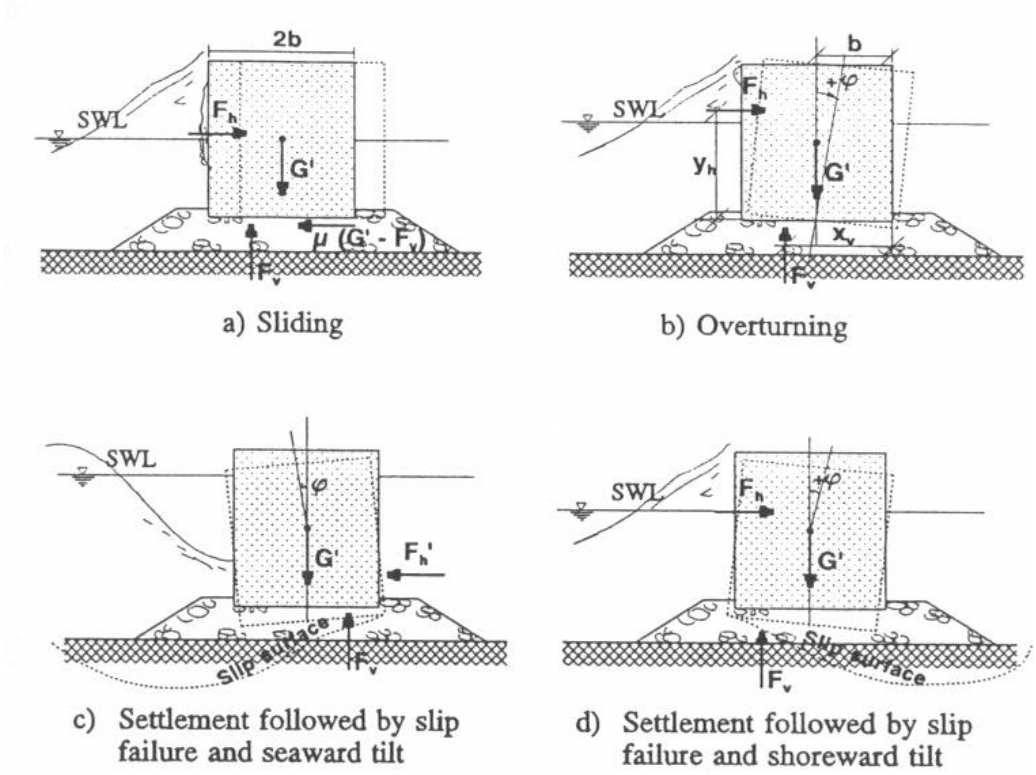

Figure 1-7: Overall failure modes [Oumeraci, 1994]

The most important mechanisms causing a vertical breakwater to fail are:

- Sliding
- Overturning
- Shear failure of the foundation
- Scouring of the seabed and erosion of the rubble-mound toe

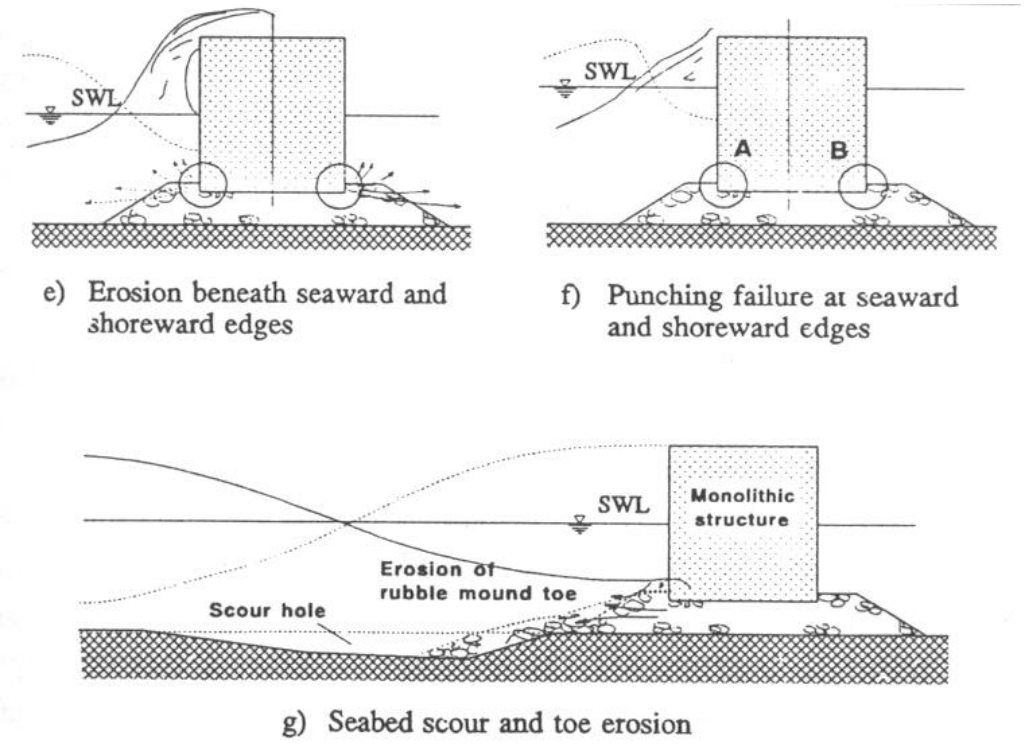

Figure 1-8: Local failure modes [Oumeraci, 1994]

From the researches done by Goda (1973) and Oumeraci (1992) it is still not clear which mechanism is responsible for the failure of vertical breakwaters and it is even questionable whether one of these mechanisms can by itself cause the collapse of a breakwater. In engineering practise some of the lessons learned are:

- "Design wave height" (PIANC, 1976) must be replaced by "design wave loads criteria", for sudden failure and repetitive loads (fatigue failure).
- Extrapolation of long-term statistics should carefully be evaluated before application.
- Determination of less dangerous locations is very difficult.
- Prediction methods for dynamic wave loads are a necessity.
- Realistic evaluation of the dynamic loading and response of the structure and its foundation for final designs is needed.
- During construction, seaward tilt should carefully be evaluated together with the work phases itself

The construction of these structures is however still essentially based on empirical approaches as well as on trial and error processes, making optimisation based on this nearly impossible.
Traditionally the stability conditions for structures are evaluated on the basis of quasi-static wave loading computed by assuming extreme wave conditions. The main weakness of this conventional approach not only consists in the uncertainty related to wave conditions and subsequent loading, but rather in the fact that it cannot explain the reason and mechanisms of the failures experienced world-wide by numerous vertical breakwaters (Oumeraci, 1991).
Breaking wave impact loads, with high irregularity and short-crestedness of the waves, still represent the most important source of damage, rather than a simple design wave criteria used with quasi-static wave loading formulae.

There also is a clear evidence that wave overtopping conditions not only represent an important functional design aspect, but also an important source of structural damage, because it can cause the low crested structure to overturn seawards.
The effect of dynamic loading on the foundation, especially that of the single maximum impact and that of the repetitive wave loads, should properly be considered in the analysis, especially for sea bed scour and toe erosion.

1.4 Framework

In the field of wave impacts on vertical walls considerable development has occurred over the last two decades. Parallel to harbour hydraulics, pollution control, replacement of breakwater armour by improved types, breakwater engineering has improved over the years. Model techniques have been improved to focus more on the combined effects of hydrodynamic, hydromechanic and geomechanic conditions combined with newly developed techniques in the field of (imprecise) wave statistics.

The main drawback with many vertical walls is the high pressure of waves breaking on the wall. Numerous publications have been written about wave forces on vertical walls. A lot of formulae for a standing (non-breaking) wave on a vertical wall have been presented. The forces acting on the wall are used for calculating the stability against overturning and sliding.

A project has been started called MAST (Marine Science and Technology programme of the European Union). Some important topics in these EU funded projects were: "Integration and development of the overall framework", "Wave action on and in coastal structures", "Wave impact loading on vertical structures" and "Berm and rubble mound breakwaters". The experience within the research programme concerning monolithic breakwaters in MAST II is the MCS-project, or the Monolithic Coastal Structures Project. In MAST III a project was started called the PROVERBS-project (Probabilistic design tools for vertical breakwaters).

Many design procedures and methods for vertical breakwaters are limited in their application and may over- or underpredict the loading under important conditions. This will then lead to overdesigned and very expensive structures or, even more dangerous, to underdesign and consequently to danger to personnel and properties.

Within PROVERBS engineering experience from various fields (hydrodynamic, foundation, structural aspects) concerned with vertical breakwaters has been brought together. Furthermore, data available from different hydraulic model tests, field surveys and experience from numerical modelling were collected and analysed to overcome the aforementioned limitations. Engineers from both universities and companies were working together to derive new methods for calculating forces and pressures under severe impact conditions taking into account the influence of salt water and aeration of the water. This new approach was then further optimised by taking into account the dynamic properties of the structure itself and of the foundation of the breakwater.

In PROVERBS a parameter map is developed classifying different types of wave loading in case of the presence of a berm. This parameter map based on small-scale model tests completed at HR Wallingford is compared with the data from the mid-scale (WKS) and large-scale (GWK) model measurements.

The goal of this study is to describe the probability of occurrence of breaking waves and wave impacts using only a few non-dimensional geometric and hydraulic parameters. I developed three theoretical models to predict the probability of breaking waves. Although it was intended to investigate the probability of impact waves, this was not done, only as a first analysis. These models are calibrated with the wave flume measurements. The reflection coefficient is used as the free parameter.

2 PERIODIC PROGRESSIVE WAVES

2.1 Introduction

A wave is defined as the maximum wave elevation difference between two successive upward zero-crossings, or between two successive downward crossings, using the distance between the level of the top of the crest and the level of the bottom of the trough. The wave period is the time between successive crests passing a certain point, or using the former definition, the period between the two zero-crossings upwards or downwards. The wavelength is the horizontal distance between two zero-crossings (see Figure 2-1).

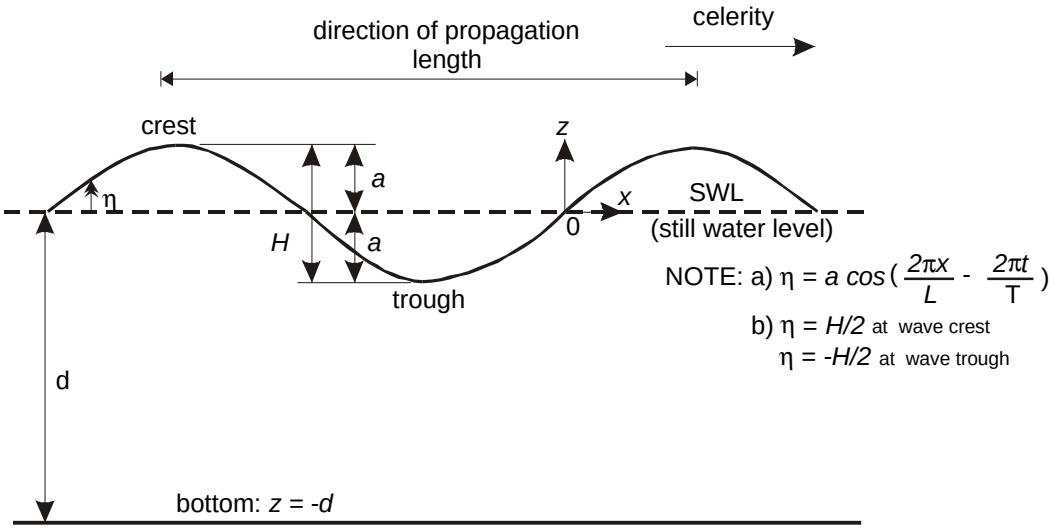

Figure 2-1: Wave characteristics (CERC, 1984)

A distinction is often made between regular and irregular waves. Regular waves are periodic repetitions of the same wave, while irregular waves show continuously different wave heights and periods. In fact, regular waves never occur in nature, but swell can come close. For an approximation of the phenomena of wave propagation, regular waves are used to solve the wave equations, and irregular wave models are based on these regular wave models.

2.2 Linear Wave Theory

The linear wave theory describes the dynamic gravity or free surface wave properties using the following conditions:

- Irrotational flow
- No Reynolds-stresses
- A sinusoidal surface profile

The Navier-Stokes equation is solved using Laplace equations with the sinusoidal surface profile defined with constant parameters: wavelength (L), maximum surface elevation (a) and propagation speed (c). The surface motions is given by

$$\eta(x,t) = \frac{H_i}{2}\sin\left(\frac{2\pi t}{T} - \frac{2\pi x}{L}\right) = \frac{H_i}{2}\cdot\sin(\omega t - kx) \qquad (2.1)$$

The velocity potential θ can be written with:

$$\theta(x,z,t) = \frac{\omega a}{k}\frac{\cosh(k(h+z))}{\sinh(kh)}\cos(\omega t - kx) \qquad (2.2)$$

Derivations for horizontal and vertical velocities show that the phase difference between them at a fixed point equals 90º. The amplitudes of horizontal and vertical velocities are equal in deep water, but differ increasingly with decreasing relative depth (~h/L) as can be seen in (2.2). The next figure shows the orbital motions of particles due to wave motion.

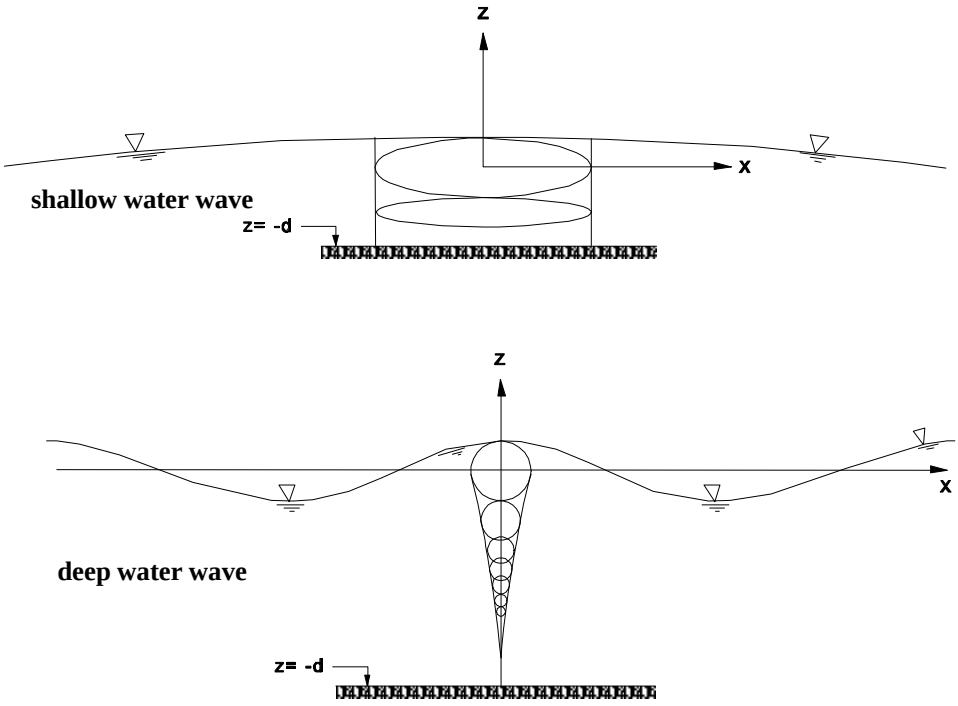

Figure 2-2: Orbital particle motions, after [d'Angremond and Bezuijen 1993]

When the relative depth becomes very small the vertical motions decrease almost linear with the depth and the horizontal velocities become equal for all vertical positions.

Dispersion relationship

If no further conditions are given the maximum surface elevation (a), phase speed (ω) and wave number (k=2π/L) are arbitrary. The dispersion relationship for linear waves states that there is a unique relation between rotational speed ù, wave number k and the water depth h:

$$\omega^2 = gk\tanh(kh) \tag{2.3}$$

The phase speed of propagation of a wave (c) can be formulated with the dispersion relation expressions for the wavelength (L):

$$c = \frac{L}{T} = \frac{\omega}{k} = \sqrt{\frac{g}{k}\tanh(kh)} \tag{2.4}$$

And when c is denoted as a function of the phase speed in deep water (c_0) the equation becomes

$$c = c_0 \tanh(kh) \tag{2.5}$$

where

$$c_0 = \frac{L_0}{T} = \frac{gT}{2\pi}\tanh\left(\frac{2\pi h}{L_0}\right) \tag{2.6}$$

The energy that is represented by a group of waves in a train does not propagate at the same speed as the individual waves that make up the group (i.e. phase speed). The group velocity is defined as:

$$c_g = \left[\frac{1}{2} + \frac{kh}{\sinh(2kh)}\right]c = nc \tag{2.7}$$

The energy flux or wave power, P, is the mean energy transmission in the direction of the propagation per unit time and per unit width. It is given by

$$P = Ec_g = Enc \tag{2.8}$$

Deformation in shallow water calculated by linear wave theory is described in section 2.4.

2.3 Non-linear Wave Theories

This chapter describes two non-linear wave theories: the Stokes theories and the shallow water theories. Both theories demonstrate a cnoidal wave shape after the mathematical equation that is used to describe this shape.

2.3.1 Stokes' higher order theory

Stokes (1847) calculated the wave equations in multiple steps. Firstly he described the wave motion using the linear wave theory neglecting the non-linear terms. Secondly he implements the parameters and again describes the wave motion, but now with the non-linear terms. The now derived velocity potential equation satisfying the (Laplace) conditions is described with

$$\theta(x,z,t) = \frac{\omega}{k^2}\sum_{j=1}^{j_{max}} C_j (ka)^j \cosh\left[jk(h+z)\right]\cos\left[j(\omega t - kx)\right] \tag{2.9}$$

In this equation the coefficients C_j are to be solved for deep water (or U_r<<1, see the following paragraph). For third and higher order theories the coefficients become rather small compared to the lower order coefficients. Using only a second order solution provides satisfactory results in most situations and gives realistic results. Wave surface profiles for higher order solutions can be described with the next equation:

$$\eta(x,t) = \hat{\eta}_1 \cos(\omega t - kx) + \hat{\eta}_2 \cos(2\omega t - 2kx) \tag{2.10}$$

when the wave crest is considered to be the position where at t=0 the phase is zero. The ratio of $\hat{\eta}_2 / \hat{\eta}_1$ is described with

$$\frac{\hat{\eta}_2}{\hat{\eta}_1} = \frac{1}{4}\frac{\cosh(kh)\left[2+\cosh(2kh)\right]}{\sinh^3(kh)}\,ka \tag{2.11}$$

For deep water this results in $\hat{\eta}_2 / \hat{\eta}_1 \approx \pi H/2L$ and for shallow water the ratio becomes $\hat{\eta}_2 / \hat{\eta}_1 \approx 0.01 * HL^2/h^3$. The wave surface profile shows a second maximum wave top when the wave becomes too high in shallow water. For shallow water a criterion is proposed to bound the conditions in which Stokes' second order wave theory is valid. This definition uses the Ursell number U_r defined as:

$$U_r = \frac{HL^2}{h^3} < 25 \tag{2.12}$$

2.3.2 Shallow water theory

This theory can be used for waves in shallow water with some steepness (contrary to the Stokes theory where the steepness must be extremely small in shallow water). This theory is based on the assumption that a certain correction for the hydrostatic pressure distribution must be added.

With consideration for flow curves parallel to the surface profile Boussinesq [1872] derived a set of equations for shallow water waves which were simplified by Korteweg and de Vries (1895) [Peregrine 1972].

For different Ursell numbers cnoidal wave profiles are shown in Figure 2-3. As can be seen the profile approaches the sinusoid shape for $U_r \sim 0$. For high Ursell values (when the relative wavelength or relative wave height becomes large) the shape demonstrates a small peak and a wide trough.

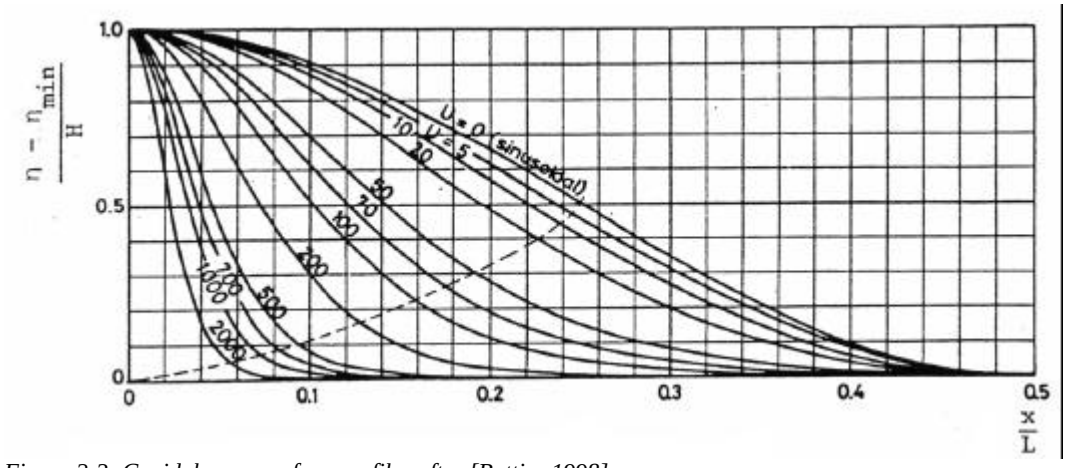

Figure 2-3: Cnoidal wave surface profiles after [Battjes 1998]

2.4 Deformation due to bathymetry or presence of structure

Most calculated deformations in shallow water are derived from analysis based on the linear wave theory. Predicted effects such as shoaling, refraction and wave set-up that are related to this theory are commonly based on monochromatic waves but describe actual phenomena sufficiently accurate for engineering purposes. With the exception of wave set-up, which is not explained in this study, all effects are transferred to coefficients of the ratio new wave height-to-deep water wave height. Waves approaching the coastline up to the point of breaking follow:

$$H = H_0 K_{refr} K_s \tag{2.13}$$

where

H = shallow water wave height
K_{refr} = refraction coefficient
K_s = shoaling coefficient
H_0 = deep water wave height

2.4.1 Shoaling

Assuming a constant wave energy transmission between adjacent lines perpendicular to the wave crest and therefore no energy dissipation (due to wave breaking) waves at normal incidence to straight parallel depth contours follow the next equation:

$$E_0 n_0 c_0 = Enc \tag{2.14}$$

with

$$\frac{H}{H_0} = K_s = \sqrt{\frac{n_0 c_0}{nc}} \tag{2.15}$$

With decreasing water depth the shoaling coefficient (K_s) decreases slightly below 1 (unity) before increasing rapidly. As the wavelength decreases with decreasing depth, the wave steepness (H/L) will increase.

2.4.2 Refraction

For a wave that is propagating over a bottom with parallel depth contours at an angle (φ) other than normal, the water depth will vary along the wave crest. Therefore, according to

(2.4) the phase speed will also vary along the wave crest. As a result the crest will tend to bend towards the depth contours. With the resulting equation:

$$Ec_g \cos\varphi = \text{constant} \tag{2.16}$$

and also

$$\frac{\sin\varphi}{c} = \text{constant} \tag{2.17}$$

The wave height variation is then equal to:

$$K_{refr} = \sqrt{\frac{\cos\varphi_0}{\cos\varphi}} \tag{2.18}$$

where K_{refr} is the refraction coefficient.

2.4.3 Diffraction

Bending of the wave crest behind a coastal structure (breakwater, island etc.) is called diffraction (see Figure 2-4).

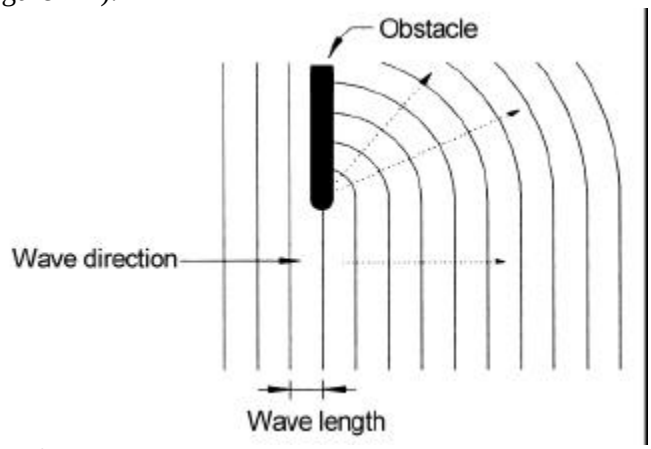

Figure 2-4: Diffraction of incoming wave [d'Angremond & Bezuijen, 1993]

The combination of the incoming wave field and the geometry of the structure creates a shadow area behind the structure. Although interaction with other wave crests can cause local wave heights to exceed the original wave heights, wave heights in this shadow area are considered to be a fraction of the original wave heights. Also marine obstacles with a crest height beneath the water level cause diffraction (e.g. shoals or sandbanks) [d'Angremond, 1993].

2.4.4 Reflection

The wave types introduced above are valid for progressive periodic waves with constant shape. This thesis considers the interaction with a structure. This occurs when waves approach the coastal area and come in the vicinity of a coastal structure. When the structure is a beach slope, the waves will break at different locations dependent on their wave height and local water depths. When the waves reach the shoreline almost all wave energy is dissipated and the reflection is nearly negligible.

With increasing steepness of the structure the reflection will increase and breaking will occur in a zone less wide compared to a milder slope. For very large steepness reflection

becomes important resulting in a standing wave pattern in front of the structure in case of monochromatic waves. The phenomena of standing waves and the resulting pressures are described in chapter 4.

2.4.5 Breaking of Waves

Physically, a wave breaks when the velocity of a particle in the top of the wave front exceeds the wave celerity. Normally two criteria are considered to induce breaking of waves. First a restricted wave height to water depth ratio (γ) and second a limiting wave steepness (s) give the point where the waves start to break.

Wave height-water depth ratio

The first, denoted by a breaker index (γ) defining a limit ratio between wave height (for monochromatic, regular or solitary waves) and water depth, calculated for the linear and non-linear wave theory:

$$\gamma = \left(\frac{H}{h}\right)_{max} = \left(\frac{H_b}{h}\right) \tag{2.19}$$

Wave steepness

Second the limiting wave steepness (s) is defined with

$$s = \frac{H}{L} \tag{2.20}$$

Models combining the limited wave height and limited wave steepness are also developed. (Miche breaking criteria). H in this case is defined as the individual incoming wave.

The non-linear wave theories (both Stokes second order wave theory and the shallow water wave theory) are valid when the velocity of the wave crest does not exceed the phase speed c. Stokes showed that this occurs when the shape of the wave crest is sharp with an inner angle of 120 degrees instead of a round wave crest (see the next figure). This analysis of the non-linear wave theory uses the steepness parameter (s) and gives a basis for different breaking criteria.

Based on the results by Stokes, Miche (1944) derived the maximum wave height for a certain wave length and water depth using this criterion and derived equation (2.22).

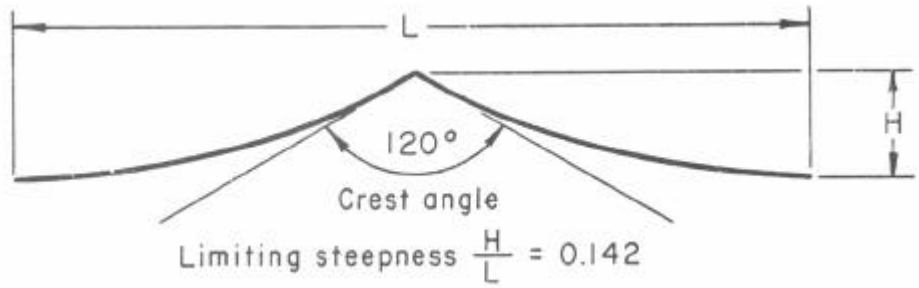

Figure 2-5: Maximum wave height for non-linear wave theories [after Battjes 1998]

2.4.5.1 Breaking criteria for monochromatic waves

Le Mehaute

Le Mehaute (1969) presented Figure 2-6 to illustrate the appropriate limits of validity for several "regular wave" theories. Implemented are breaking criteria for the linear wave theory, the Miche breaker limit and Stokes 2nd, 3rd and 4th order theory. The vertical axis is a measure for the wave steepness (:: H/L) and the horizontal axis for the relative water depth (:: h/L). The very existence of waves is limited by breaking due to steepness (upwards) and due to restricted water depth (leftwards).

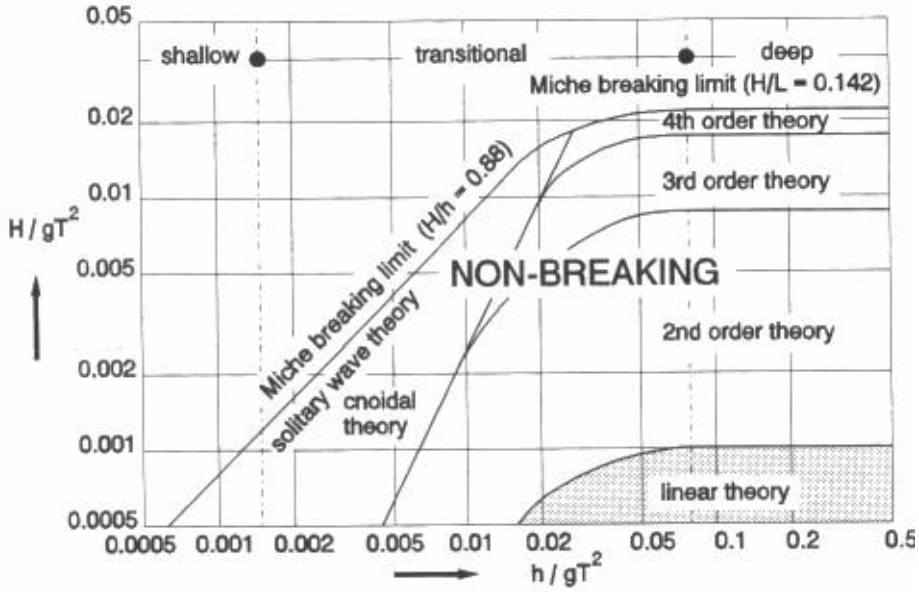

Figure 2-6: Regions of validity for various wave theories (after Le Mehaute, 1969)

McCowan (1891) defined a maximum wave height for solitary waves in a given water depth with a value given by

$$\gamma = 0.78 \tag{2.21}$$

Munk (1949) derived an expression for the shoaling effect and comes to the (same) conclusion that the breaker index γ is equal to 0.78.

Miche

The general form describes the limiting steepness for progressive periodic waves in any water depth according to Miche (1944):

$$\frac{a_b k}{\pi} = \frac{H_b}{L} = \beta \tanh\left(\frac{2\pi h}{L}\right) \tag{2.22}$$

where

a_b = breaker height (maximum water surface elevation)
β = criterion constant
H_b = breaker height (wave height)
L = local wave length

In the Miche breaker criterion, β equals 0.142. A breaker index can be derived from this equation:

$$\gamma = \frac{H_b}{h} = \frac{0.88}{kh}\tanh(kh) \qquad (2.23)$$

Oumeraci

[Oumeraci, 1994b] derived an adjusted Miche criterion for partially reflected waves. The influence of the reflection on the wave-breaking criterion is implemented in the constant β (see equation (2.22)) with the reflection coefficient K_r defined as the wave height ratio of the reflected and incoming wave (H_r/H_i). The breaker criterion, assumed to be the ratio between the incident wave height in front of the structure and the local wave length at depth h_s, is defined as:

$$\frac{H_b}{L} = \left(0.109 + 0.033\frac{1-K_r}{1+K_r}\right)\tanh\left(\frac{2\pi h}{L}\right) \qquad (2.24)$$

In this equation the part 0.033(1-kr)/(1+Kr) is an empirical relation and follows from laboratory data. This equation yields the same results as the Miche criterion for non-reflected waves (K_r=0).

Camfield and Street

Camfield and Street (1969) tested single solitary waves on slopes from m=0.01 to m=0.20 and found an empirical relationship between the slope and the breaker height-to-water depth ratio given by

$$\gamma = 0.75 + 25m - 112m^2 + 3870m^3 \qquad (2.25)$$

Equation (2.25) is based on empirical data only and should therefore be used only in the range of observations.

Weggel

Weggel (1972) developed also an empirical relationship for ã for periodic waves that is based on small-scale laboratory tests:

$$\gamma = b(m) - a(m)\frac{H_b}{gT^2} \qquad (2.26)$$

where

$$a = 43.75 * (1\text{-}e^{-19m})$$

$$b = \frac{1.56}{1+e^{-19.5m}}$$

If $H_b=\gamma h$ and $T^2=(2\pi)^2/k$ is substituted (this is true for deep water waves) equation (2.26) can be used when the different breaker indices are compared for varying relative depths (see Figure 2-7).

Kaminsky and Kraus

An extensive study of the breaker parameter was carried out by Kaminsky and Kraus [1993]. Kaminsky analysed a large data set containing laboratory test cases from several authors. Depth limited wave breaking was analysed for regular waves, incident to plane sloping beaches. An empirical relation for the breaker index as a function of the Irribarren parameter was developed.

$$\gamma = 1.20\xi^{0.27} \tag{2.27}$$

Nelson
Field data, from an experiment undertaken on the Great Barrier Reef, was used by Nelson [1994] to determine the maximum individual design wave height on a horizontal bed. Both for laboratory and field data a maximum value of 0.55 as the ratio between the maximum individual wave height and the water depth was found. For varying bed slopes the maximum wave height-to-depth ratio is given by:

$$\gamma = 0.55 + 0.88e^{-0.012/m} \text{ , for } 0<m<0.01 \tag{2.28}$$

An overview of these limit wave height criteria is given in the following figure. The breaker functions of McCowan and Nelson are not a function of kh and appear as constants. The breaker function of Miche and Weggel decrease with increasing value of kh. Various steepnesses for Weggel and Nelson are given. For kh = 0.6, all criteria are in the range of 0.55-0.88. For shallower water Weggel estimates a higher breaker heights for steep foreshores and for the lowest breaker heights Nelson can be used to defined a lower limit. For deeper waters Weggel gives the smallest breaker heights and McCowan (γ = 0.78) gives the largest breaker heights.

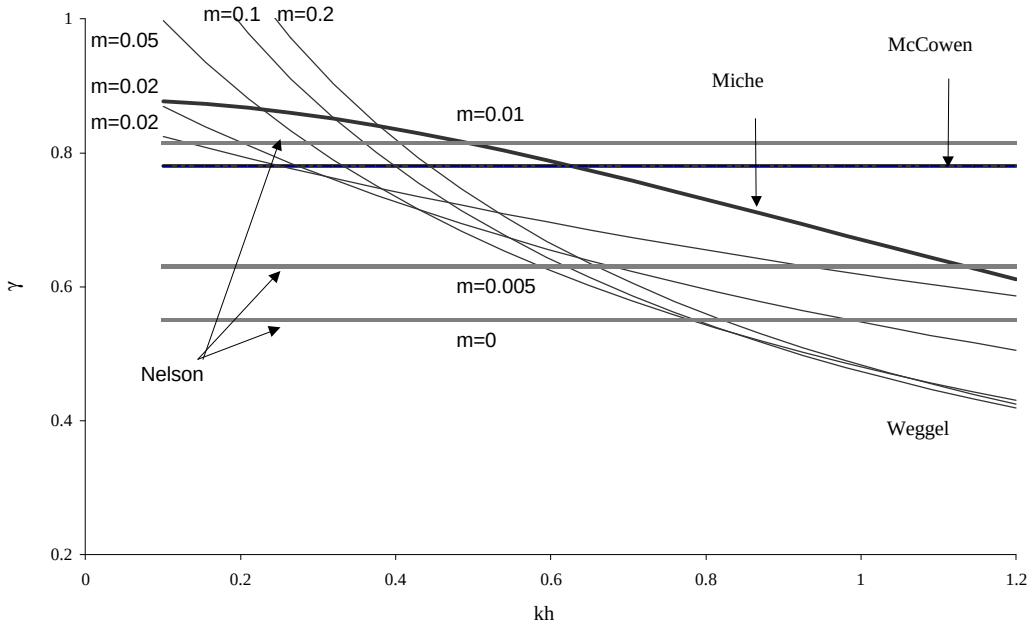

Figure 2-7: Breaker criteria for regular wave fields versus relative depth (kh)

Some criteria are given as the ratio between the breaker height H_b and the breaker depth, here defined as h. Others are given as the ratio between this breaker height and the local wave length L. When this value is multiplied with 2ð / kh the breaker index occurs. This multiplication is used for deriving a formula for the breaker index as a function of kh when it is not originally given.

2.4.5.2 Breaking criteria for irregular wave fields

For irregular waves fewer criteria have been developed. Most of the developed criteria for irregular wave fields are based on regular wave criteria. In order to apply wave height

criteria for such a wave field, characteristic values representing the irregular wave field are used, called the significant wave heights.

When this ratio is applied to the significant wave height irregular waves (H_s/h), values of $\gamma = 0.4\text{-}0.5$ are usually found, representing the maximum significant wave height for progressive irregular waves for a given water depth [Schiereck 1998].

v. Marle

While Miche was used for regular waves, application of this criterion was proposed for irregular waves. Van Marle [1979] found that $\beta = 0.093$ resulting in the following criterion could better approximate the coefficient β, resulting in:

$$\frac{H_{s;b}}{L} = 0.093\tanh\left(\frac{2\pi h}{L}\right) \tag{2.29}$$

A breaker index can be derived from van Marles result:

$$\gamma = \frac{H_b}{h} = \frac{0.58}{kh}\tanh(kh) \tag{2.30}$$

Oumeraci

Oumeraci [1994b] derived an adjusted Miche criterion for partially reflected irregular waves. The influence of the reflection on the wave breaking criterion, using the incident wave height in front of the structure, is included by the reflection coefficient K_r and implemented in β follows with:

$$\frac{H_b}{L} = \left(0.1025 + 0.0217\frac{1-K_r}{1+K_r}\right)\tanh\left(\frac{2\pi h}{L}\right) \tag{2.31}$$

Vincent and Smith

Vincent and Smith [2000] formulate another expression for a breaker function for random waves.

$$\gamma = \left(\frac{H_s}{h}\right) = 0.996e^{-50\frac{h}{gT_{mn}^2}} \tag{2.32}$$

in which the T_{mn} is defined as the reciprocal of the mean frequency $T_{mn}=1/f_{mn}$.

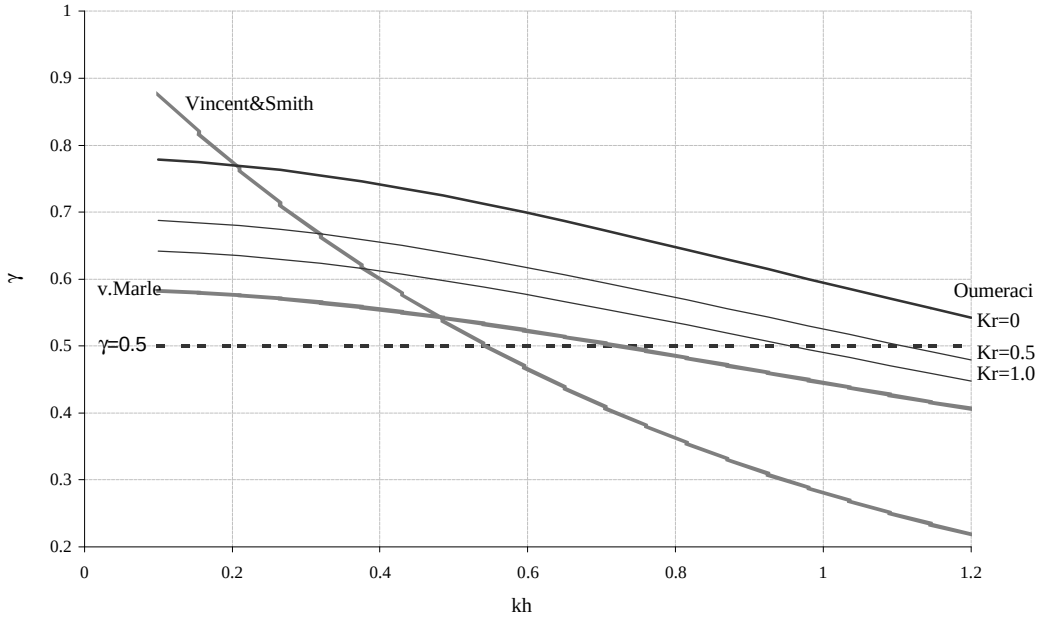

Figure 2-8: Breaker criteria for irregular wave fields versus relative depth (kh)

The model of Vincent and Smith gives qualitatively different results for varying relative depths. The criteria derived by Oumeraci and van Marle give similar results.

3 WAVE CLIMATES

3.1 Hydraulic conditions

Fluctuations of the water level are caused by numerous phenomena and can be characterised by defining a wave with an amplitude and period. The most important types of these waves are listed below in order of period:

wind waves
Induced by a wind field, these waves are generated and vary in size from ripples to ocean waves with wave heights as high as 30 m. Periods in the range of 5 to 15 seconds are often observed.

swell
This dispersed wave field induced by distant storms shows wave lengths ranging from 30 to more than 500 times the wave heights. Due to their travelled distance the waves have decayed and short steep waves are transformed into relatively long waves with small amplitudes. Periods occur in a range up to 30 seconds.

tsunamis
Phenomena like earthquakes or other tectonic disturbances on the open ocean can cause gravity waves. Showing no significant wave heights in deeper parts of the ocean (depths up to 1000 m), they can become very large when travelling into coastal areas. Their periods range from 10 to 100 minutes.

tides
Induced by the gravitational forces of the moon and the sun, tidal motions of ocean water cause a rise and fall of the water surface. Normally the tide follows the period of the force attracting the earth water mass, but changes when reaching shorelines or relatively shallow waters. At most locations one or two tides per day occur. Along the Dutch coast, the tide has a period of 12 hours and 25 minutes.

storm surges
Caused by local minima of atmospheric pressures or depressions the water surface lowers or rises (barometric effect). Also a wind set-up can be the result of extreme large wind speeds, and is explained in section 3.2.2. A storm surge behaves as a long wave with a wavelength approximately equal to the width of the centre of the depression. The height of these long waves may increase considerably due to shoaling effects. The period of these long waves may be in the order of a day or more.

In hydrodynamic studies with waves with large periods, two types of waves can be distinguished; short waves and long waves. In case of long waves, vertical accelerations are negligible. As a result the pressure distribution is assumed to be hydrostatic. Ships and wind mainly cause short waves. The term wind wave is often used when the driving wind force is still active. In contrast, swell is defined as waves that were caused by wind, but possibly long ago (days) and far away on the ocean (1000 km and more) travelling on with the slowly dissipating energy gained from the wind. Swell in shallow water can also be seen as a transition to long waves. [Schiereck, 1998] (see section 2.1).

In section 3.2 the following section the slow varying fluctuations of the water level is explained while 3.3 introduces the wind waves.

3.2 Water Levels

The still water level oscillation can be considered a superposition of a the water levels caused by the following phenomena:

- Astronomical tide
- Wind set-up
- set-up due to atmospheric pressures
- higher water levels due to river discharges (in tidal inlets or estuaries)

In this section the component of the tidal wave, the component caused by storm surges and the component caused by atmospheric pressure are explained. Included are design philosophies used for the design of the Storm Surge Barrier Oosterschelde. Probabilistic tools are implemented to give an idea on how the maximum storm surge level can be calculated in this case.

3.2.1 Tide

With a steady repeating rhythm the ocean water level changes in a significant way. Due to the orbit of the moon around the earth and the earth around the sun, each of these planetary objects influences all masses on earth. The sun induces a periodic response of the water mass, which is called S_2 and has a period of 12 hours (S_2 denotes solar tides twice a day). The influence of the moon on the tidal motion is approximately twice the influence of the sun because of the smaller distance to the earth (380.000 km) and causes a periodic wave with a period of 12 hours and 25 minutes. Two following high tides differ each “day” (every 24.50u) because the axis of the rotation of the earth is not exactly perpendicular to the plane of the orbit of the moon. This non-perpendicularity is called inclination and causes a phenomenon called the daily inequality. This daily inequality is different in each longitude and causes a tidal period of 24.50h in some places on earth.

The fluctuating water level can be described with a series of harmonic oscillations:

$$z(t) = z_0 + \Sigma A_i \cos(\omega_i t - a_i) \qquad (3.1)$$

where:

z_0 = average water level [m]
A_i = amplitude of component i [m]
ω_i = frequency of component i [rad/s]
α_i = phase of component i [rad]

By the Dutch Institute for Coastal and Marine Management (RIKZ) of the Ministry of Public Works the daily high and low waters are predicted for a number of locations along the Dutch coast. Figure 3-1 shows the water levels for Vlissingen in the South of the Netherlands. The following figure shows different mean high and low waters for other locations along the coast.

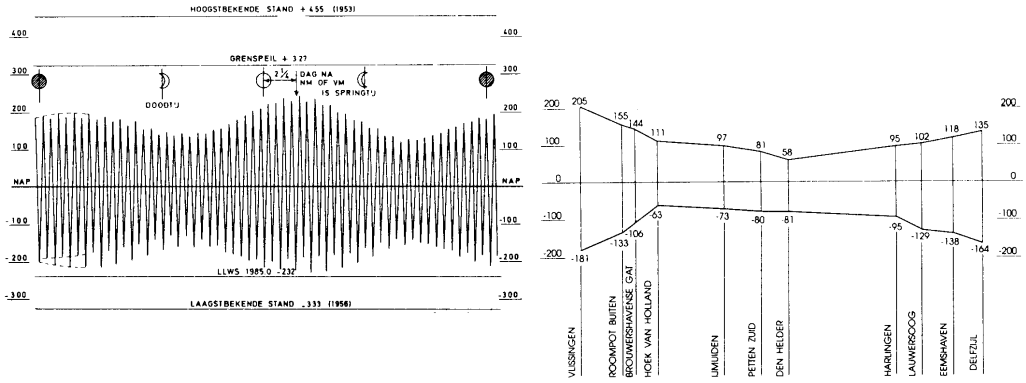

Figure 3-1: Waterlevels at Vlissingen and tidal fluctuations along the Dutch Coast [after d'Angremond & Bezuijen, 1993]

3.2.2 Wind set-up

Wind set-up is caused by the friction of a wind field above a water mass causing a water set-up at the end of the water basin (e.g. a lake) and a wind set-down at the start of the basin. Because the wind set-up parameters wind direction and atmospheric pressure have stochastic properties and cannot be calculated beforehand, the wind set-up is considered to be a stochastic phenomenon. Collected water level statistics form the basis for an analysis of water level occurrences.

The properties of the wind set-up have been studied by subtracting the astronomical tide from the still water level variations recorded during storms. In case of the storm surge barrier Oosterschelde the variation of the wind set-up in a storm could be approximated by [RWS, 1994]:

$$s(t) = s_m \cos^2\left(\frac{\pi t}{D}\right) \tag{3.2}$$

where s_m = maximum wind set-up during storm
D = duration of the wind set-up

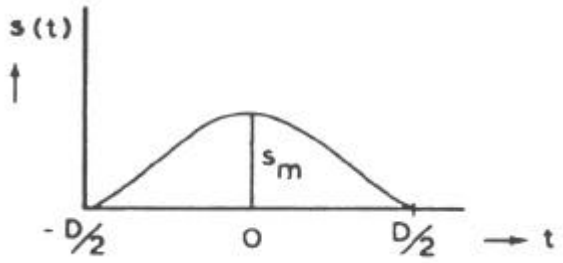

Figure 3-2: The wind set-up as a function of time [after RWS, 1994]

For the surge level duration and exceedance, probability of occurrence curves were developed by Dantzig [1960], using optimisations of the (logarithmic) exponential function $e^{(a-u)/b}$:

$$p(s_m > s) = e^{\frac{1.53-s}{0.3026}}$$
$$p(D) = \frac{1}{D\ln(1.4)\sqrt{2\pi}} e^{-\frac{1}{2}\left(\frac{\ln(D)-\ln(51.3)}{\ln(1.4)}\right)^2} \tag{3.3}$$

where

s_m = maximum wind set-up during storm
D = duration of storm (in hours)

3.2.3 Extreme surge levels

A common way to get an impression of the maximum storm surge level (called z_m during the design process of the storm surge barrier Oosterschelde) is simply to add the maximum wind set-up and the astronomical high water level.

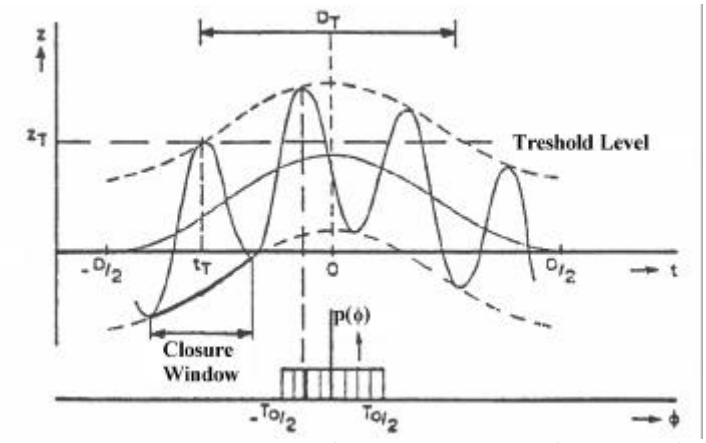

Figure 3-3: A storm surge level as a superposition of wind set-up and tidal fluctuation after [RWS 1994]

The marginal probability function of z then follows from:

$$p(z_m) = \iiint p(z_m \mid h_{HW}, D, s_m) p(h_{HW}) p(D) p(s_m) dh_{HW} dD ds_m \tag{3.4}$$

The exceedance curve of the maximum storm surge level compared to the observed data gives a close resemblance and supports the accuracy of the developed model.

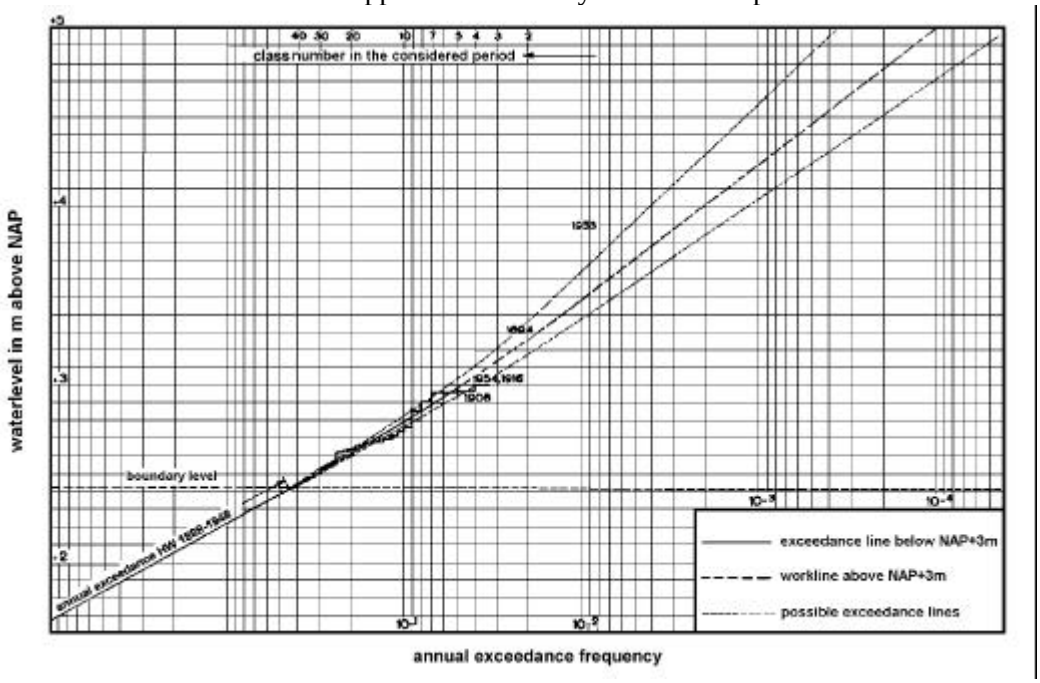

Figure 3-4: Example of frequency exceedance curve for the Dutch coast [after d'Angremond, 2000]

When the high water levels are written linear on the vertical axis and the exceedance frequencies logarithmically on the horizontal axis an almost straight line can often be seen. Figure 3-4 shows the water level distribution following from statistical analysis of water levels observed in the period 1889-1954. With a Poisson distribution this frequency of occurrences can be transformed into a probability density function. Now the probability of non-exceedance of any storm surge level (h) larger than a certain design level (h_d) in one year can be calculated with:

$$P(\underline{h} < h_d) = e^{-f} \tag{3.5}$$

where

f = frequency of exceedance per year

The following equation is used to predict the probability of non-exceedance during the lifetime of a structure in which T stands for the period in years (e.g. lifetime):

$$P(\underline{h} < h_d) = e^{-fT} \tag{3.6}$$

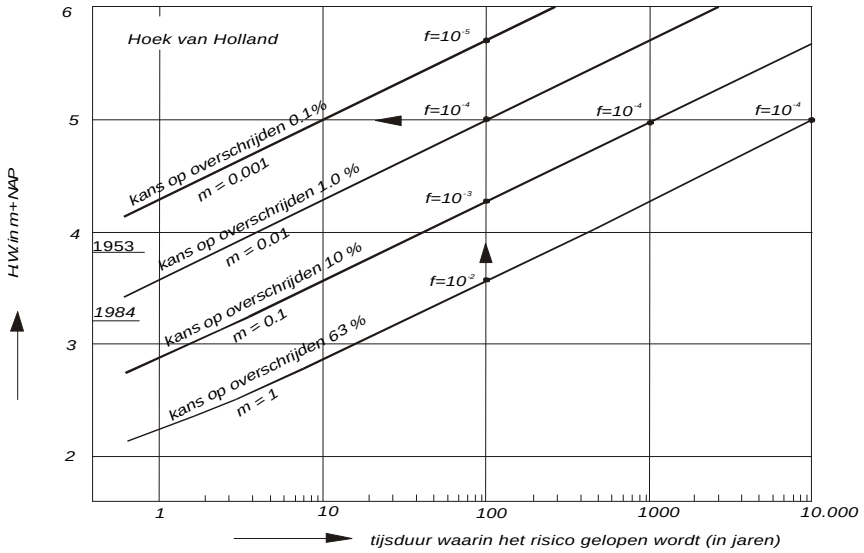

Figure 3-5: Lifetime design water levels [after d'Angremond & Bezuijen, 1993]

The result of (3.6) is shown in Figure 3-5 and gives a design water level for a given lifetime and probability of exceedance.

3.3 Wind Waves

When a turbulent wind field with irregular wind velocities blows over a water surface, the wave profile shows no regular periodic (progressive) waves but an irregular wave field will be induced.

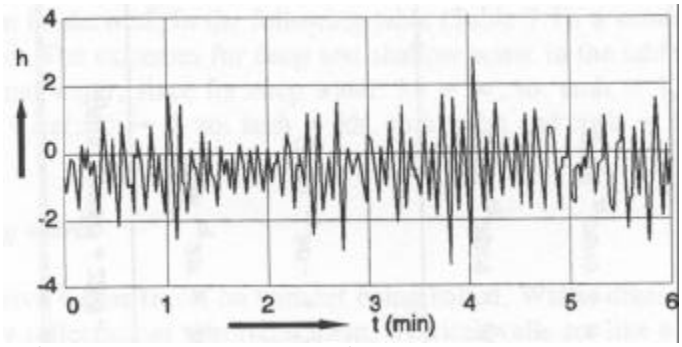

Figure 3-6: Example of North Sea wave registration (after Groen & Dorrestein, 1976)

A short look at a fluctuating water level registration like Figure 3-6 shows that it is impossible to describe the water level fluctuation deterministically. The wind waves should be treated as a stochastic phenomenon in time.

Spectral analysis can be applied to the time series of wave registrations. From the wave spectrum, distributions of different aspects of the wave field can be derived.

3.4 Spectral Analysis

Simplification of all conditions to sinusoid shaped waves profiles can be done both for increasing insight in hydraulic processes and for calculations of the response of linear systems on these processes but only for non-breaking waves. In this section the analysis of the water surface elevation due to waves $\eta(t)$ is considered.

3.4.1 Fourier-series

A set of multiple cosine- and sinus functions can be combined forming Fourier-series. The Fourier transformation will be discussed briefly to demonstrate its importance and give an introduction to dependent sections.
The Fourier-series can be an infinite number of cosine (or more complex with sine, but neglected here) waves described with:

$$\eta(t) = \sum_{n=0}^{\infty} a_n \cos\left(2\pi f_n t + \alpha_n\right) \tag{3.7}$$

To use a more physical basis for describing the wave field Parseval proposed a theorem which describes the mean square energy $\eta(t)^2$ of the wave field as a function of the frequency [Battjes, 1992a].

3.4.2 Variance density spectrum

When the process is assumed to be stationary and Gaussian, it can be characterised by a mean value (still water level) and the auto-covariance function. The variance density spectrum is the Fourier transform of the auto-covariance function and describes the contribution of each frequency to the variance of the random variable $\underline{\eta}$.

An example of a variance density spectrum is given in the following figure. As explained in section 3.1, two types of wind waves can be discovered looking at this graph; wind waves with periods ranging up to 5 seconds and swell with periods ranging from 5 seconds.

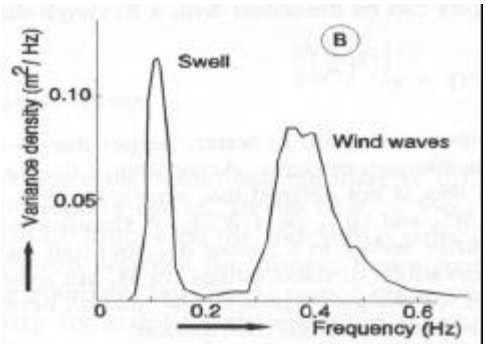

Figure 3-7: Spectrum of a North Sea registration

3.5 Level crossing probability

3.5.1 Maxima of water surface elevation

The distribution of the maximum of η in a certain time is often needed in stead of the distribution of the elevation $p_{\underline{\eta}}(\eta)$. Two sets of maxima can be used:

- All maxima, negative and positive of the still water level, see Figure 3-8a
- Only positive maxima between zero-crossings, see Figure 3-8b

The first set of maxima is demonstrated often for wide spectra. In this case more maxima exist between two upward or downward zero-crossings (see Figure 3-8a). For narrower spectra the number of negative maxima decreases and becomes zero for very narrow spectra.

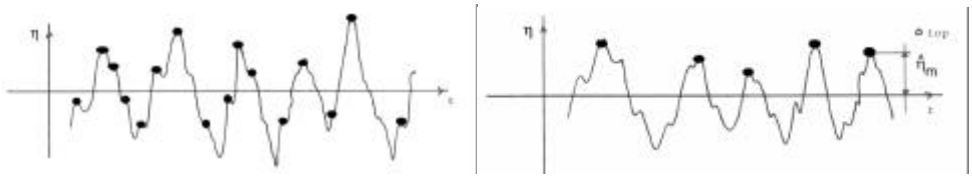

Figure 3-8:a) All maxima (wide spectrum); b) all positive maxima

Considering a narrow spectrum with no positive minima or negative maxima the number of maxima is equal to the number of downward zero-crossings. The method of treating a wide spectrum as a narrow spectrum (only positive maxima) is demonstrated in Figure 3-8b.

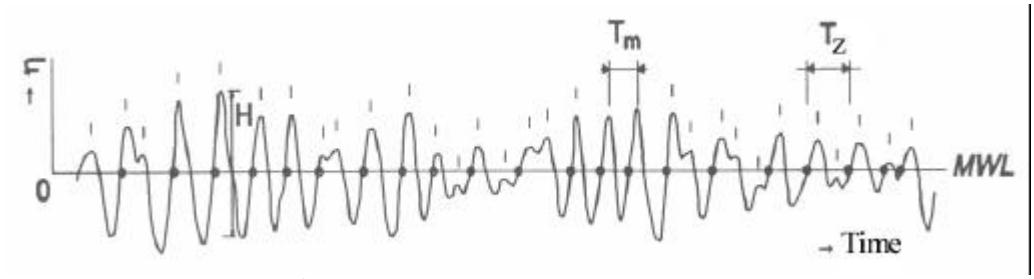

Figure 3-9: Time registration for calculating wave height spectrum

The probability density function and the probability of non-exceedance (cumulative probability function) becomes:

$$f_{\underline{\eta}_m}(\eta) = \frac{\eta}{m_0} e^{-\frac{\eta^2}{2m_0}} \tag{3.8}$$

$$F_{\underline{\eta}_m}(\eta) = 1 - e^{-\frac{\eta^2}{2m_0}} \tag{3.9}$$

These functions are considered to be of the Rayleigh type and are proposed by Longuet-Higgins.

As explained in section 2.2 a wave height is defined as the difference between the maximum and the minimum in between two zero-crossings. In the case of a narrow wave spectrum the wave height is (approximately) twice the maximum elevation. As a result the wave height distribution is also Rayleigh distributed. The expected value of $\underline{H}$ and the root-mean-square value of $\underline{H}$ are defined with

$$\begin{aligned} \mu_H &\equiv E\{\underline{H}\} = \sqrt{2\pi m_0} \cong 2.5\sqrt{m_0} \\ H_{rms} &\equiv 2\sqrt{2}\sqrt{m_0} \end{aligned} \tag{3.10}$$

where

m_0 = zero-moment of wave spectrum

To describe a Rayleigh distribution with one parameter another parameter is used. This parameter denotes the average of the highest $1/3^{th}$ of all wave heights, $H_{1/3}$ or H_s. All the former parameters can be defined using the significant wave height:

$$H_s = 4.004...\sqrt{m_0} = 1.41 H_{rms} = \frac{4}{\sqrt{2\pi}}\mu_H \tag{3.11}$$

3.5.2 Extreme Wave Heights

As explained in chapter 1 probabilistic tools are often used to calculate the frequency of exceedance of a certain wave height ($P_{\underline{H}}$). For structures which are designed to withstand the natural conditions for a certain time, a new wave height probability type is introduced: the extreme wave heights in a certain period ($P_{\underline{Hm}}$).

The probability of non-exceedance of the maximum wave height is defined as

$$P_{\underline{H}_m}(H;N) = P_{\underline{H}}(H)^N \tag{3.12}$$

where N = number of waves = $N = \lambda_0 D = \sqrt{\frac{m_2}{m_0}} D$

D = duration of storm

λ_0 = average frequency of zero-crossings in a stationary Gaussian process

3.5.3 Long term wave height prediction

For the short time scales, Longuet-Higgens (1952) already showed that the Rayleigh distribution (see Table 3-1) is the most appropriate to describe the distribution of the wave heights. Without using a spectral analysis various parameter estimation methods are

available in literature to determine the free parameter of the Rayleigh distribution. [Vrijling et al. 2000].

For predicting wave heights on long time scales the significant wave heights H_s have to be predicted. Numerous authors have intensively investigated wave height distributions on long-term scales. To investigate the probability of failure, extreme value distributions are used to describe the distributions of significant wave heights. The Weibull and Fréchet distributions are often used for the long term wave height distribution.

Long term distribution	
Type II maxima (Fréchet)	$F_{\underline{H}}(H)=\exp(-(H/\beta)^{-\gamma})$
Type III minima (Weibull)	$F_{\underline{H}}(H)=1-\exp(-(H/\beta)\gamma)$
Other distributions	
Type I maxima (Gumbel)[4]	$F_{\underline{H}}(H)=\exp(-e^{-\alpha(H-\beta)})$
Type III maxima	$F_{\underline{H}}(H)=\exp(-(H/\beta)\gamma)$
Type I minima	$F_{\underline{H}}(H)=1-\exp(-e^{+\alpha(H-\beta)})$
Type II minima	$F_{\underline{H}}(H)=1-\exp(-(H/\beta)^{-\gamma})$

Table 3-1: Important distribution types for wave height prediction

[4] For predicting yearly maxima of wave heights, river discharges, water levels etc. the Type I maxima distribution or Gumbel distribution is often used [Vrijling 1996]. However due to the discovery of slowly running stochastic processes (e.g. sea level rise, climate change) the uncertainty in choosing the appropriate distribution type may increase. [Vrijling et al. 2000]

4 HYDRAULIC PRESSURES ON VERTICAL WALLS

4.1 Physical processes

When waves approaching the shoreline hit a vertical wall structure, they are (partially) reflected. When the steepness or heights of the waves in front of the structure are relatively small, the pulsating wave pressures induce a similar response of the structure. In other words, if small sinusoidal standing waves exist in front of a vertical reflective wall, they exert similar pressure fluctuations, which are sinusoidal in time (see Figure 4-1).

When waves translate in shallower water and come near breaking conditions, the shape of the waves and hence in a way the pressure-time history changes and becomes more asymmetric. Deformation due to the breaking process results in a steeper wave front and a more asymmetric pressure time history (see Figure 4-1,a-b). Then the waves start to break (Figure 4-1c). A pressure peak, shaped as a spike, can be seen on top of the quasi-static pressure time history. The duration of the shock pressure is much smaller than that of the quasi-static pressure period (Figure 4-1d).
For broken waves hitting the wall, the double peak of the pressure time history (Figure 4-1e) is still apparent, their magnitude and duration depending on the distance between the breaking point and the upright section.

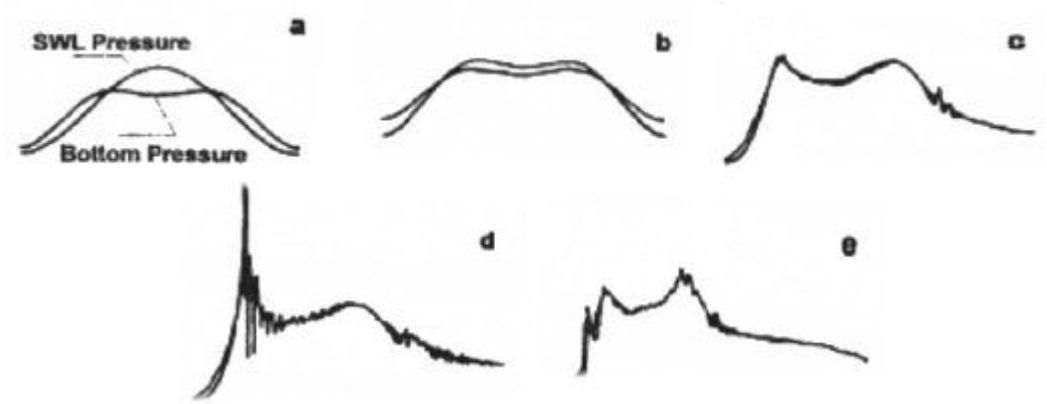

Figure 4-1: Pressure patterns due to different wave types

4.2 Pressures due to Non-Breaking Waves

4.2.1 Linear Wave Theory

The prediction of periodic progressive (regular) wave loads is used traditionally to design a structure, which endures pressure from waves. With relatively simple design methods, the quasi-static response can be calculated, neglecting the response caused by sudden shocks induced by waves breaking directly at the structure. In case of small amplitudes and large wave periods the period of the pressure increase and decrease is much larger than the eigenperiod of the structure. In that case the response of the structure is quasi-static. Pressure distributions due to non-breaking waves are shown in Figure 4-2.

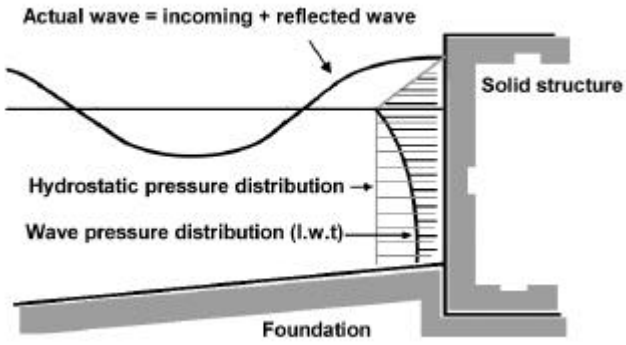

Figure 4-2: Presentation of wave pressures

The magnitude of the pressures when the response of the structure is quasi-static, is substantially smaller than the impact wave pressures associated with breaking waves, as explained in the next chapter. If a wave is stopped by a wall a part is reflected. The result is a superposition of the incoming and reflected waves. The resulting wave height is approximately twice the incoming wave, if the incoming wave is fully reflected.

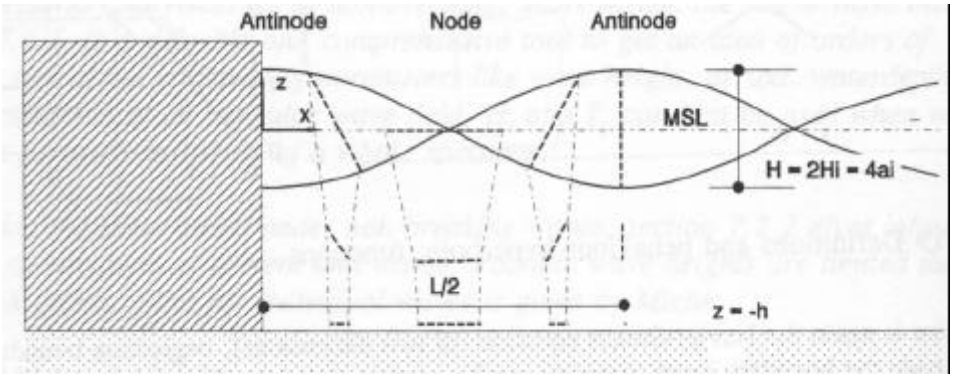

Figure 4-3: Standing wave [Battjes, 1998]

When a monochromatic wave field is present with incoming wave height H_i and length L, a standing wave occurs with nodes and antinodes. This phenomenon is also called "Clapotis" and the circular orbits of the particle movements have degenerated into straight lines. This results in only vertical velocities at the antinodes and horizontal velocities at the nodes. The equation for the surface elevation according to the linear wave theory is given by the following equation as a function of the incoming non-reflected wave H_i:

$$\eta(x,t) = H_i \cos(kx)\sin(\omega t) \tag{4.1}$$

A few categories can be distinguished when the integrated pressure on a vertical wall structure is looked upon: pulsating wave loads and dynamic impact waves loads. Within the linear wave theory the pressure distribution along the vertical is described with the following equation:

$$p(z) = \rho g \eta(0,t) \frac{\cosh(k(h+z))}{\cosh(kh)} - \rho g z \qquad \text{for } -h < z < 0 \qquad (4.2)$$

$$p(z) = (1 - \frac{2z}{H_i}) \rho g H_i \qquad \text{for } 0 < z < H_i/2 \qquad (4.3)$$

where

z = elevation above water level

Assuming a hydrostatic pressure distribution above still water level, the resulting wave forces acting on the caisson can be calculated. Integration of the pressure distribution over the water depth results in the formulae for the wave forces. Also, with these formulae, the lever arms with respect to the centre of the base plate and the tilting moment due to the horizontal (and vertical) forces can be calculated.

4.2.2 Design Formulae for non-breaking pressure distributions

4.2.2.1 Hiroi

Hiroi's formula gives the following pressure equation as a function of the incoming non-reflected wave height H_i:

$$p_{max} = 1.5 \rho g H_i \qquad (4.4)$$

where the pressure distribution is constant along the vertical wall, hence $p(z)=p_{max}$, from a depth less than twice the wave height to a height of 1.25 times that wave height (see Figure 4-4).

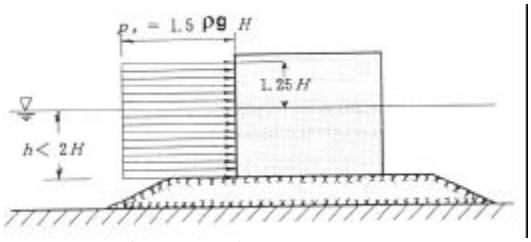

Figure 4-4: Wave pressure distribution of the Hiroi formula

4.2.2.2 Sainflou

Sainflou published a theory of trochoidal waves in front of a vertical wall in 1928 and presented a simplified formula for pressure estimation. Sainflou uses a second order Stokes theory and full reflection ($H_r=H_i$) and expresses the pressure as a function of the incoming non-reflected wave H_i. The pressure distribution is sketched as in Figure 4-5 and the pressure intensities and the quantity of water level rise $ä_0$ are given as

$$p_{max} = p_1 = \rho g H_i \qquad (4.5)$$

with

$$p_2 = \rho g \frac{H_i}{\cosh kh} \qquad (4.6)$$

$$\delta_0 = \frac{1}{2} k H_i^2 \coth kh \qquad (4.7)$$

where

L = wave length

k = wave number = 2ð/L

δ_0 = difference between mean water level and still water level

This maximum pressure is exerted at the mean water level.

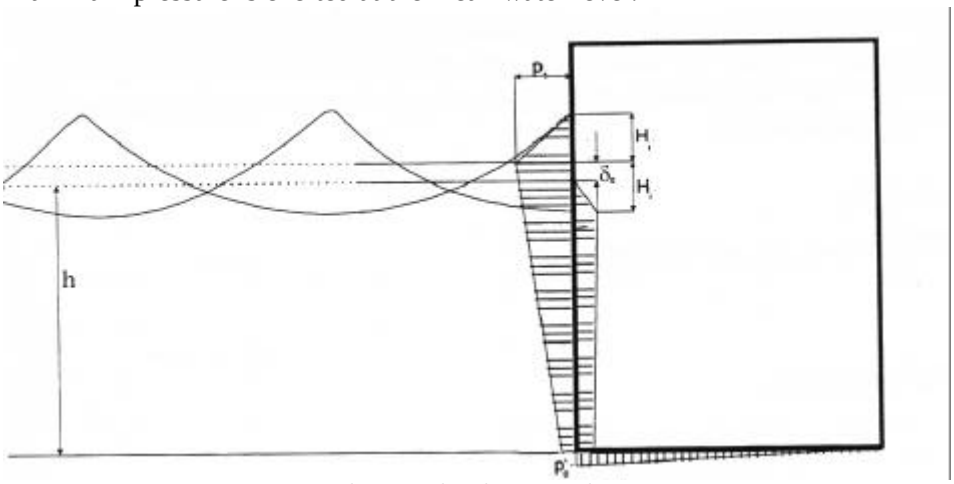

Figure 4-5: Wave pressure distribution of the Sainflou formula [after Kuijper, 1999]

The pressure is linear between surface elevation and bottom level. The average of calculated pressures is approximately (0.8-1.0)ñgH_i in ordinary design conditions with Sainflou's formula. It was customarily in Japan to use $H_{1/3}$ with Sainflou's formula but in a modified form. This leads to design forces much smaller than resulting from Hiroi's formula. Reduction of pressure due to overtopping and oblique wave direction is not included in the Sainflou formula. Experiments by many researchers, particularly by Nagai, proved that Sainflou's method was an oversimplification. Research done by Rundgren showed an exaggeration of pressure loads for steep waves. The adjusted formula resulted in the CERC formula (4.22)

By examining several minor damages of breakwaters, it has been revealed that a simple application of Sainflou's formula had yielded underestimation of wave pressure under storm conditions. For the zone extending +/- $H_i/2$ around the design water level, the wave pressure by Sainflou was replaced with that by Hiroi's formula. This partial breaking wave pressure formula has been the recommended engineering practice of breakwater design in Japan for the period from around 1940 to the early 1980's (Goda, 1984).

4.2.2.3 Goda

The wave pressure formula proposed by Goda [1984] for the design of vertical breakwaters assumes the existence of a trapezoidal pressure distribution along a vertical wall, regardless whether the waves are breaking or non-breaking waves. Goda takes H_{max} as the highest wave out of 250 waves. This has a probability of exceedance of 0.4%. Furthermore, the wave height is taken seaward of the surf zone. Within the surf zone the height is taken as the highest of the random breaking waves H_{max} at a distance of 5 $H_{1/3}$ seaward of the breakwater. The assumption of a trapezoidal pressure distribution results from measurements in which he found the distribution shown in Figure 4-6.

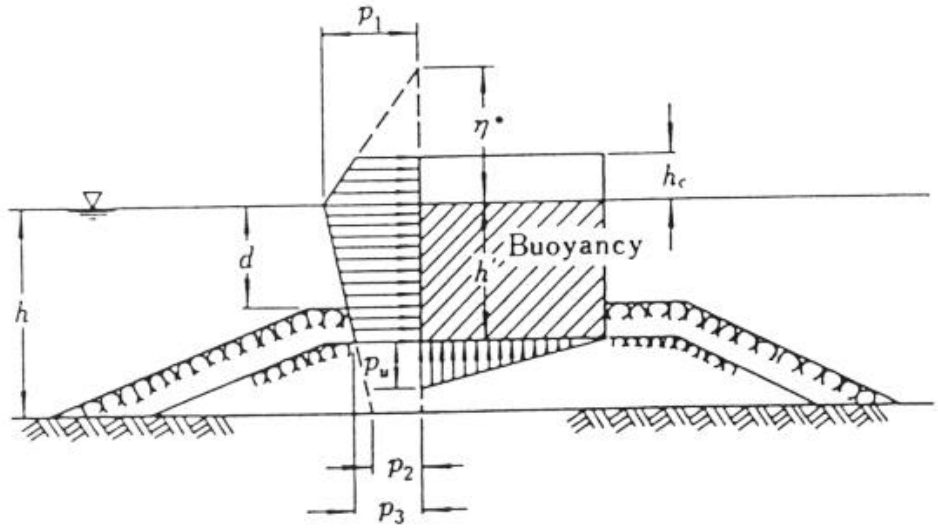

Figure 4-6: Wave distribution according to the Goda formula

In the experiments done by Goda [1984] regular waves were used. The maximum pressure at the still water level is defined by:

$$p_{max} = \frac{1}{2}(1+\cos ß)(a_1 + a_2 \cos^2 ß)\rho g H_{max} \qquad (4.8)$$

where

β = angle of wave direction

Other parameters included in the Goda formulae are:

Param.	Formula	Description
p_1	p_{max}	pressure at still water level
p_2	$p_1 / \cosh(2\pi h/L)$	pressure at bottom of super structure
p_3	$\alpha_3 p_1$	pressure at toe depth
p_u	$½(1+\cos\beta)\,\alpha_1\alpha_3\rho g H_{max}$	pressure under structure at wave side
β^*	$0.75(1+\cos\beta)H_{max}$	

Table 4-1: Pressures in Goda model

Influence factors are given as:

Influence factor	Formula	Description
α_1	$0.6+½[\,(4\pi hs/L) / (\sinh(4\pi h/L)\,]^2$	wave period influence
α_2	$\min\left(\frac{(1-d/h_b)(H_{max}/d)^2}{3}, \frac{2d}{H_{max}}\right)$	foundation height influence
α_3	$1-(h'/h)\left(1-\frac{1}{\cosh(kh)}\right)$	interpolation between α_1 and α_2

where

h_b = water depth at $5H_{1/3}$ seaward of the breakwater
d = depth in front of the breakwater

Table 4-2: Influence factors for Goda formula

The amount of wave overtopping due to a low crest height of the breakwater is assumed to exercise no effect on the distribution and magnitude of the wave pressures for the sake of simplicity.

The presence of a rubble mound foundation is a crucial point in the formula of Goda. If no rubble mound is present, the coefficient á$_2$ is almost zero. If a horizontal foreshore is present this means that h_b=d and that á$_2$ can be neglected and only á$_1$ remain.
Van der Meer et al. (1993) have investigated the horizontal force, F_h, on vertical breakwaters. The horizontal force was compared with the formula of Goda (1985). For all forces, moments and arms the following conclusions have been drawn:
Goda overestimates the total uplift force by 40%. Goda assumes that the superstructure has no influence on the total uplift force, while the experiments show otherwise. Goda also does not take into account the consequences of an inclined superstructure.
Probability calculations show that the scatter around the Goda formula has the largest influence of all parameters on the probability of failure [van der Meer et al., 1993].

4.3 Pressures due to Breaking Waves

4.3.1 Wave Impact Pressure models

In the following sections models are described which are often used to calculate the maximum pressure and the pressure distribution. In case of no air pocket entrapment, the impact pressure is described with the hammer shock model. In case of air pocket entrapment, three models have been developed. First the ventilated shock model (flow models) when the air hardly can escape the onrushing wave mass. Second, a transition model developed by Takahashi using the Wagner type pressure model. And third and an air compression model using the formula of the Bagnold model.

4.3.1.1 Hammer shock pressures (no air entrapment)

One of the first impact wave pressure models is the hammer shock pressure model. This model describes the perpendicular approaching water mass hitting a vertical rigid wall. At the moment of the water impact, the water cannot escape, the water is compressed and a shock wave, which moves away from the wall is created. The velocity of sound in water is equal to the velocity of the shock wave. The added water pressure above the atmospheric pressure, as a result of such a hammer shock is defined as

$$p_{max} = \rho c_w u_0 = p_0 + u_0 \sqrt{K_w \rho} \tag{4.9}$$

where

c_w = velocity of sound in pure water (≈ 1480 m/s)
K_w = compressibility modulus
ρ = mass density of fresh water (assumed to be constant in this model)
u_0 = wave front velocity

Because of the assumptions underlying the model, this model gives an upper limit for the impact wave pressure.

When the water is mixed with air, the compressibility modulus changes and the maximum wave impact pressure can be defined by

$$p_{max} = u_0 \sqrt{\frac{\gamma p_0 (1-\alpha)\rho}{\alpha}} \tag{4.10}$$

where

γ = Poisson constant (factor between isothermal and adiabatic compression)
α = Air content

When the wall is not rigid but flexible in some way, and can be considered compressible, a shock wave will be created both in the wall and in the water. If ε is considered to be the ratio between the shock wave velocity in the wall c_c and that of the approaching wave front, v, and the decline of the pressure over the compression waves is equal to

$$p_{max} = \rho c_w u_0 (1-\varepsilon) = \rho_c c_c u_0 \varepsilon \qquad (4.11)$$

where

ρ_c = mass density of the structure

$c_c = \sqrt{\frac{E_c}{\rho_c}}$ (Dieterman et al, 1993)

This equation can also be written with the densities and sound velocities of both water ($\tilde{n}_w$, c_w) and structure ($\tilde{n}_c$, c_c) (Kamel, 1970):

$$p_{max} = \rho_c c_c \frac{\rho_w c_w u_0}{\rho_w c_w + \rho_c c_c} \qquad (4.12)$$

The reduction due to the compressibility of the water can normally be neglected, compared with the reduction as a result of air content. Flowing aside of water, which impinges upon a vertical wall, has a greater influence on the reduction of wave impact pressures than the compressibility of the wall of the structure. (Delft Hydraulics, 1994)

4.3.1.2 Air layer models

When waves hitting a vertical wall are considered, the shape of the breaking waves indicates the wave impact type. When a wave is not breaking, the wave is not so impulsive. When the wave hits just before it breaks, the wave front hits the wall severely without entrapping an air layer, causing the wave pressure to significantly increase (about 10ρgH). When a wave starts breaking, a small air layer is entrapped and compressed, with this compression generating the impulsive pressure (about 10ρgH). As the breaking progresses, the size of the air layer increases and the pressure intensity decrease. In fact, for waves hitting a vertical wall after breaking, the impulsive pressure intensity is significantly reduced [Takahashi, 1996].

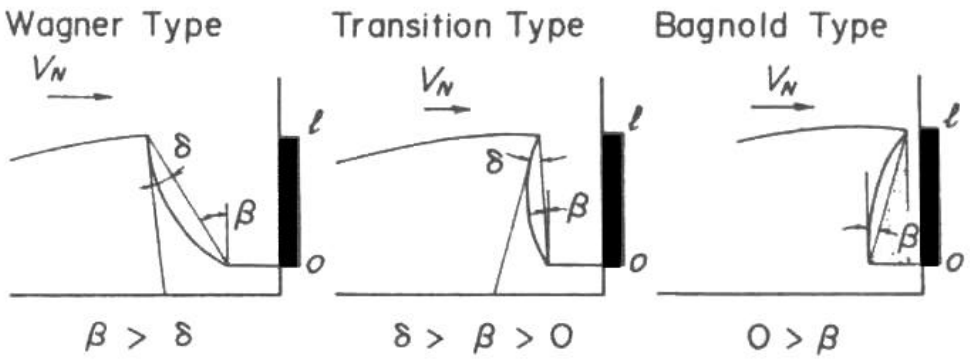

Figure 4-7: Three types of impulsive pressures [Takahashi, 1996]

Ventilated shocks

In this model, the compression of the water can be neglected because it is assumed that the water can escape fast enough to the sides. Wagner type pressure was recently termed as "flip through" due to the occurrence of a pile-up effect of water at the intersection

point [Cooker and Peregrine, 1990]. [Goda 1967] called this type of pressure "single peak pressure" and Lundgren (1969) and Horikawa and Horikawa and Noguchi (1970) called it a "ventilated shock" which from now on will be the term used to refer to this type of impact wave explained in this section. Impact processes due to the “flip-through” action [Cooker and Peregrine, 1991] is observed when incident waves break as an upward deflected breaker at the wall [Oumeraci et al 1993].
A flow pressure model can describe the wave impact pressure of the ventilated shock

$$p_{max} = k\left(\frac{1}{2}\rho u_0^2\right) \tag{4.13}$$

where

k = coefficient which determines the impact pressure

In maritime engineering the slamming-coefficient c_s is used instead of k. Also Chuang (1967) investigated the expression of a shock (slamming) pressure in case the water can escape sideways. His type of wave impact can therefore also be considered as a ventilated shock.

Takahashi et al. [1993] have developed a theoretical model to describe the generation of impact pressures. The type of impact pressure changes with the amount of trapped air. Using the Wagner theory [Takahashi et al, 1983], the maximum wave impact pressure is:

$$p_{max} = \frac{1}{2}\rho u_0^2\left(\frac{\pi^2}{4}\cot^2\beta + 1\right) \tag{4.14}$$

[Takahashi et al. 1993] found that at $\beta \approx 20^o$ the transition is between the Wagner type pressure and the transition type pressure. When $\beta \approx 20^o$ the maximum pressure of the Wagner type occurs.

Transition type pressure models (Takahashi model)
When the angle β of the wave front is smaller than the curvature angle δ (see Figure 4-7) of the wave front but β has not become negative, transition type pressures arise. (Takahasi et al. 1983, 1992). Breaking of waves with the almost vertical or very slightly curled wave front exerts an impulsive pressure on the wall with very high magnitude and short duration.

$$p_{max} = \rho g H\left(0.4\pi\kappa_m^2\kappa_i/\kappa_a\right)\left(\frac{h + 0.75H}{h' + h_c}\right) \tag{4.15}$$

where

κ_a = air thickness coefficient (related to β and δ, minimum ix approx. 0.4 to 0.9)
κ_i = impulsive height coefficient (ratio between wave front height and H)
κ_m = added mass correction factor (assumed to be 0.83)
h' = water depth at the bottom of the wall
h_c = crest elevation of wall

Another model by Takahashi et al uses the Wagner type pressure model. When $0 < \beta < \delta$, it is assumed that the impact can be modelled with the Wagner type pressure model. The effect of the pressure reduction due to air entrapment is expressed by the equivalent angle β^* which is used in this region instead of β:

$$\beta^* = \beta_0 + \frac{\delta - \beta_0}{\delta}\beta \tag{4.16}$$

where

$$\beta_0 = \tan\left\{\frac{2}{\pi\kappa_m^2}\left[\frac{p_{max}}{\frac{1}{2}\rho u_0^2}\right]_{\beta=0}\right\} \tag{4.17}$$

Within this type of impact pressures little oscillations occur at the still water level due to the entrapped air bubbles, which are caused by the irregularity in the vertical wave front. Kirköz (1982) states that the severest shock pressure occurs when a breaking wave, having a vertical front face ($\beta \approx 0$ and $\delta \approx 0$) strikes the plane wall without trapping any air pockets between the wave front and the wall. Whereas Wallis (1969) states that a great reduction of the peak pressure maxima is caused by the acoustic radiation as well as the energy dissipation in bubbly water.

Air compression model

The first model that formulates the compression of air behind a water mass is the piston model of Bagnold (1939). The air in this model, also called the Bagnold type pressure model, acts like a spring element where the water is the piston.

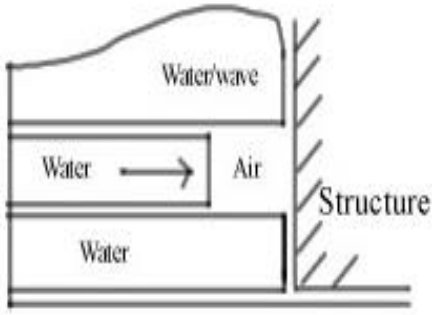

Figure 4-8: Air compression model

The solution of differential equations results in an oscillation that is not damped. The equation, which defines the maximum wave impact pressure, is:

$$p_{max} = u_0\sqrt{\frac{\gamma p_0 \rho L}{D}} \tag{4.18}$$

Takahashi et al. (1993) developed an air compression model that includes bagnold type pressure, but the air layer is defined by the curvature of the wave front (see Figure 4-7). The air compression can be approximated by a damping oscillation (see with p_{max} being:

$$p_{max} = 1.6\left(\frac{\rho L u_0^2}{D p_0}\right)p_0 \tag{4.19}$$

where p_0 = atmospheric pressure

The impact pressure is assumed to act simultaneously only within $z=0$ and $z=\lambda$ with the same intensity, even though the air compression pressure propagates through the water. Although an approximated solution is obtained which does not include air leakage during air compression this model provides a good approximation of the exact solution.
A rapid pressure decrease is caused by expansion of the compressed air pocket. The occurrence of the negative pressure seems to be one of the special characters of the

impact pressure accompanied by damped pressure oscillations. The minimum dimensionless pressure, recorded and scaled during experiments performed by Hattori et al (1990) and experiments performed by Witte (1988), amounts to $p_{min}/\rho gH$= -28 to -34.

4.3.2 Schematisations of Wave Impact Loads

In a preparatory phase of a design process waves can be classified as standing wave, slightly breaking wave, plunging breaker and fully broken waves (see Figure 4-9). The pressure and forces of the first type can easily be calculated using the linear wave theory for standing waves or the more complex Goda formula for slightly breaking waves. To model the pressures and loads on the structure in case of a plunging breaker, a method is needed to transform the pressures into a pressure peak and impulse pressure duration.

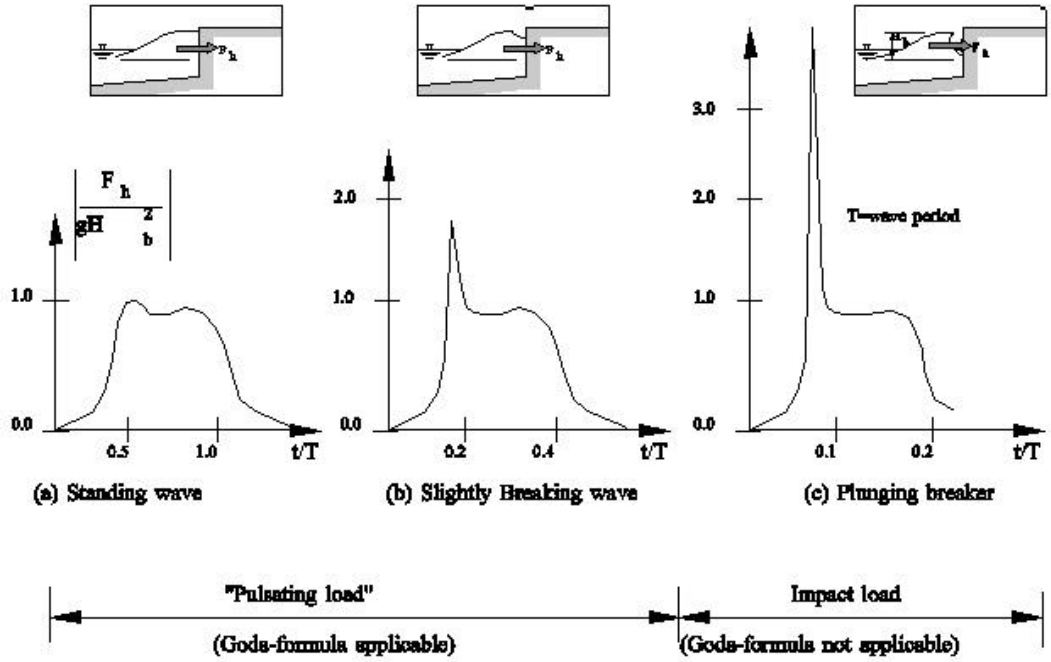

Figure 4-9: Pulsating and impact load - problem definition (Kortenhaus et al 1997)

The typical time history of a wave impact is shown in Figure 4-10. This is an example of a (non-scaled to prototype) wave impact against the upper girder of the Storm Surge Barrier Oosterschelde at mean water level, during scale model experiments. Two parts can be distinguished: a non-oscillating part with an impact time of 30-70 ms and an oscillating part with an oscillating frequency of 200-500 Hz. The non-oscillating part has been schematised in two triangles as can be seen in the right example in Figure 4-10. The smaller triangle will partly consist of the oscillation but a further subdivision is rarely made.

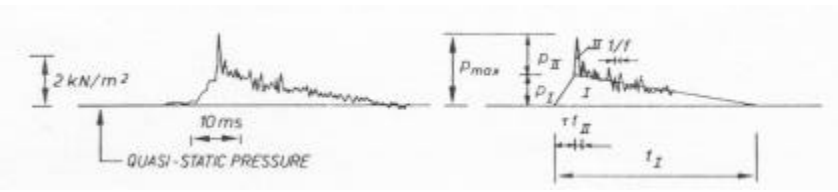

Figure 4-10: Typical time history of wave impact type and schematisation (model scale)

The water mass following the wave front will exert pressures during a certain period referred as t_t. This impulse ($I_{hd}=½F_{h,max}t_t$) exerted on the wall caused by a breaking wave gives pressures which are small compared to the possible impact pressures at impact time.

These pressures are mostly calculated using the formula of Goda considering the response of the structure to be quasi-static.

The combination of these two pressure-time functions is often schematised as a church-roof (see Figure 4-11), where the peak of the church is the important large impact pressure of the pressure time history. It is suggested to substitute the load history by a single peak load with a triangular shape. Also the effect of the quasi-static component in the church-roof shaped load (the church-ship shaped load) was found to have no significant effect on the oscillatory motions and the permanent displacement of the structure [Oumeraci, 1997]. The quasi-static component is often neglected in impact calculations and only the maximum impact pressure is used. This church-roof peak, from now on referred to simply as the church-roof, transfers a total impulse equal to $I_{hd}=½F_{h,max}t_d$.

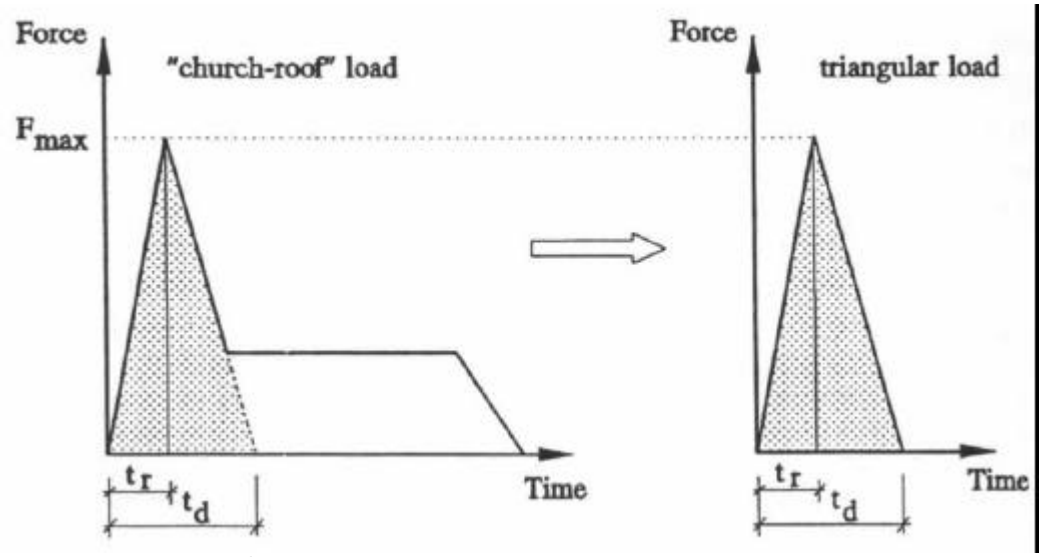

Figure 4-11: Church-roof impact load exerted on a vertical breakwater

A wave with an overhanging wave front can entrap air that will be compressed and expand afterwards creating a large pressure decrease. This mechanism results in a pressure oscillation. In Figure 4-10 and in Figure 4-12, the time history of a model respectively a schematisation can be seen demonstrating a peak pressure followed by a pressure oscillation.

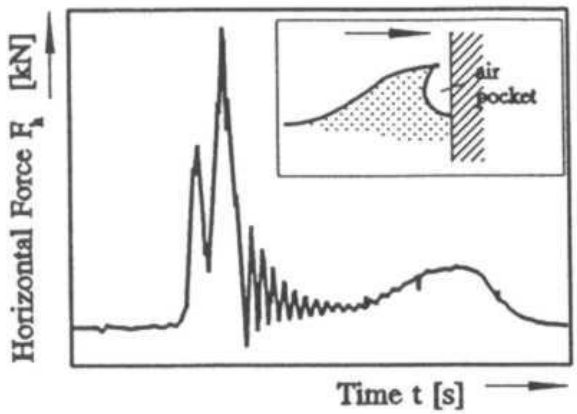

Figure 4-12: Curved overhanging wave front with oscillating pressure history

Experimental research emphasises that with increasing maximum impact pressure the duration of the peak pressure will decrease. Much research is done finding a formula for the impact pressure impulse.

4.3.3 Design Formulae

4.3.3.1 Minikin Design formula

Minikin (1950) proposed a breaking wave pressure formula that includes impulsive pressures. The Minikin model is based on model experiments and on prototype measurements. The model consists of a maximum dynamic pressure at still water elevation and a parabolic pressure decrease, which becomes zero at distance H/2 above and beneath the still water level plus a hydrostatic pressure increase due to the wave elevation above the still water level. The Shore Protection manual (1984) recommends this model. The dynamic pressure becomes:

$$p_{dynamic}(z) = p_{max;dynamic}\left(1-\frac{2|z|}{H}\right)^2, \text{ for } |z| \quad H/2 \tag{4.20}$$

where

z = elevation above still water level

The maximum wave pressure becomes:

$$p_{max;dynamic} = \frac{1}{2}C_{mk}\rho g H\frac{\pi d_s}{L_D D}(h_L + d) \quad (= p_m \text{ in Figure 4-13}) \tag{4.21}$$

where

C_{mk} = impact coefficient, $C_{mk} = 2$
d = water depth at vertical wall
h_L = water depth at wave length distance
L_D = wave length

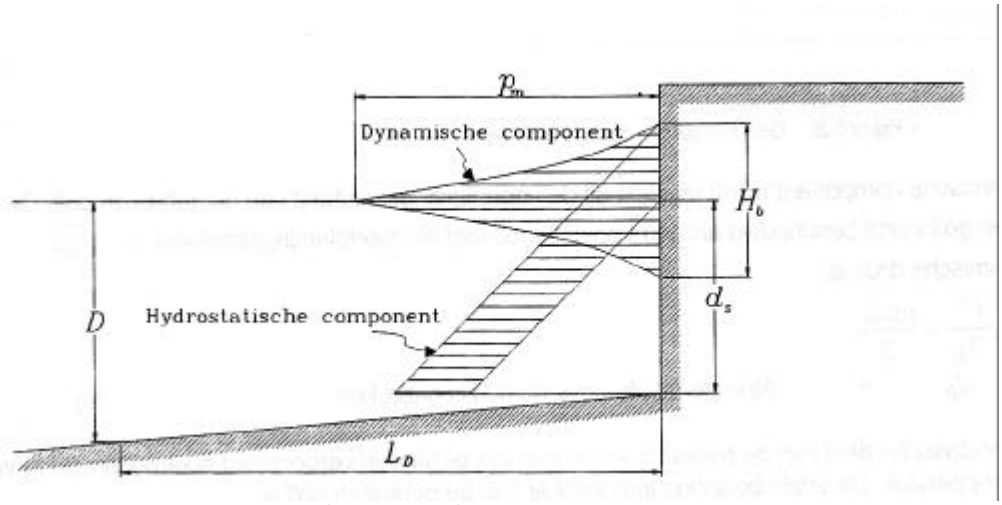

Figure 4-13: Pressure distribution of the Minikin formula

If the wall slopes at an angle α to the vertical, then the dynamic pressure $p_{max;dynamic}$ must be multiplied by $\cos^2\alpha$.
It should be mentioned here that the Minikin formula for breaking wave pressure was never used in breakwater design in Japan, though the information of that formula was well shared among Japanese engineers soon after its publication in 1950. The main reason

for its unpopularity was its prediction of excessively high value of wave pressure, which would necessitate a very broad upright section say two to three times the section designed by the Hiroi formula. Japanese engineers could not find any good reason to build such an excessively large breakwater in the place where a conventionally designed breakwater would serve satisfactorily [Kobayashi, 1995].
The formulae does not properly describe changes in the impulsive pressures due to the shape of the rubble foundation.

4.3.3.2 CERC Design formula

The Coastal Engineering Research Centre (CERC) uses a model that gives an indication of the wave pressures. It also handles a hydrostatic and dynamic component, similar to the Minikin model. The celerity of the broken wave leads to the dynamic component, with $C=\sqrt{gh_{br}}$. The dynamic pressure becomes

$$p_{max;dynamic} = \frac{1}{2}\rho C^2 = \frac{1}{2}\rho g h_{br} \tag{4.22}$$

where

h_{br} = water depth at breaking point at distance L_D (design wave length)

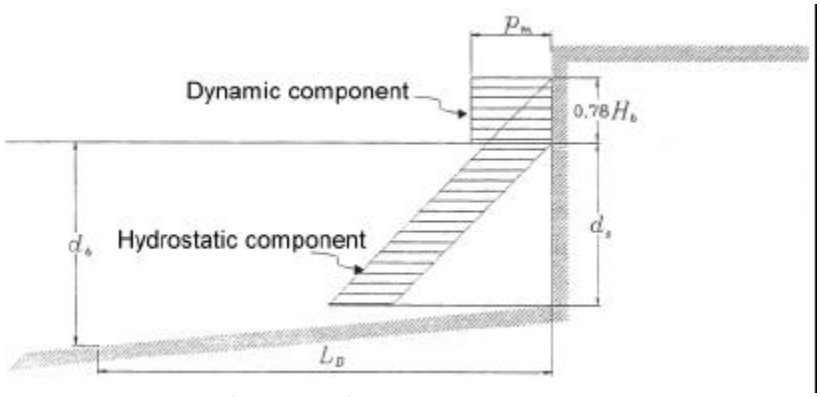

Figure 4-14: Pressure distribution of the CERC formula

4.3.3.3 Nagai

Nagai (1969) divided the conditions where breaking wave impact pressures occur into two formula types: high and low rubble-mound wave pressure formulas. The characteristics of the incoming wave, the depths of water and the shape of the breakwater are schematised in Figure 4-15.

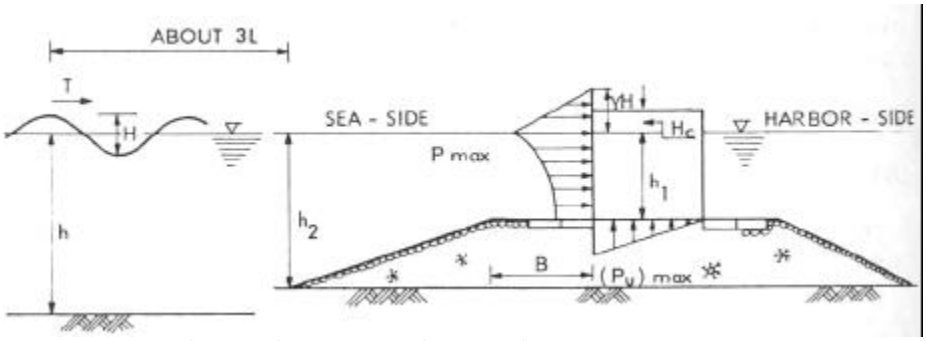

Figure 4-15: Schematic definition of symbols used for Nagai formula

The high rubble mound breakwater approach is used for a relative small depth in front of a vertical breakwater (h1/h2 < 0.40 to 0.50) and the H1/10 and the T1/10 are used for maximum wave characteristics.

The low rubble mound breakwater approach is used when 0.40 to 0.50 < h1/h2 < 0.75. Waves, occurring in front of the vertical walls of composite-type breakwaters with low rubble-mounds as defined above, vary over a wide range from perfect breaking wave to standing waves depending upon the ratios of h_1/h_2, B/h_2, h/L and h_2/H [Nagai et al, 1974].

4.3.3.4 Extended Goda formula by Takahashi

The original Goda formula has many advantages like the ability to be employed both for standing and slightly breaking waves and the clarification of uplift pressures. To use this formula for impact waves, it was subsequently extended with the incident wave direction (Tanimoto et al., 1976), modification factors applicable to other types of vertical walls and the impulsive pressure coefficient (Takahashi et al., 1994).

$$p_{max} = \frac{1}{2}(1+\cos ß)(\lambda_1 a_1 + \lambda_2 a^* \cos^2 ß)\rho g H_{max} \qquad (4.23)$$

where

β = angle of wave direction

For unchanged Goda formula parameters, see section 4.2.2.3. Changed pressures and Influence factors are defined as:

parameter	**Formula**	**Description**
p_u	½(1+cosâ)λ_3 $\alpha_1\alpha_3$ñgH_{max}	pressure under structure at wave side
ç*	0.75(1+cosâ)$\lambda_1 H_{max}$	virtual crest height (p(η*) = 0)
α*	max{α_2,α_I}	(α_I = impulse. press. coefficient)
λ1		slow varying pressure component
λ2		dynamic pressure component
λ3		changes in uplift pressure

Table 4-3: Parameters for extended Goda formula (Takahashi 1994)

parameters α_I	**Formula**	**Condition**
α_I	$\alpha_{I0}+\alpha_{I1}$	
α_{I0}	H/d	H 2d
	2	H > 2d
α_{I1}	cos δ_2/cosh δ_1	δ_2 0
	1/(cosh δ_1 (cosh δ_2)0.5)	δ_2 > 0
δ_1	20 δ_{11}	δ_{11} 0
	15 δ_{11}	δ_{11} > 0
δ_2	4.9 δ_{22}	δ_{22} 0
	3 δ_{22}	δ_{22} >0
δ_{11}	0.93 (B_M/L - 0.12) + 0.36 {(h-d) /h -0.6}	
δ_{22}	-0.36(B_M/L - 0.12) + 0.93 {(h-d) /h -0.6}	

Table 4-4: Additional parameters for extended Goda formula (Takahashi 1994)

5 PROTOTYPE MEASUREMENTS ON COASTAL STRUCTURES

5.1 Introduction

This chapter shows three examples of prototype measurements done on coastal structures. The first coastal structure is the storm-surge barrier Oosterschelde, built in the ninety's to serve as a partial closure dam. Also the Dieppe breakwater is demonstrated. The third example is prototype measurements carried out on Japanese ships.

5.2 Storm-surge Barrier Oosterschelde

5.2.1 Design

The Oosterschelde Barrier is located in the Southwest part of the Netherlands. The barrier has been built across three main channels of the mouth of the Oosterschelde, respectively one kilometre, one kilometre and two kilometres wide. The actual barrier consists of 62 basic sections that are 45 meters wide. Figure 5-1 shows the sand bed covered by a filtermat. On this mat concrete piers are placed. The flow opening is between two concrete beams. A steel gate, driven by hydraulic cylinders can close the opening. On top of the piers a motorway bridge is located. The piers and sill beam are packed in by a rubble sill structure. The barrier has been completed in 1986. Until 1994 11 storm closures have been performed.

Under storm conditions the barrier is subject to wave attack from the North Sea. During the more severe storm surges the gates of the barrier will be closed. These gates are subject to wave impact during the closure operation of the barrier, when the girders of the gates, which are located at the North Sea side of the barrier, cross the water level. Wave impacts were measured during three different scale models measurements campaigns:

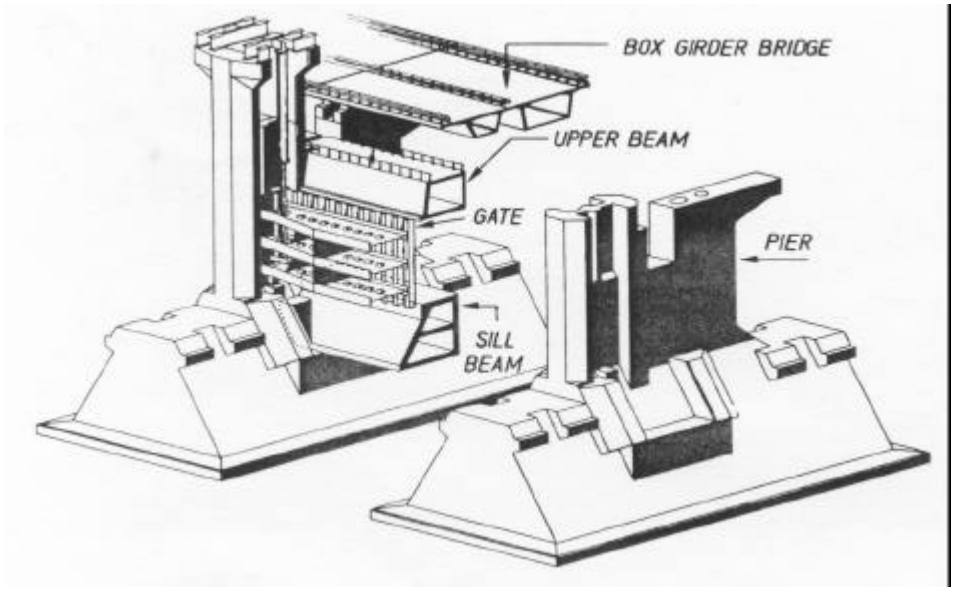

Figure 5-1: SVKO elements

Box girder design
One of the designs included two gates, which were similar to two grills translating parallel to each other resulting in an open barrier when the girders are positioned behind each other and (partly) closed when positioned otherwise.
Most frequent wave impacts on girders were experienced when the mean water level was just below one of the girders. Air entrapment occurred frequently during these impacts on the girders and as a result pressure oscillations due to the entrapment of air pockets were observed.

Caisson-type barrier
An alternative barrier design was the caisson-type barrier. In these caissons two steel plate gates were placed behind each other. Most impact occurred when the mean water level was located just beneath the upper girder, similar to the Box girder design.

Design with Piers and gates
The final design of the storm-surge barrier evolved to a concept of sunken piers founded on seabed reinforcements. Wave impacts on the girders of the gates generated such large impact pressures that the design of the gate had to be adapted several times to reduce these pressures. In the model maximum pressures were measured of approximately 100 kN/m2 (design values) but local pressure maxima exceeded this (pressures of 250 kN/m2 were measured and scaled using ventilated shock scale laws). The final gate/girder design included round girders forming the rigid structure fixing the gate. Wave impacts in the model using the altered design showed peak pressures of 150 kN/m2 under extreme conditions.
The measurements gave insight in impact phenomena and conditions inducing wave impacts. Frequency of occurrence of wave impacts was high during the closure operation of the barrier, when the girders of the gates, which are located at the North Sea side of the barrier, crossed the water level. Air entrapment occurred frequently during these impacts on the girders.

5.2.2 Monitoring program

To evaluate the hydraulic aspects of the barrier a monitoring program has been set up. This program consisted of field measurements of hydraulic loads on the barrier and the response of the structure (Klatter 1990). In this program wave impacts were included. For the upper beam wave impacts against the bottom of the beam were regarded to be critical, because the relatively light weight prestressed concrete beam could be lifted from its supports. For the monitoring of the wave impacts, one gate and one upper beam were instrumented with accelerometers, pressures gauges, a water level gauge and force gauges.

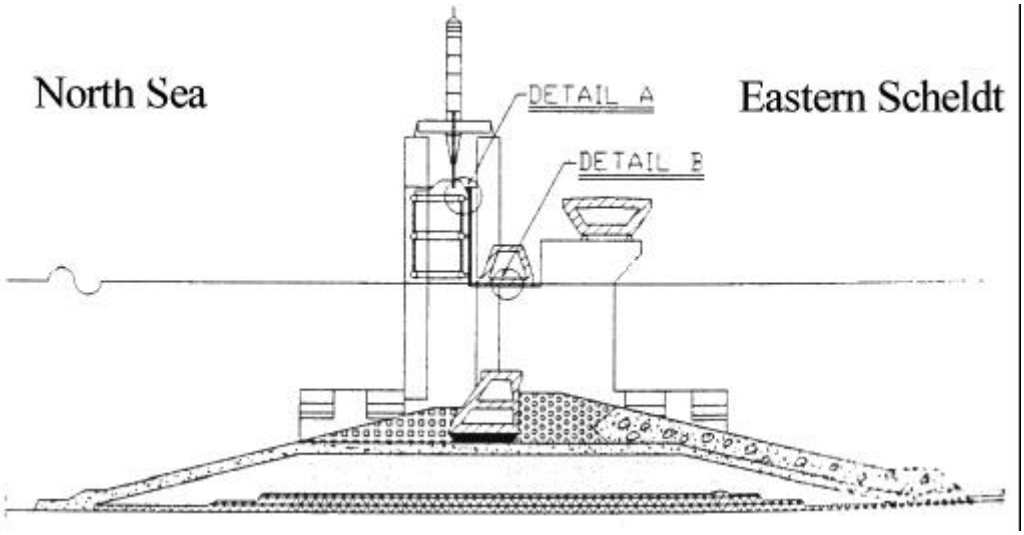

Figure 5-2: Details upper beam and upper gate girder

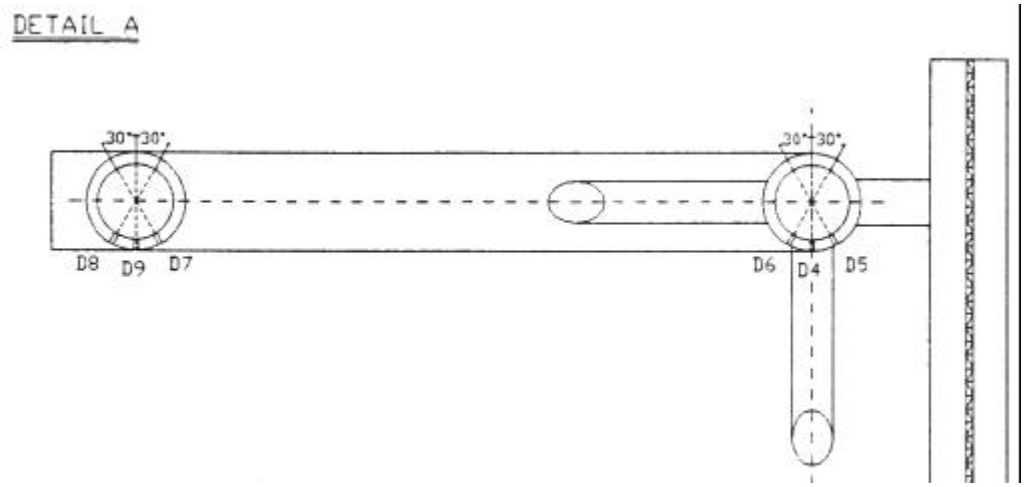

Figure 5-3: Detail A: Upper gate girder [Klatter et al, 1994]

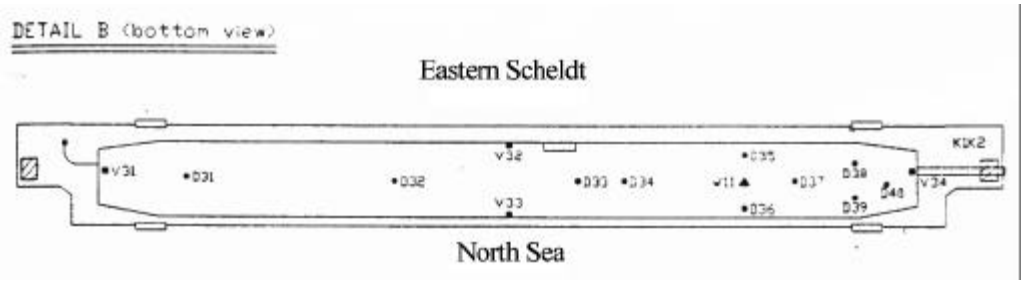

Figure 5-4: Detail B: Bottom view of upper beam

5.2.3 Upper gate girder

The most severe wave impacts occurred when the upper girder was positioned just above the mean water level.

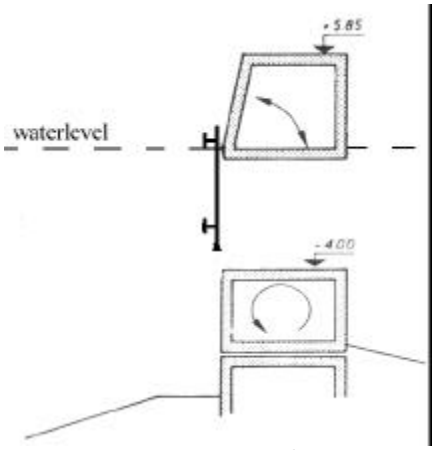

Figure 5-5: Schematisation of SVKO model and water level

Wave impacts occurred not simultaneously but with a certain phase shift. This phenomenon was considered a ventilated shock, even for parallel wave crests when the phase shift was very small. The gates designed with round girders instead of plate girders showed no air entrapment, either when the girder was above the water level or submerged.
Extreme conditions showed maximum local peak pressures up to 230 kN/m^2 on the main girders. Against the bottom of the upper girder maximum impact pressures were measured up to 60 kN/m2 showing a wide spatial variation. Also the measured impacts on prototype scale showed no air entrapment and hence pressure oscillations and the impacts were considered similar to the ventilated shock model.
The measurements of wave impacts on the top girders of the gate were performed during the closure operations of the gates, when the girders cross the water level. The most severe impacts were selected out of 10 successful measurement series. These measured maximum pressures over 50 kN/m^2 on one of the sensors are shown in the next table.

Date	**Time**	**Hs [m]**	**Maximum impact pressures [kN/m^2]**					
			D4	**D5**	**D6**	**D7**	**D8**	**D9**
27-feb-90	14:33:59.5	2.15	72	38	39	-	21	21
27-feb-90	14:35:47	2.15	24	5	43	16	5	117
27-feb-90	14:36:25	2.20	81	66	46	11	19	1
27-feb-90	14:36:29.5	2.20	227	14	44	10	-	-
27-feb-90	14:36:43.5	2.20	110	18	53	58	1	8
27-feb-90	14:43:47	2.20	217	33	18	-	11	12
14-feb-89	06:33:59.5	2.15	72	12	9	-	26	53

Table 5-1: Maximum Impact Pressures Gate Girder [Klatter et al., 1994]

In this table the results for pressure gauge D4 (at the bottom of the upper beam, see Figure 5-3), gives the maximum pressure 227 kN/m^2.

The maximum impact pressure registered is 227 kN/m^2 with a significant wave height of 2.20m. The prototype pressure history is shown in detail in Figure 5-6 (although this peak registration does not seem to reach this point)

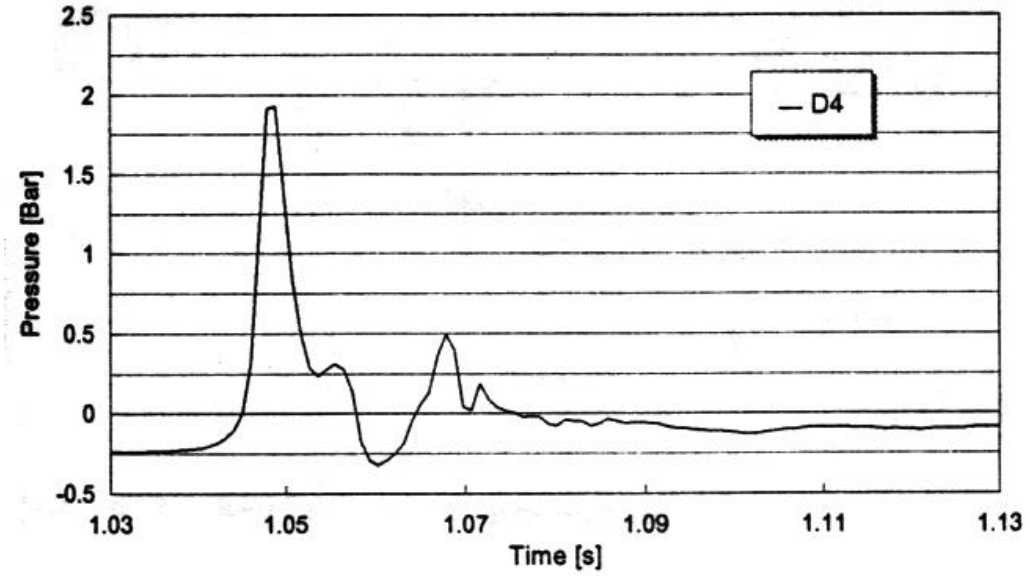

Figure 5-6: Typical prototype pressure history [Klatter et al, 1994]

5.2.4 Upper Beam

The wave impact measurements against the bottom of the upper beam started with an outside water level 1 meter below the bottom level of the beam and ended with the start of the closure of the gates.

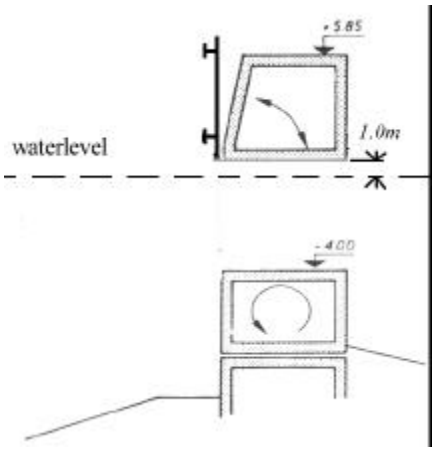

Figure 5-7: Schematisation of SVKO model and water level

The maximum pressure recorded on the upper beam equals 59 kN/m^2. This was recorded at approximately 1/4th of the gate length from the pier at the North Sea side on the bottom.

To illustrate the wave impact on the upper beam and the response of the beam the impact pressure time history of D35 (Oosterschelde side) and D36 (North Sea side) are shown in the following figure. The delay is about 0.2 seconds. The oscillation behind both peaks, together with registration of the acceleration of the beam, demonstrates the response of the beam, vibrating in its own frequency of approximately 5 Hz. The short (vertical) wave impact force is considered to be small (675 kN) compared to the stationary support force (of approximately 6000 kN)

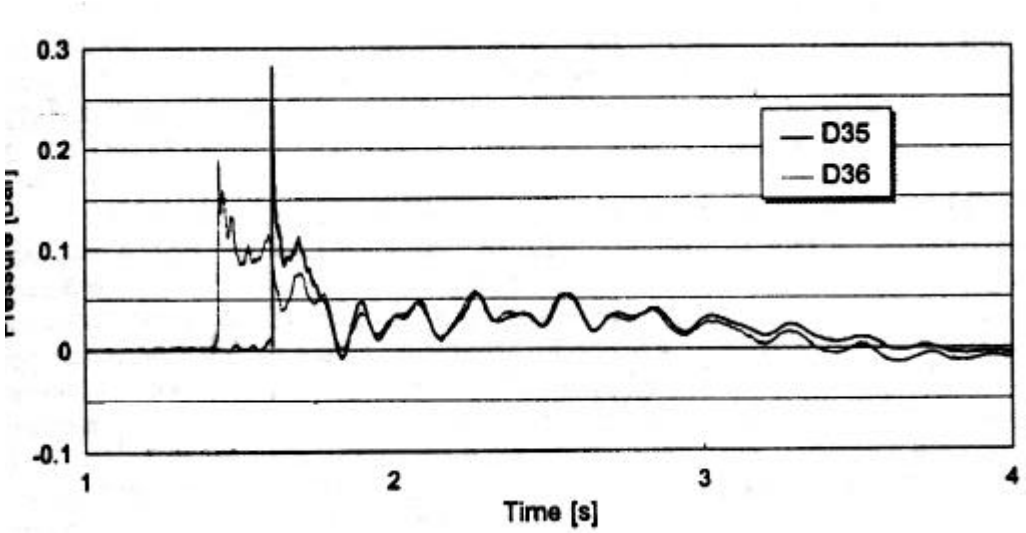

Figure 5-8: Registration of Impact pressures at Upper Beam [Klatter et al., 1994]

5.2.5 Conclusions

The frequency of exceedance of the maximum impact pressure on the gate girders and the upper beam is estimated between 1% and 0.1%, based on the total number of waves recorded during measurements. This is certainly important when the storm surge barrier is been evaluated. These maximum pressures are higher than the design values (45 kN/m2 to 60 kN/m2). The design values were determined for larger impact areas, however. The measured peak pressures are representative for only a small area related to the dimension of the sensors (diameter approximately 1 cm). The maximum pressures measured in the field show a very large spatial variation. Because of this variation the impact pressure averaged over a larger area will be relatively small; smaller than the design values (Klatter, 1994). The observed oscillations are related to the vibration of the structural elements. The rise time was in the order of 0.01 s and the decline time in the order of twice the rise time. Altogether the maximum wave impact pressures did exceed the design values but their influence on failure mechanisms was considered to be small because of the large spatial variance.

5.3 Dieppe breakwater

5.3.1 Introduction

Bagnold (1939) has examined the problem of wave impact pressures. Rouville and Petry carried out full-scale measurements on the Dieppe breakwater (see Figure 5-9) and Bagnold added the results to his paper.

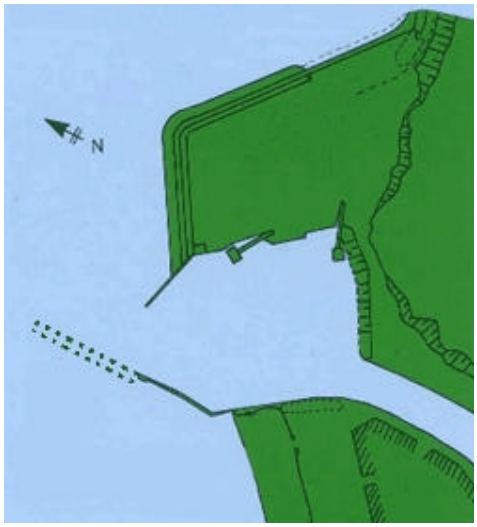

Figure 5-9a,b: Dieppe plan view and port picture

5.3.2 Impact loads

The maximum observed pressure at Dieppe according to Bagnold (1939) is 677 kPa (see Table 5-2) during a storm with a wave height of 1.8 m at open sea and an observed wave height at the structure of 2.0 m. The wave length was 40 m.

Open sea			**At shock**		**Vertical Velocity**	**Pressure (kPa) Above base**	
L(m)	**H(m)**	**v(m/s)**	**H(m)**	**v_{hor}(m/s)**	**v_{vert}(m/s)**	**0.35m**	**1.35m**
40	1.50	6.0	2.0	12.0	77	-	-
40	1.50	6.0	2.0	12.0	77	177	69
40	1.50	6.0	2.0	12.0	77	196	186
40	1.50	6.0	2.0	12.0	77	510	245
40	1.50	6.0	2.0	12.0	77	226	304
40	1.50	6.0	2.0	12.0	77	177	265
45	2.50	6.0	3.50	6.50	31.0	157	78
45	2.50	6.0	3.50	7.50	37.0	392	98
40	*1.80*	*6.0*	*2.50*	*8.50*	*23.0*	*677*	*69*
40	1.80	6.0	2.50	6.80	25.0	608	29
40	2.50	5.50	3.50	11.50	32.0	363	39

Table 5-2: Peak pressures observed at Dieppe, France (Minikin 1950)

5.4 Ship hulls

5.4.1 Introduction

In maritime design wave impacts are classified in four types: Bottom slamming, bow flare slamming, breaking wave impacts and wetdeck slamming (see Figure 5-10). When emerged bottoms re-enter the water surface bottom slamming occurs. When travelling with high speed, bow-flare slamming occurs in deep seas. Breaking wave impact is a result of superposition of breaking wave and bow waves hitting the bow of a blunt ship.

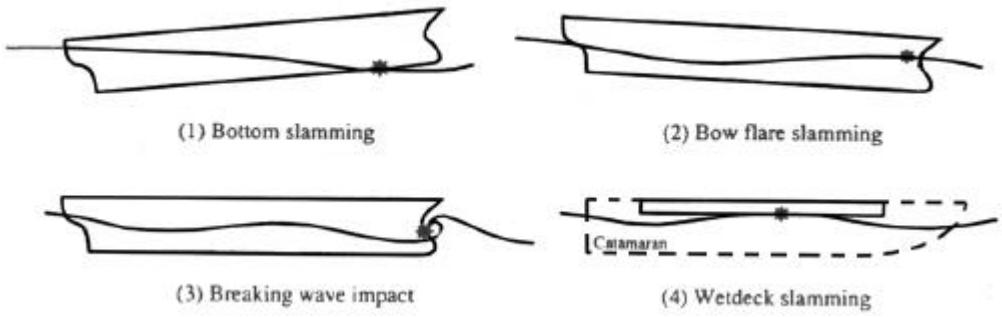

Figure 5-10: Slamming impact types of ship hulls

The most important load exerted on a ship is the bottom slamming. During the history of naval architecture ship design is based on this phenomenon. Despite its importance, few data from full scale experiments is obtained. Many researches done on this subject tried to give a design pressure value predicting the load. Measured peak pressures are about 3 to 6 ρgH, where H is the observed individual incident wave height. To result in similar maximum wave pressures as Dieppe (677 m), a sea wave of about 11 m should be implemented in this formula.
Takahashi et al carried out an experimental model study on bow flare impacts on two bow forms. The maximum measured pressure observed is about 491 kPa (full-scale value).

5.4.2 Impact loads

The Japan Shipbuilding Research Association performed full-scale measurements on a large ore carrier (length of vessel = 247m, displacement = 135,950 t). Together with measured impact duration, magnitudes of wave impacts were measured. Throughout the trials the impact duration was less than 0.1 s, with average impact duration of 20 ms. The maximum impact pressure was about 570 kPa. These wave impacts were measured during seastate 6, speed 13 knots, at 7 Beaufort of wind. The accompanying significant wave height is in the order of 7.5 m[5].

[5] Seastate 6 with Beaufort 7 of wind (Moderate Gale) with storm duration over 3 hours gives a significant wave height between 6 and 9 (7.5) m (fully developed sea state) with a peak period of 10.0-17.2 s (15 s) according to Bales 1983, 17th ITTC 1984; North Pacific Open Ocean Channel Sea States graphs.

6 DEVELOPMENT OF A BREAKER MODEL FOR COASTAL STRUCTURES

6.1 Introduction

In hydraulic engineering the focus of many research projects is on the maximum pressure and the pressure distribution. As a result many researches are focussed on recording maximum pressures. Often experiments have been carried out during which the amount of wave impacts and the maximum impact pressures are maximised by changing the berm configuration. The coverage of model configuration parameters is usually small and often ill-suited for coastal design because these situations do not occur frequently near modern harbours. As a result researchers with different backgrounds, such as hydraulic engineers and maritime engineers find many upper bound values for these pressures.

A different perspective is to focus on the probability of breaking of waves instead of on maximum pressures. This will be the subject of the model calculations done this study.

The way the presence of a berm in a irregular wave field affects the probability of occurrence of breaking waves and the probability of occurrence of impact waves is studied. Because an optimal design could reduce the probability of occurrence of breaking waves it is important to understand the phenomena inducing the resulting forces.

Different wave types, breaking phenomena and structure response ranging from incoming waves entering the vicinity of a coastal structure to severe wave impacts are visualised in Figure 6-1. The waves tend to break or not under the influence of other conditions like depth / water level, flow, shoals etc..

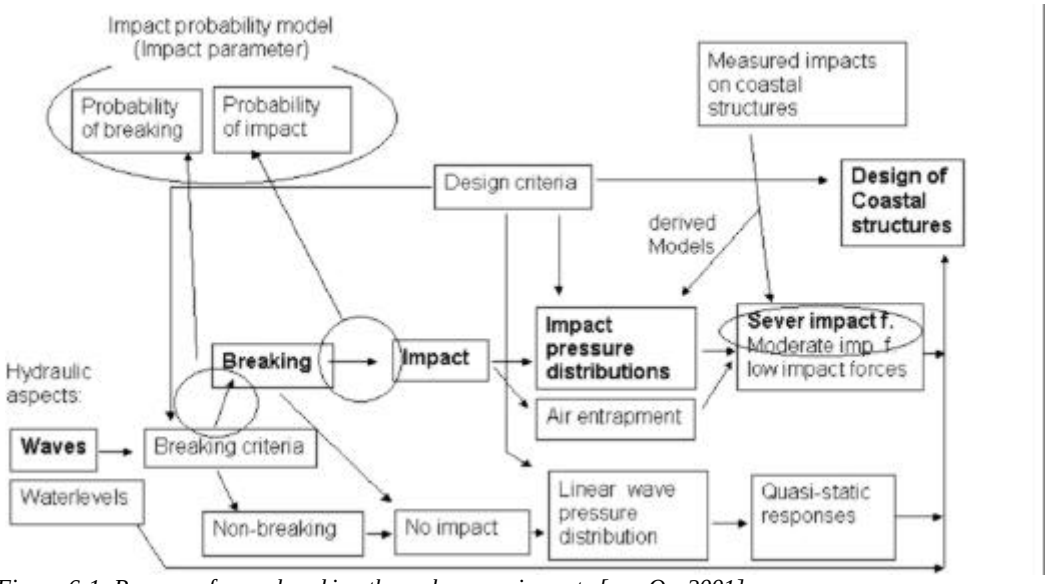

Figure 6-1: Process of wave breaking through severe impacts [van Os, 2001]

As explained in chapter 4, breaking waves can exert impact wave pressures on a structure, which in some cases can result in severe impact forces. Many times, as is said

before, only maximum wave pressures are recorded and the probability of occurrence of the wave-breaking phenomenon is neglected.

Because the exact shape of the “breaking wave” is difficult to predict, the resulting pressure distributions can not be predicted very accurately. Because in most cases information is present about a few parameters representing the irregular wave field (see section 3.3) only rough estimates with rules of thumb have been carried out.

This chapter focuses on the occurrence of wave breaking and the occurrence of wave impacts and in particular their probabilities of occurrence. In the PROVERBS project a parameter map has been developed indicating the type of wave load (quasi-standing, breaking or broken) dependent on relative wave height (wave height over depth) and relative berm height (berm height over depth). The background of the classifications in this parameter map is fully empirical. The parameter map is clarified in section 6.6.2.

Three models have been developed (see section 6.6) to give a theoretical background to the criteria developed for the parameter map. The models use the probability distribution of wave heights together with breaker criteria for individual waves. The berm influence is introduced using a berm influence parameter, which will be explained, in section 6.4.1.

6.2 Wave flume data

6.2.1 Hydraulic model tests

Different hydraulic model tests have been carried out. In this study the data has been analysed. The tests are summarised in the next table where the most important information is given. Furthermore, references are added where more detailed information on these tests is available.

Location,	**Year**	**Scale**	**f_{sam}[Hz]**	**Waves**	**Slope**	**Tests**	**References**
WKS	*1993*	*1:15*	*600*	*90*	*1:50*	*121*	*[Oumeraci et al., 1995]*
GWK	*1993/94*	*1:5*	*100*	*100*	*1:50*	*62*	*[McConnell & Kortenhaus, 1996]*
HR94	1994	1:20	400	500	1:50	217	,,
PIV	1994	1:50	400	1	1:20	77	[Oumeraci et al., 1995]
HR97	1997	1:20	1000	1000	1:50		[McConnell & Allsop, 1998]
					1:20		,,
					1:10		,,
					1:7		,,
QUB	1997	1:30	1000	800	1:50	12	[Kortenhaus & Löffler, 1998]

Table 6-1: Hydraulic model tests with reference

The two data sets used to clarify the parameter map and compare the model results are the mid-scale wave channel data set (WKS) and the Large Wave Flume data set (GWK). The mid-scale wave channel tests have been carried out at Franzius-Institut (WKS) at Hannover. The large wave flume tests have been carried out at the Coastal Research Centre, a joint institution of the University of Hannover and the Technical University of Braunschweig.

The hydraulic model tests for random waves analysed by Oumeraci et al (1995) and McConnel and Kortenhaus (1996) are the basis of all comparisons in this chapter. The scale used in the large wave flume of Hannover (GWK) is approximately 1:5. This is a larger scale compared to common used model scales. The data set with the smaller scale wave heights (scale 1:15) is called the WKS data set throughout the rest of this study. The data set with the larger scale wave heights will be called the GWK data set. The size of the WKS data set, containing 122 tests is almost twice as large as the GWK data set, containing 62 tests. Although the hydraulic model tests used in the PROVERBS project, see Table 6-1, consists of 121 test, a data set consisting of 122 tests has been used in this project.

6.2.2 Definition of data set parameters

This data set contains the following parameters:

Par.	Description	Type
H_{si}	Incoming significant wave height	Hydraulic
h_s	Water depth in front of the berm	Hydraulic
d	Water depth above berm	Hydraulic
L_{hs}	Waves length corresponding with the peak frequency of wave spectrum	Hydraulic
h_b	Berm height	Geometric
B_b	Berm width	Geometric
m	Slope of berm (sea side)	Geometric
P_{nbr}	Probability of non-breaking waves	Result
P_{br}	Probability of breaking waves (=1-P_{nbr})	Result
P_{fh}	Probability of horizontal wave impact force	Result
P_{fu}	Probability of vertical wave impact force	Result

Figure 6-2: Data set parameters

An effective berm length (B_{eq}/L_{hs}) is derived from the berm height (h_b) and the slope of the berm front (m). This effective berm length (in meters) is defined as:

$$B_{eq} = B_b + \frac{1}{2} m \cdot h_b \qquad (6.1)$$

These parameters are based on the standard PROVERBS notation [after Kortenhaus 1997] as shown in Figure 6-3.

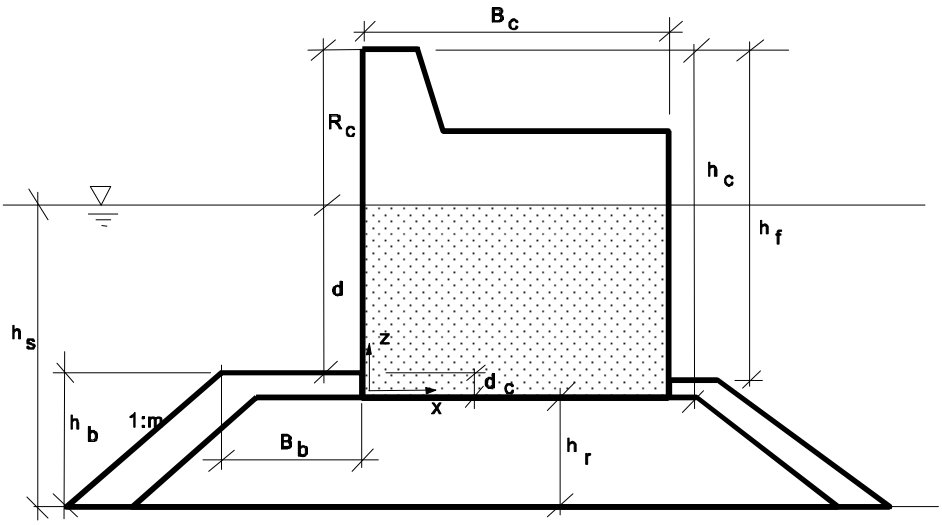

Figure 6-3: Definition sketch of parameters (PROVERBS) [after Kortenhaus, 1997]

Each of the 184 tests (62 GWK and 122 WKS) describes the incoming wave field, the breakwater configuration and the measured probabilities of occurrences of breaking waves and impact waves. As shown in Table 6-1, each wave field runs for 90 to 100 individual waves.

The complex irregular wave field is represented by a few parameters (H_s and L_{hs}). The large set of important environmental parameters is represented by two or three dimensionless influence parameters.

6.2.3 Definition of breaking waves and impact waves

The shape of the individual waves is used to distinguish whether a wave is a non-breaking or breaking wave. A wave demonstrating a shape indicating particle velocities at the top of the wave crest exceeding the wave celerity is called a "breaking wave" (see also section 2.4.5). P_{br} is the fraction of breaking waves during one test. The measurement of the shape of the waves is performed with video analysis. This was performed for selected tests only and was mainly used for calibration of P_{Fh} (probability of wave impacts, see next paragraph) since it was thought that video analysis for all tests is too time consuming and too costly. In the data set the criterion $P_{br}=0$ is implemented separating the data in non-breaking wave observations ($P_{br}=0$) and breaking wave observations ($P_{br}>0$) (Kortenhaus 2001)

The definition of an impact wave is based on the time series of pressures. The maximum pressure in a time series is used to calculate the maximum horizontal forces on the structure (per unit length). An impact (using the derived force) is defined as follows:

- If the impact peak of the time series (1st peak of the church roof) is at least 2.5 times higher than the second (quasi-static) peak ($F_{h;max}>2.5\ F_{h;q}$) AND
- If the relative impact peak ($F_{h;max}/\rho*g*H_s^2$) is larger than 2.5

If this definition (see Figure 6-4) is applied to all waves in a test the fraction of impacts as P_{fh} = (number of impact waves) / (number of all waves) can be derived. In the data set the criterion $P_{fh}=0$ is implemented separating the data in non-impact wave observations ($P_{fh}=0$) and impact wave observations ($P_{fh}>0$).

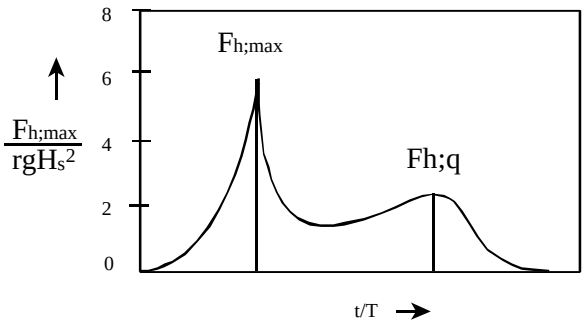

Figure 6-4: Definition sketch for impact wave

6.2.4 Analysis of data set

In the next figure the data is plotted against the relative incoming significant wave height and the relative depth ($2\pi h/L$). Also four lines indicating a constant wave steepness calculated with the significant wave height and the wave length at deep water ($s_s=H_{si}/L_{hs}$) are shown.

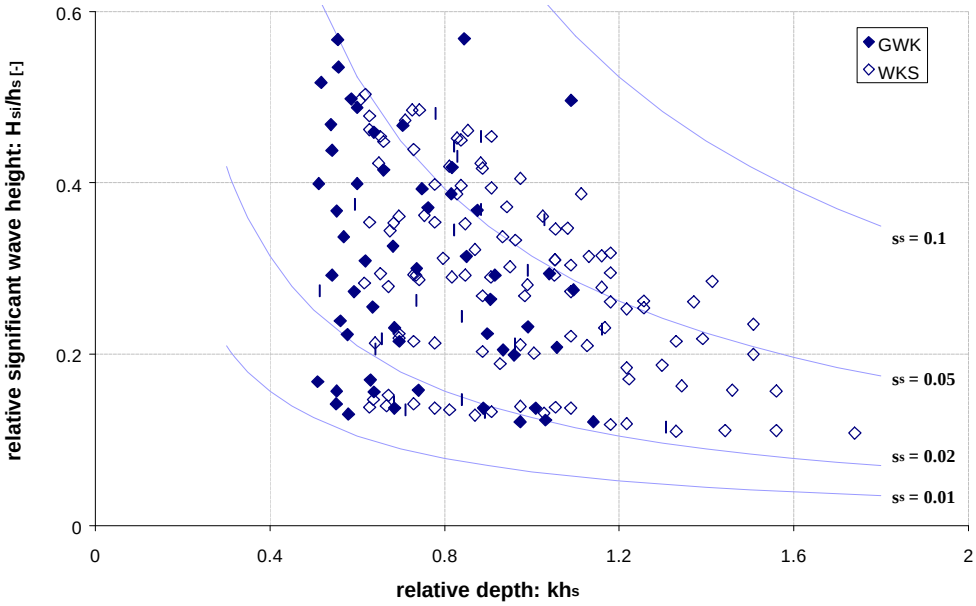

Figure 6-5: Data plot with relative depth and significant wave steepness

All data points, containing the results of measurements performed with 90-100 individual waves, are plotted between khs=0.5 and 1.5. This means that the measurements are performed with transition depth configurations; shallow water is defined as $h/L< {}^1/_{20}$ and deep water is defined as $h/L<{}^1/_2$. Therefore all waves are in "transition depth" water, defined with ${}^1/_{20}<h/L<{}^1/_2$, or ${}^1/_{10}ð<kh<ð$ [Schiereck, 1998].

In the following two figures the GWK and WKS data sets are plotted against the relative incoming unreflected significant wave height for the probability of breaking waves and for the probability of breaking waves.

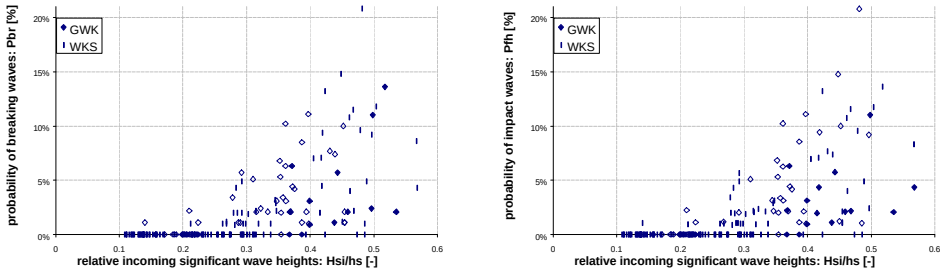

Figure 6-6: Data plot of probability of breaking waves and probability of impact waves

The figures show almost equal probability values while normally not all breaking waves should result in wave impacts at the structure.
To emphasise this problem the data sets are plotted with the data set parameters P_{br} (probability of breaking waves) against the data set parameter P_{fh} (probability of waves causing severe horizontal forces). Also a line corresponding with $P_{br}=P_{fh}$ is shown in this figure.

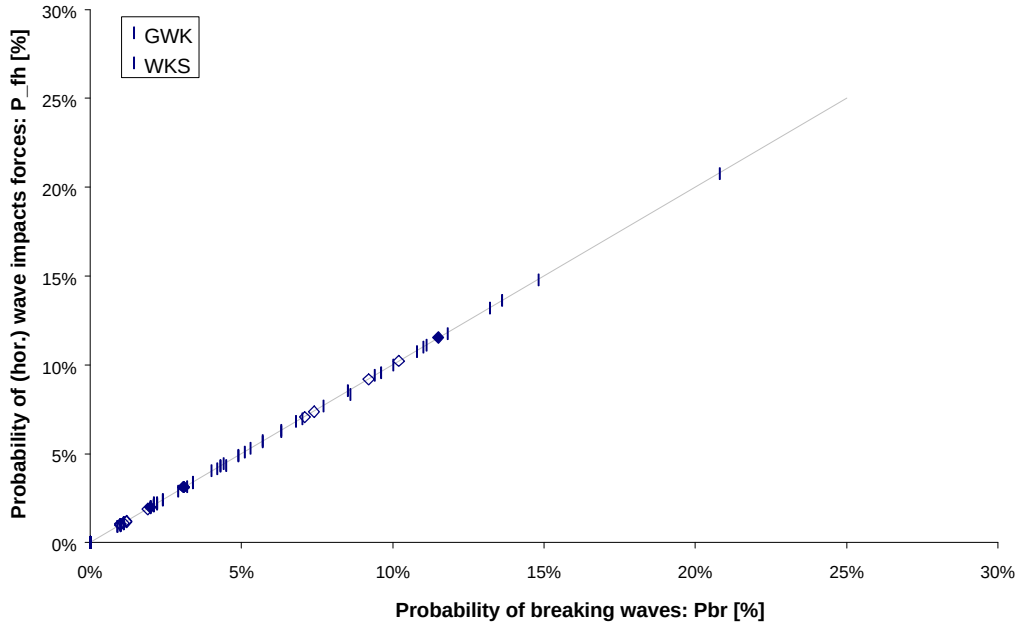

Figure 6-7: Probability of impact forces against probability of breaking waves

When the two probabilities are shown against each other (see Figure 6-7) the almost straight line of data points indicates a large dependency between the two probabilities. The ratio impact waves/breaking waves should be less than 1 because not all breaking waves cause impacts (impact force history defined in 6.2.3). This phenomenon can be seen more clearly in the following figure.

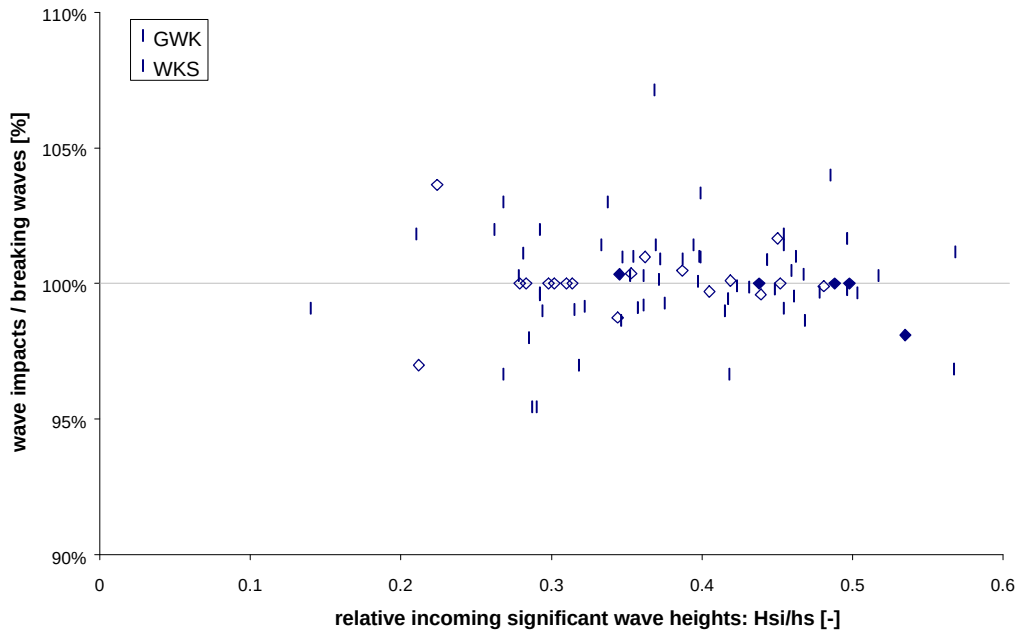

Figure 6-8: Dependence of probabilities of horizontal impact forces and breaking waves.

This figure clearly shows ratio's larger than 1, indicating more waves causing wave impacts than there are breaking waves. This should be impossible. Figure 6-7 demonstrates the dependence of the parameters, which clearly is large and P_{br}/P_{fh} is for the combined data set (GWK and WKS) between 0.95 and 1.05 (as can be seen in Figure 6-8). Also no correlation can be seen between this ratio and the relative incoming significant wave height or between the ratio and the relative berm height (not shown). The wave heights or berm configurations do not influence this phenomenon.

A more strange phenomenon is the fact that the number of impact waves is clearly not a fraction of the number of breaking waves as can be seen in Figure 6-1. Not all breaking waves should result in impact waves. Depending on the configurations and hydraulic conditions only a part of it should result in impact waves. This is rather strange and clearly is dependent on the definitions of the parameters P_{fh} and P_{br}.

Viewing Figure 6-8, it may be concluded that with the use of the aforementioned data sets GWK and WKS the probability of occurrences of horizontal impact forces can be considered equal ($P_{br} \approx P_{fh}$) to the probability of occurrence of breaking waves (both defined in section 6.2.3). In spite of the background of the parameters P_{br} and P_{fh}, explained in the previous paragraph, these probabilities will be used for comparison, calibration and optimisation (sections 6.5 and 6.8).

In the next sections the probability of occurrence of impact waves is considered to be equal to the probability of breaking of waves. Although this statement gives the idea that the probability of occurrence of impact waves should be neglected, this is not plausible, but will be used from now on.

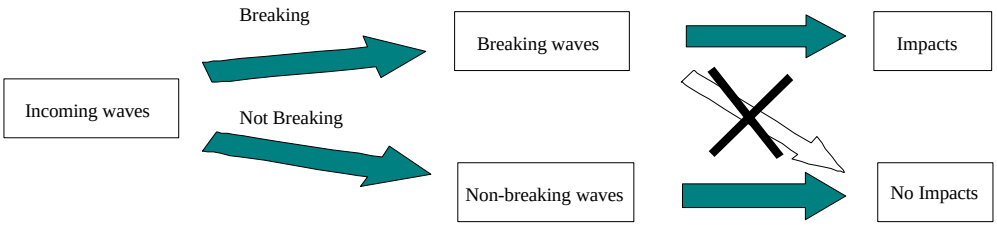

Figure 6-9: All breaking waves cause wave impacts

6.3 Inspection of PROVERBS Parameter Map

A parameter response map for prediction of the type of wave loading on vertical and vertically composite breakwaters based on structure geometry and wave conditions was first suggested by Allsop et al (1996a), Figure 6-10. The parameter map was constructed with analysed data from a series of small-scale model tests completed at HR Wallingford for vertical and composite breakwaters termed the HR94 tests, see Table 6-1 [McConnell, 1998].

The parameter map concept is based on the use of three non-dimensional input parameters (see Table 6-6). These parameters are related to the structure geometry as well as to the water depth and wave conditions at the structure. They are used to decide at a first stage on the type of monolithic structure (relative height h_b/h_s) and at a second and third decision level on the loading case (relative wave height H_s/h_s and relative berm width B_{eq}/L). The practical parameter map for wave load classification has been developed and validated on the basis of laboratory testing at four different institutes. It particularly allows us to distinguish between (i) impact loads for which the load duration/time history is most relevant for the dynamic response of the structure and which therefore need to be handled with special care and (ii) those "pulsating" wave loads for which the expected response of the structure is such that "quasi-static approaches" might apply (see Figure 6-10).

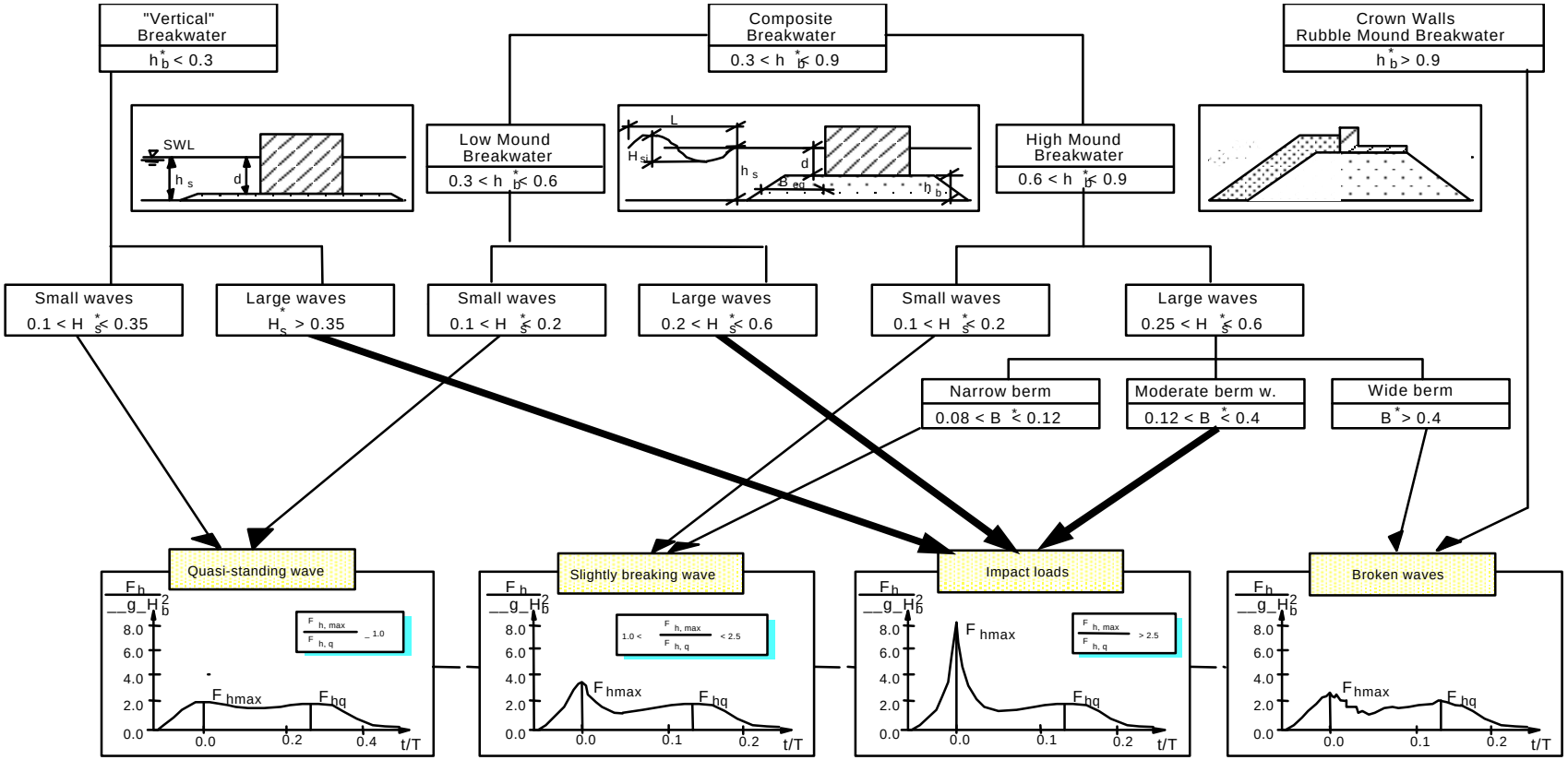

where $h_b^* = h_b/h_s$, $H_s^* = H_{si}/h_s$, $B^* = B_{eq}/L_{pi}$

Figure 6-10: Parameter map (PROVERBS), after [Allsop et al 1996]

This parameter map is based on model scale measurements and uses the following geometric and hydraulic parameters:

Parameters	Description	Type
H_{si}/h_s	Relative significant (incoming, unreflected) wave height	Hydraulic
h_b/h_s	Relative berm height	Geometric
B_{eq}/L	Relative berm length	Geometric

Figure 6-11: Non-dimensional parameters used for the Parameter Map [after Kortenhaus]

The map gives an indication of the loading conditions to be expected:

- quasi-standing waves without any account for load duration
- slightly breaking waves
- impacts with account for load duration
- broken waves, i.e. the waves already broke before reaching the structure.

The background of the classification for the aforementioned loading conditions is fully empirical and no theoretical background supports these results. The geometric and hydraulic conditions for wave impacts (see Figure 6-10) can also be defined with a lower bound and an upper bound condition for the relative incoming significant wave height, given the relative berm height. Within these conditions (lowerbound<H_{si}/h_s<upperbound), the wave series should contain wave impacts, defined in section 6.2.3. The lower and upper bound conditions are shown in the more comprehensible table, Table 6-2.

Beneath the lower bound condition for the relative incoming significant wave height (H_{si}/h_s) quasi-static wave response can be expected and for larger berm height-water depth ratios slightly breaking waves can also be expected. Although no definition is given in the parameter map for ratios of the relative incoming significant wave heights larger than the upper bound condition. large values for these ratios (H_{si}/h_s larger than 0.6) are not expected nor measured during the tests. Therefore this upperbound condition could be neglected but is shown anyway.

rel. berm height (h_b/h_s)	**rel. sign. wave heights (H_s/h_s)**	**rel. berm width (B_{eq}/L)**
0.0-0.3	$0.35 < H_s/h_s$	-
0.3-0.6	$0.20 < H_s/h_s < 0.6$	-
0.6-0.9	$0.25 < H_s/h_s < 0.6$	$0.12 < B_{eq}/L < 0.4$
>0.9	never	-

Table 6-2: Breaking conditions with parameter map

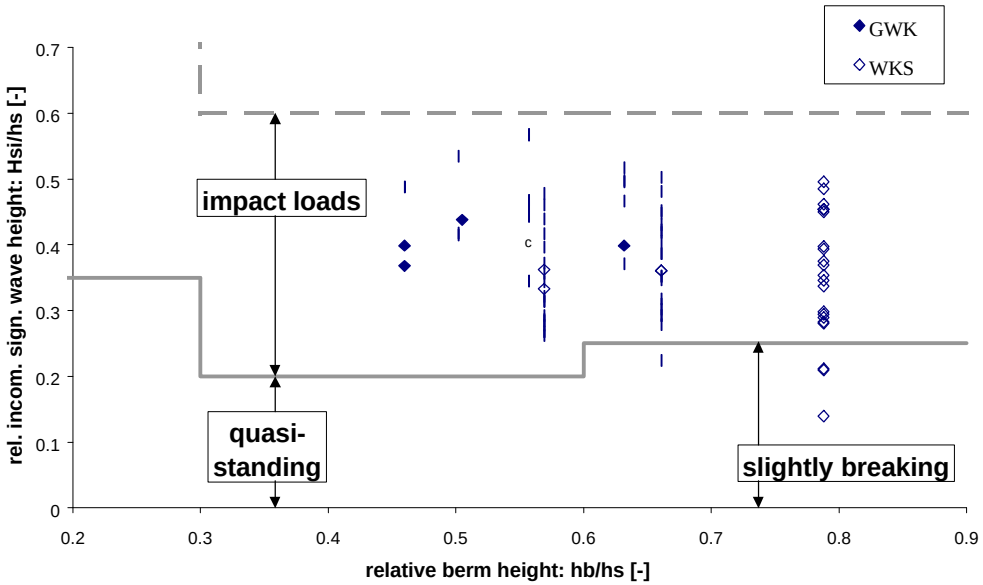

Figure 6-12: Data plot (only breaking waves) with parameter map conditions

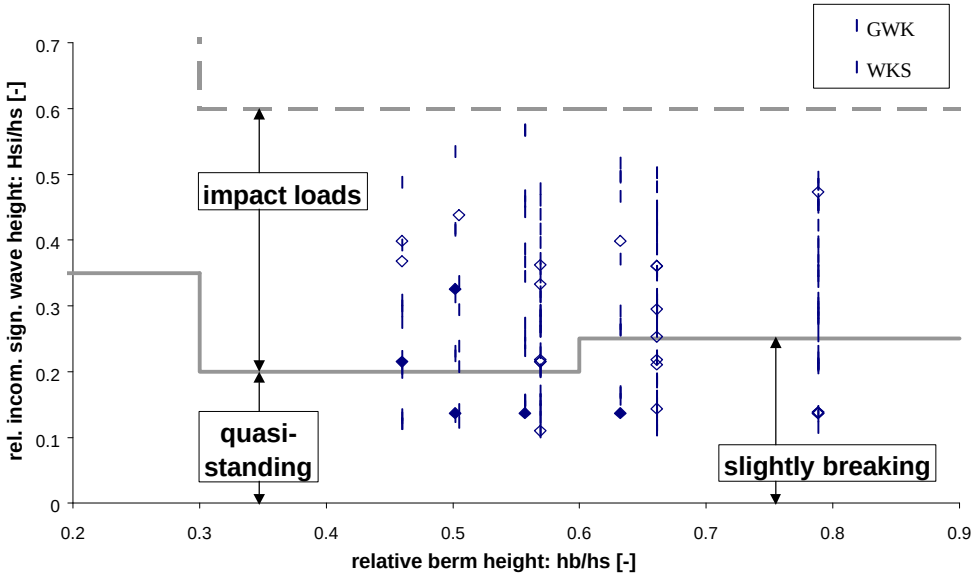

Figure 6-13: Data plot (only non-breaking waves) with parameter map conditions

The plots of these conditions and the data configurations, Figure 6-12 and Figure 6-13, demonstrate the accuracy of the parameter map for the data set WKS and GWK. In Figure 6-12 only the data with observed wave impacts (P_{fh}>0) are shown. In Figure 6-13 all non-impact wave observations (tests with P_{fh}=0) are shown. Figure 6-12, showing observed impact waves (P_{fh} > 0), clearly demonstrates a very good agreement (100% for GWK dataset) with the parameter map conditions; all observed data with impact waves are within the impact wave conditions of the parameter map. Only the small scale wave flume data set (WKS) shows little disagreement (6%) for relatively higher berm heights. The plot with non-impact wave observations (Figure 6-13) shows that the parameter map conditions (H_{si}/h_s<0.2 for h_b/h_s<0.6 and H_{si}/h_s<0.25 for h_b/h_s>0.6) are not good upper bound conditions for non-impact waves. This can be seen by the fact that almost half the

full data set (WKS and GWK) shows a large number of data points in the “impact load area” where it should be in the “quasi-standing” load area. In can be concluded that no good distinction can be made with only the two parameters h_b/h_s and H_{si}/h_s in case of waves giving non-impact loads.

The following table gives an overview of the number of observations, which are within and outside parameter map conditions. The third column shows the amount of tests with configurations (H_{si}/h_s and h_b/h_s) within Impact conditions of the parameter map. For full agreement, the first two values (Impact waves observations) should be 100% (all tests) and the last two values (Non-Impact observations) should be 0% (none of the tests).

Wave type	**Dataset**	**within Impact conditions** observations agree with p.map	**outside Impact conditions** observations disagree with p.map
Impacts	GWK	100.0%	0.0%
	WKS	93.8%	6.3%
Non-impacts	GWK	60.5%	39.5%
	WKS	37.9%	62.1%

Table 6-3: Comparison of data with Parameter map Impact conditions

Evidently the parameter set is more accurate for breaking waves. For non-breaking waves the parameter map's lower limit is too small. Although the parameter map was based on data from a series of small-scale model tests completed at HR Wallingford consisting of 217 tests, the smaller test series (GWK 62 and WKS 122) do not agree well. Conclusions drawn from the comparison will not give satisfactory results, because the general statements above are based on only 184 tests.

6.4 Clarification of model parameters

6.4.1 Berm influence parameter

A configuration is used implementing the water depth in front of the total structure (foundation included), defined as h_s, and the water depth above the foundation, defined as d.

Three options will be studied:

i. Only the water depth in front of the structure h_s is considered and no berm/foundation is present
ii. Only the water depth above the berm d is considered and the water depth in front of the berm is deep
iii. A water depth between h_s and d is used, depending on a so-called "berm influence parameter"

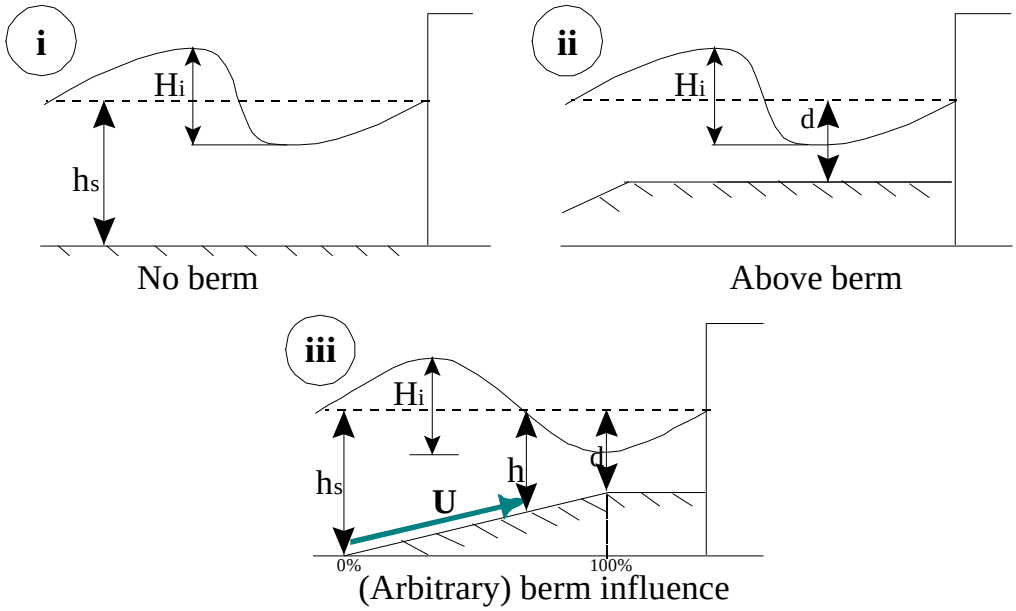

Figure 6-14: Overview of berm influence options for model configuration

No berm (i)
The waterdepth in front of the berm is only used ($h=h_s$)

Above berm (ii)
The waterdepth above the berm is only used (h=d)

Berm influence parameter (iii)
This option is in fact a linear interpolation between the two depths h_s and d. The parameter U is introduced defining the linear influence of the berm on the model (see Figure 6-14). When no berm is included in the model, or its influence is very small, U becomes zero (U=0), similar to option (i). When the influence of the berm is supposed to be large, U approaches unity (U=1). In this case, similar to option (ii), the water depth is taken as the depth above the berm (d). The following function defines the water depth, which is implemented in the formula:

$$h = h_s - U(h_s - d) \tag{6.2}$$

This depth is used to relate the wave heights to the environment (H_{si}/h) giving a non-dimensional parameter for model input.

6.4.2 Breaker index

In section 2.4.5 some breaker indices are given for regular and irregular wave fields. Because the wave field is treated as a set of individual waves the breaker function giving the maximum individual wave height for a given water depth should therefore be a regular wave field-breaker function.

No foreshore steepness is included in any of the models. Therefore the following breaker functions are considered to be relevant:

Breaker index	**Index**
McCowan breaker index for regular waves	A
Miche breaker index for regular waves	B
Oumeraci breaker index for regular waves (derived from Miche)	C

Table 6-4: Breaker indices used in the models

For example, when the simple wave reflection model is used with the Miche breaker index function the combination will be called: model 1B. These breaker heights can all be written as the ratio of the breaker height and the local depth (see also section 2.4.5.1):

$$\gamma = \frac{H_b}{h} = 0.78 \text{ (McCowan)} \tag{6.3}$$

$$\gamma = \frac{H_b}{h} = 0.892 * \frac{\tanh(kh)}{kh} \text{ (Miche)} \tag{6.4}$$

$$\gamma = \frac{H_b}{h} = \left[0.644 + 0.136 \frac{1 - K_r}{1 + K_r} \right] \frac{\tanh(kh)}{kh} \text{ (Oumeraci)} \tag{6.5}$$

NOTE: The McCowan and Miche breaker criteria derived for regular wave fields with progressive waves are used. Although the incoming waves are supposed to be progressive waves, in front of the structure due to reflection they are supposed to become standing waves. Therefore an invalid application is used in this study for the sub-model A and B. Because the Oumeraci breaker criterion is equal to the McCowan breaker criterion for K_r=0 (no reflection), this criterion is also condidered to derived for progressive waves in stead of standing waves. This will influence the reflection coefficient, analysed in section 6.8. The values of the proportionality constants should be smaller, but the standing wave equation (left) does not implement the reflection coefficient and uses therefore only the incoming (unreflected) wave height H_i (considering a reflection coefficient value equal to 1).

$$\left[\frac{H_i}{L_{hs}} \right]_{max} \cong 0.20 \tanh\left(\frac{2\pi h_s}{L_{hs}} \right) \text{ instead of } \left[\frac{H_i (1 + K_r)}{L_{hs}} \right]_{max} = 0.142 \tanh\left(\frac{2\pi h_s}{L_{hs}} \right).$$

Although the optimal reflection coefficient corresponding to a minimum error (will be explained in the next section) is in this case not accurate, the aforementioned error is not influenced by a change of the proportionality constant.

The different breaker index values for varying relative depth (Miche) and multiple values for the reflection coefficient (Oumeraci) are displayed in the next figure.

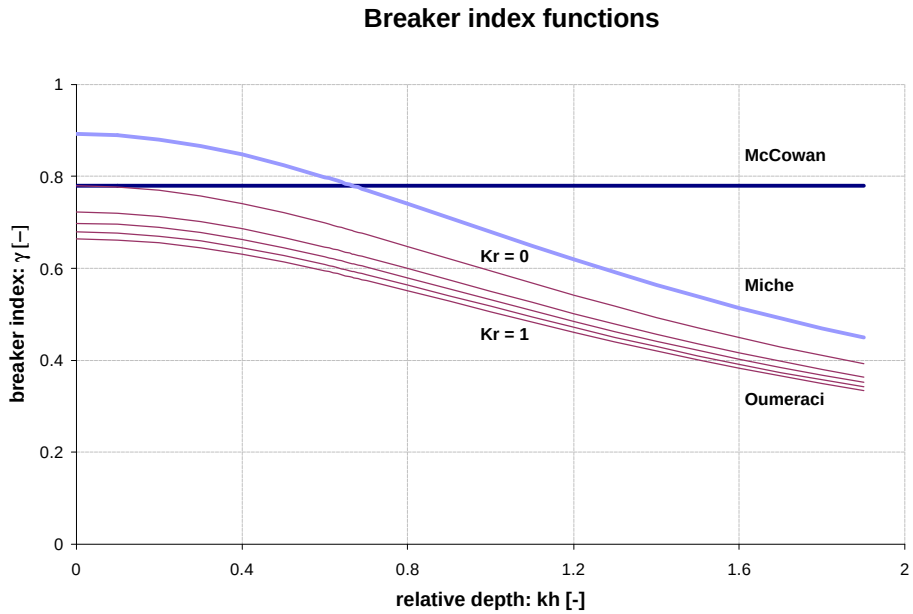

Figure 6-15: Breaker indices against relative water depth and reflection coefficient

The Miche and McCowan breaker functions give equal values for a relative water depth of $2\pi h/L = 0.666$. Only the Oumeraci breaker function calculated for no reflection approximates the McCowan breaker function for relative depths smaller than $kh<0.4$ (shallow water).

6.5 Model calibration

6.5.1 Free parameter

To investigate the error between measured and predicted probabilities of breaking waves in a random wave field with added geometric parameters a free parameter is needed. For different values of this parameter the error can be calculated.

Because the theories on which the models are based are not perfect and assumptions have to be made, the reflection parameter is used as a calibration parameter.

6.5.2 Error derivation

The following assumptions are made for error derivation and optimisation of the free parameter. The difference between the calculated and predicted probability of breaking waves is called the error (ε) (or residue) and is added to the model results. The distribution of the error $f(\varepsilon)$ is supposed to be normal.

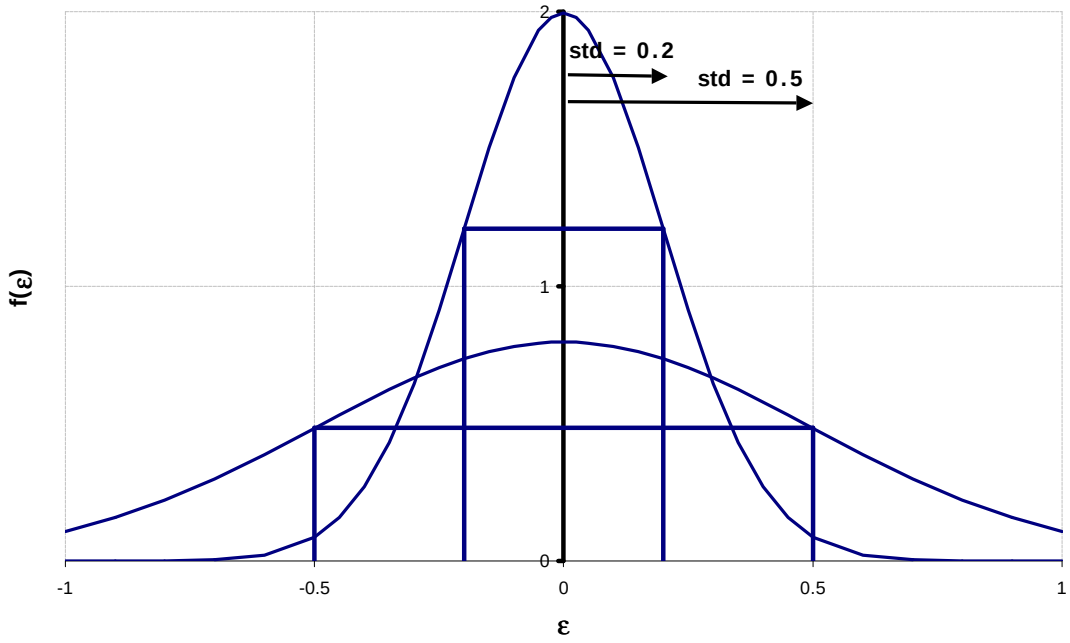

Figure 6-16: Representation of standard deviation of the error

The standard deviation ("wideness" of the (error) distribution) is used as an indicator for the accuracy implying a lower accuracy of a model for increasing standard deviation. The squared standard deviation or variance of the error is therefore also a good indicator for indicating the accuracy. Instead the variance is used in further comparisons.

The error can be derived in two ways by using different representations, if the model function is denoted by g or
$P_{br} = g(H_{si}/h_s)$:

1. $y_i = g^{-1}(P_{br;i}) + \underline{\varepsilon}$ (linear model representations)
2. $P_{br;i} = g(H_{si}/h) + \underline{\varepsilon}$ (real model representations)

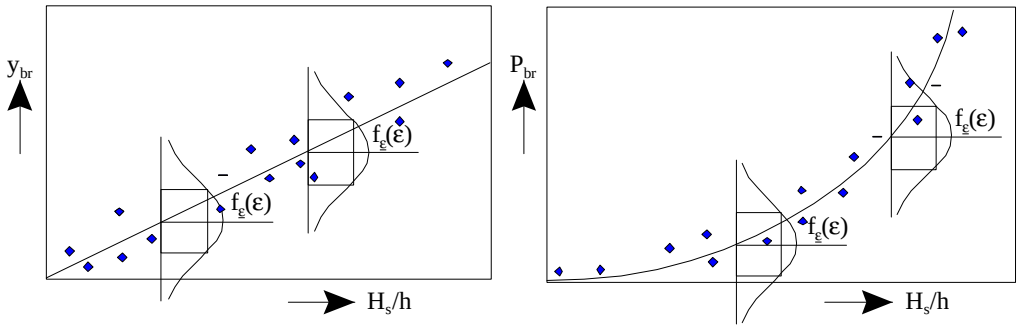

Figure 6-17: Leased square error method for linear- and real model-presentations

Using the transformed model function of equation (6.15) the measured probabilities are transformed so that the free parameter (reflection coefficient Kr) and the independent parameter (Hs/hs) can express all transformed probabilities with a certain "best fit". Both options should give similar results. Otherwise the transformation of the model function is not valid. Because of a large numerical error in case of small probabilities in case of the linearisation method, the second option is used for optimisation.

6.5.3 Free parameter optimisation

Choosing an optimal value for the free parameter the deviations around the predicting model becomes minimal. Normally this is done expressing the probability function of the deviations or errors as a Gaussian distribution. The variance and hence the standard deviation indicates the "accuracy" of the used model. This way the second power of all differences between the predicted and measured values becomes the parameter, which has to be minimised. This parameter, the Sum of Squared Errors (SSE) is described by:

$$\chi^2 = \sum_{i=1}^{N} \left\{ P_{br;i} - P_{br;model} \right\}^2 \tag{6.6}$$

where

i = observation index
N = Number of observations (184 observations for WKS + GWK)

And is minimised with

$$\text{MIN}(\chi^2) = \underset{Kr=0}{\overset{1}{\text{MIN}}} \left[\sum_{i=1}^{N} \left\{ P_{br;i} - P_{br;model} \right\}^2 \right] \tag{6.7}$$

This should be true when

$$\frac{\partial \chi^2}{\partial K_r} = 0 \tag{6.8}$$

Important in the analysis is the minimisation of the scatter around the prediction model. The variance of the error, σ_ε^2 or var(ε), being the second central moment of the error can be predicted by the following parameter:

$$s_{\varepsilon;b}^2 = \frac{\sum \left(P_{br;i} - P_{br;i;model} \right)^2}{N} = \frac{SSE}{N} \tag{6.9}$$

where $s^2_{\varepsilon;b}$ is the (biased) predictor for the variance of the error: var(ε).

Because the parameter is biased, hence the subscript b, the order in which the SSE has to be divided has to be one less than the size of the data set, N, giving (subscript u means unbiased):

$$s_{\varepsilon;u}^2 = \frac{\sum \left(P_{br;i} - P_{br;i;model} \right)^2}{N-1} = \frac{SSE}{N-1} \tag{6.10}$$

where $s^2_{\varepsilon;u}$ is the (unbiased) predictor for the variance of the error: var(ε).

6.6 Development of models for the probability of breaking waves

6.6.1 Introduction

The aim of this study is to develop a model for the probability of occurrence of breaking waves. Three models are developed in the following sections and their agreement with observations is compared.

The models are based on the following assumptions. An irregular wave field can be treated as a set of successive individual waves with an equal wave height distribution (see

model definitions, section 6.6.3 through 6.6.5). The wave heights are assumed to be Rayleigh distributed using the incoming unreflected significant wave height as the nominal parameter. Each individual wave can be classified as a breaking wave, or non-breaking wave, depending on the breaker function (see section 6.4.2). The berm is introduced with only one parameter: the berm height (see also section 6.6.2).

In the next sections three probability functions will be developed to describe the probability of breaking waves. This is done by combining the probability of exceedance of the individual wave height, say $p(H_i)$ and check whether this individual wave follows the condition for breaking waves, explained in section 2.4.5.1. Adding these probabilities will result in the probability of occurrence of breaking for the total irregular wave field.

The different models are:

Description of model	**Model number**
Simple wave reflection model	1
Truncated distribution model	2
Random wave reflection model	3

Table 6-5: Denotation of Models

With the use of influence parameters geometric and hydraulic dimensions will be implemented in these models.

6.6.2 Model Parameters

Although more parameters are used in the GWK and WKS data sets (following the PROVERBS notation) only a few are used in the models developed in section 6.6. They are visualised in the following figure.

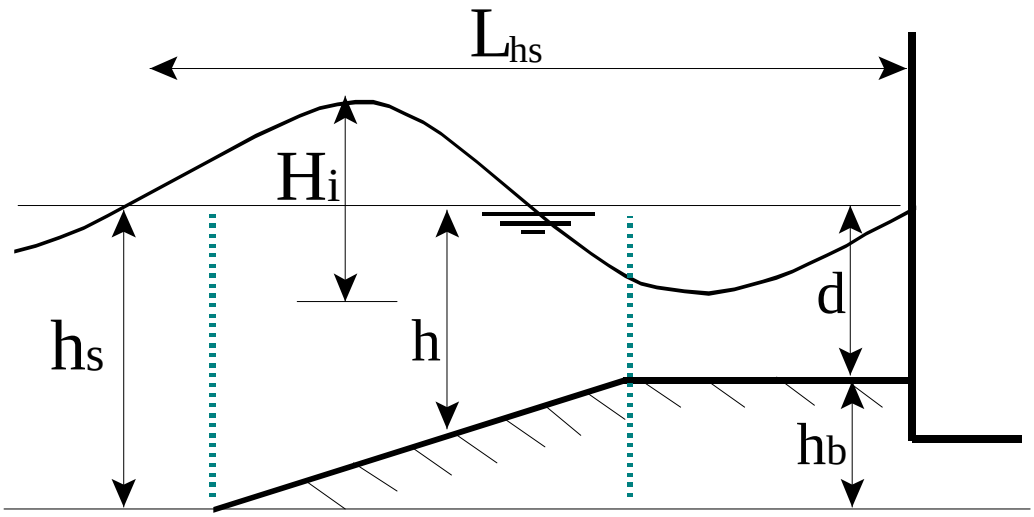

Figure 6-18: Definition sketch of parameters

Three water depths are used, h_s as the waterdepth in front of the berm, d as the waterdepth on top of the berm, and h as a depth between the first two mentioned depths. If only one depth is to be used, the water depth in front of the berm, h_s is used.

All these parameters can be reduced to two important non-dimensional ratios:

Parameters	Description
H_{si}/h_s	Relative significant (incoming, unreflected) wave height
h_b/h_s	Relative berm height
$2\pi h_s/L_{hs}$	Relative water depth

Table 6-6: Important relative parameters

These ratios should give similar results for different scales. Difficult phenomena such as aeration of the water, air entrapment or salinity of the (sea) water could influence the results, but this is not studied in this report.

6.6.3 Simple wave reflection model (1)

This model is based on the assumption that the wave height of reflected waves is superposed onto the wave height of incoming waves. When the properties of the incoming wave are similar to the reflected wave a standing wave is to be expected. Every new wave in an irregular wave field has a different wave height. Second order phenomena as the result of interaction between incoming and reflected waves can be expected in reality but are neglected in this model

All individual waves with wave heights (H) above the "breaker height" (H_b) are considered to break. The breaker height can be derived from different geometric properties (see section 6.4.2). The part of all waves in a Rayleigh distribution exceeding this breaker height forms the basis for predicting the parameter $P_{br;model}$ (model prediction of probability of breaking waves). This distribution is restricted with several assumptions:

- The registration on which the calculation of the significant wave height is based is a short-term registration for deep-water waves.
- The Rayleigh distribution is used to predict the probabilities of occurrence of wave heights.
- The influence of the water depth seawards of the structure on the wave height distribution is neglected

The significant wave height H_s together with the mean wavelength L are considered to be the only parameters describing the wave field properties. Using a breaker index the relative wave height becomes the variable with which the other properties are to be calculated.

Considering a regular wave field the superposition of the incoming and reflected wave in front of a structure (such as a vertical wall) can be described as

$$H_c = H_i + H_r = H_i(1 + K_r) \tag{6.11}$$

or

$$H_i = \frac{H_c}{1 + K_r} \tag{6.12}$$

This occurs only at the wall. Because the berm length is considered to be very small compared to the wave length (derived from the peak period of the observations), it is proposed to use this equation above the berm.

As said before all individual (in case of no reflection) or combined waves (in case of reflection) with wave heights exceeding the breaker height are considered to break. This breaker height, in its simplest form a ratio between the maximum wave height and the water depth, can be defined using the breaker index. McCowan uses a constant value,

Miche implements the relative depth (kh) and Oumeraci on his turn implements the reflection coefficient K_r (see sections 2.4.5 and 6.4.2). When this breaker index is simply denoted as "γ" neglecting its properties (K_r and kh_s), the breaker (wave) height is defined by:

$$H_b = H_{max;non-breaking} = \gamma h_s \tag{6.13}$$

When these definitions (H_b and $H_i(1+K_r)$) are combined with a probability distribution for wave heights in an irregular wave fields the probability of non-breaking waves can be calculated. The breaker height is considered to be the criterion for the exceedance value. The Rayleigh distribution giving the probability of non-exceedance of a certain value H is the basis for the probability calculations:

$$F_{\underline{H}}(\underline{H} < H \,|\, H_s) = 1 - e^{-2\left(\frac{H}{H_s}\right)^2} \tag{6.14}$$

Substituting the breaker height (6.13) leads to the probability of breaking waves:

$$P_{br}(\underline{H} > H_b \,|\, H_s / h_s; H_{b;c} / h_s = \gamma, H_{b;i} = \frac{H_{b;c}}{1+K_r}) = e^{-2\left(\frac{\gamma h_s}{H_s(1+K_r)}\right)^2} \tag{6.15}$$

which can be written as a function of the hydraulic input parameter H_s/h_s:

$$P_{br;MODEL1} = e^{-2\left(\frac{\gamma}{(H_s/h_s)(1+Kr)}\right)^2} \tag{6.16}$$

The probability of breaking waves is therefore now calculated using the reflection, geometry of the structure and the berm and hydraulic input.

Different breaker index functions (γ) will be explained in 6.4.2.

6.6.4 Truncated distribution model (2)

The philosophy of this second model, is that the Rayleigh distribution giving the probabilities of occurrence of the wave heights is influenced before it reaches the berm. The water depth and the wave steepness reduce the larger wave heights. They become smaller and hence give larger probabilities for the smaller waves heights.

This model calculates the part of all waves with heights exceeding the breaker height for the water depth h_s and redistributes the probabilities over the lower wave heights. Other redistribution models are also possible such as a redistribution into one spike at the location of the now largest possible wave height [see Vrijling 2000, Battjes 2000].

In this model two probabilities of breaking waves will be calculated. The first is denoted by Q_{br} and is calculated by:

$$Q_{br} = e^{-2\left(\frac{\gamma}{(H_s/h_s)(1+K_r)}\right)^2} \tag{6.17}$$

which is similar to model 1 (equation (6.16)). Using the complement of the parameter Q_{br} $1/(1-Q_{br})$ the probabilities of smaller waves can be multiplied by it, creating a truncated

wave height distribution. For wave heights smaller than the breaker height the truncated distribution gives a non-exceedance probability equal to 1:

$$F_{model2}(\underline{H} < H_b) = 1 \tag{6.18}$$

The truncated probability density function now becomes:

$$f_{\underline{H}}^{tr}(H) = \frac{1}{1-Q_{br}} f_{\underline{H}}^{0}(H) \tag{6.19}$$

where

$$f_{\underline{H}}^{0} = \frac{4H}{H_s^2} e^{-2\left(\frac{H}{H_s}\right)^2} \tag{6.20}$$

This applies to all wave heights smaller than the breaker height ($H<H_b$), because for larger wave heights the probability of non-exceedance (F_H^0) will be larger than 1, which should be impossible.

Substituting the breaker height (6.13) and using the water depth above the berm (d instead of h_s) the probability of non-exceedance of the breaker height becomes:

$$F_{\underline{H}}^{TR}(H/d < \gamma) = \frac{1}{1-Q_{br}} F_{\underline{H}}^{0} = \frac{1}{1-Q_{br}} \left(1 - e^{-2\left(\frac{\gamma}{(H_s/d)(1+K_r)}\right)^2} \right) \tag{6.21}$$

The probability of occurrence of breaking waves becomes:

$$P_{br} = 1 - F_{\underline{H}}^{tr}(H_s/d < \gamma) = 1 - \left[\frac{1}{1-Q_{br}} F_{\underline{H}}^{0}\left(H_{si}/d < \gamma\right) \right] = 1 - \left[\frac{1}{1-Q_{br}} \left(1 - e^{-2\left(\frac{\gamma}{(H_s/d)(1+K_r)}\right)^2} \right) \right] \tag{6.22}$$

And, using the parameter a, defined as $a = \frac{1}{1-Q_{br}}$ the equation reduces to

$$P_{br;MODEL2} = 1 - a + a e^{-2\left(\frac{\gamma}{(H_s/d)(1+K_r)}\right)^2} \tag{6.23}$$

Note: When again the depth h_s is used as the water depth above the berm (hence neglecting the berm presence) and the probability of breaking waves over the water depth h_s is calculated, the probability of breaking waves (P_{br}) becomes zero. This is the result of the factor a, which was introduced to do so (giving P_{br}=100% for wave heights above the breaker height for h_s).

To demonstrate how the distribution changes when truncation of the probabilities for the larger wave heights is used, two figures are shown neglecting reflection (for simplicity). First the probability density function (pdf) is shown and second the cumulative probability density function (cdf) of the unreflected wave heights is shown. In this example, no reflection is implemented, only progressive waves are considered.

The continuous lines show the (normal) Rayleigh distribution and the discontinuous lines the truncated Rayleigh distribution of normalised wave heights for the normalised breaker height (H_b).

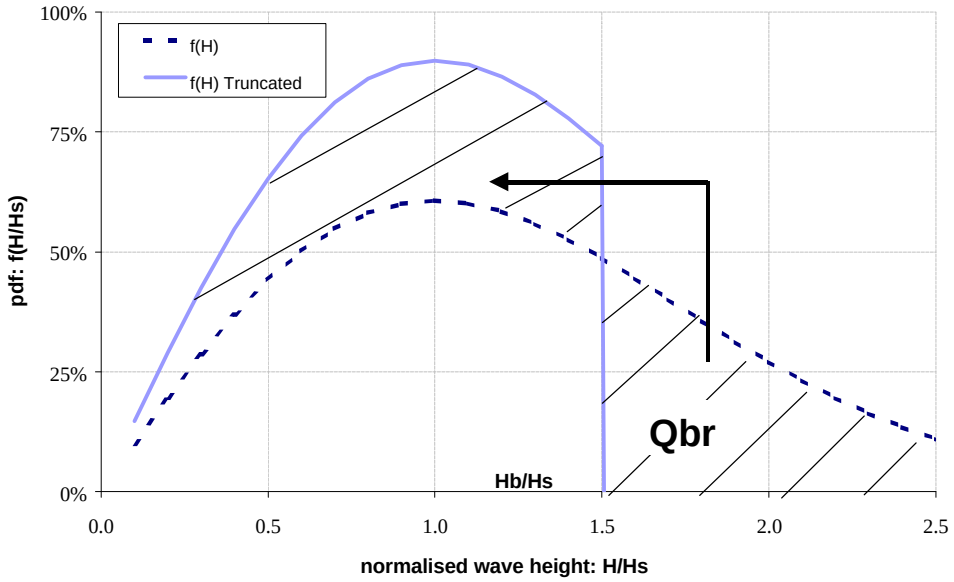

Figure 6-19: Pdf of normal and truncated wave height distribution

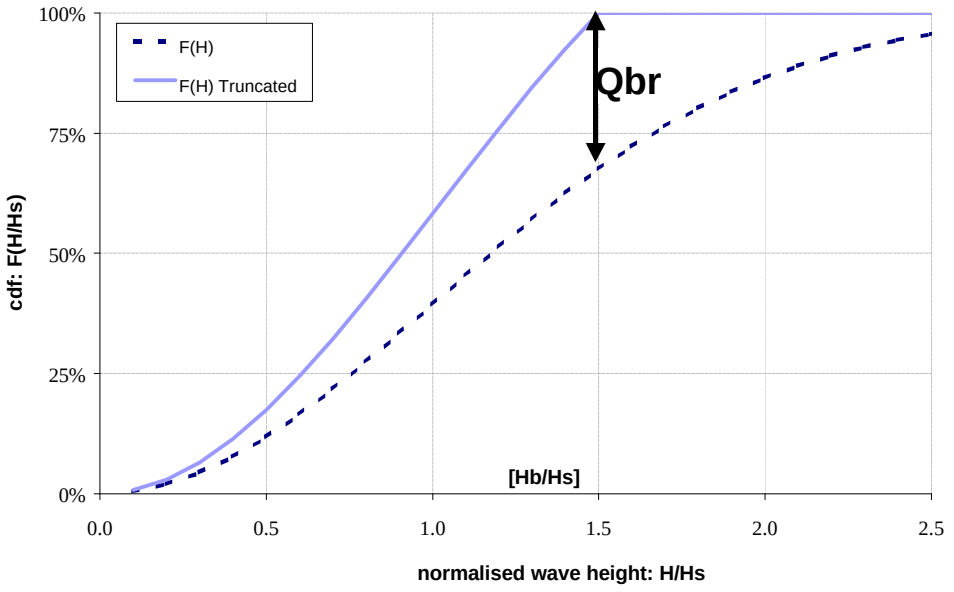

Figure 6-20: Cdf of normal and truncated wave height distribution

6.6.5 Random wave reflection model (3)

In this case two waves with independent wave heights and similar wave height distributions travel towards the structure. The first wave (H_1) will be partially reflected and its height becomes K_rH_1. Following linear wave theory, its surface elevation can be

superposed onto that of the second incoming wave H_2. This cannot occur at the wall (because only one wave can occur at the time at the wall), but is considered to occur above the whole berm.

The wave on top of the berm with a wave height H equal to the sum of the reflected wave (H_1) and the new incoming wave (H_2) follow the equation:

$$H_2 + K_r H_1 = H \tag{6.24}$$

The probability of the wave height above the berm can be calculated using all combined probabilities that follow equation (6.24).

The probability of occurrence of a wave height H is equals to the sum of the multiplied probabilities of occurrence of K_rH_1 and H_2 following (6.24). The probability of wave height H could be calculated with the probability of H_2 and the dependent probability of the derived H_1: $H_1=(H-H_2)/K_r$.

So the probability of a wave height in front of a structure H follows with:

$$f_{RND}(H) = \int_0^H f_{\underline{H}}(H_2) f_{\underline{H}}\left(\frac{H - H_2}{K_r}\right) dH_2 \tag{6.25}$$

In this equation it can be seen that all combination of H_2 and the derived $H_1(=(H-H_2)/K_r$ are used to integrate their probabilities. The probability of exceedance of the breaker height follows with:

$$P_{br}(H_b) = 1 - \int_0^{H_b} f_{RND}(H) \partial H \tag{6.26}$$

This integral is difficult to solve analytically. Monte Carlo simulation is applied to find Pbr in this model.

6.7 Plotting the theoretical model results with scale model observations

The measured data of the parameter P_{br} or measured probability of occurrence of breaking waves is plotted against the relative incoming unreflected significant wave height (H_{si}/h_s) for the models 1A, 2A and 3A in the next figures. Both data sets are shown; dark diamonds for the GWK data set (large scale wave flume data) and open diamonds for the WKS data set (small scale wave flume data).

If most of the data points are plotted between the lines corresponding with no reflection respectively full reflection, an optimal reflection coefficient exists. For this optimal reflection coefficient the variance of the error should reach a minimum.

First, the probability of occurrence of breaking waves is plotted for model 1A. Figure 6-21 shows the results.

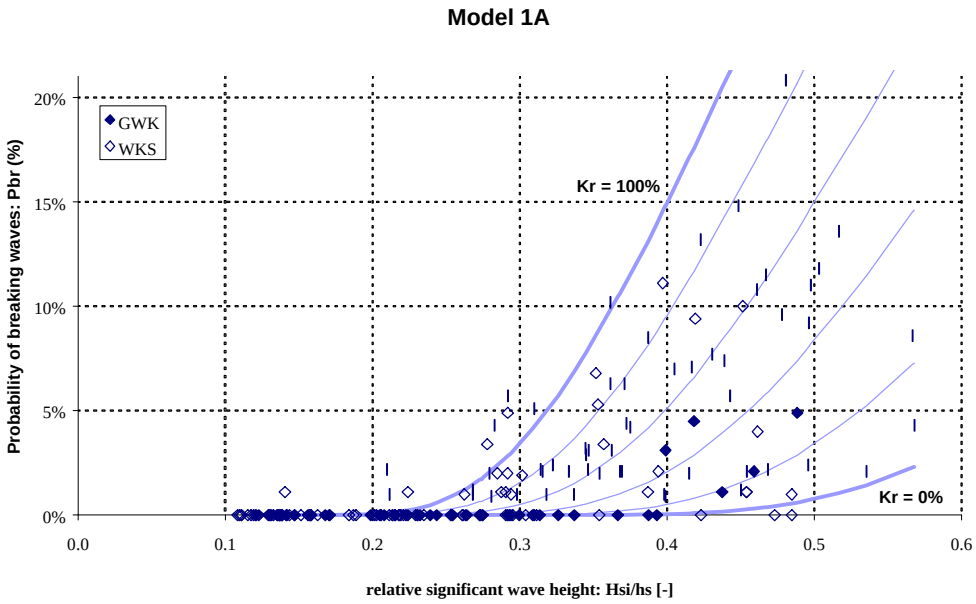

Figure 6-21: Data compared with normal reflection model 1(A)

In this figure the thin lines represent the probability of occurrence of partial reflected breaking waves as a function of the relative incoming unreflected significant wave height with steps of 20%. The thick lines describe the non- (K_r = 0%) and fully-reflected (K_r=100%) breaking waves probabilities. This also applies to Figure 6-23 through Figure 6-25.

More difficult is the presentation of model 2. The independent model parameters include the water depth in front of the berm (h_s) and the water depth above the berm (d). In Figure 6-22, all configurations are plotted against both water depths. The plot shows the configurations together with two lines. These lines indicate a lower and an upper boundary condition for all configurations. They are defined as

Condition	**Definition**	**Description**	$\mathbf{h_b/h_s}$	$\mathbf{d/h_s}$
lower bound:	$H_s/d = 1.5\ H_{si}/h_s$	low berms	1/3	2/3
upper bound:	$H_s/d = 5.0\ H_{si}/h_s$	high berms	4/5	1/5

Table 6-7: Conditions for truncated distribution model (2A), high and low berms

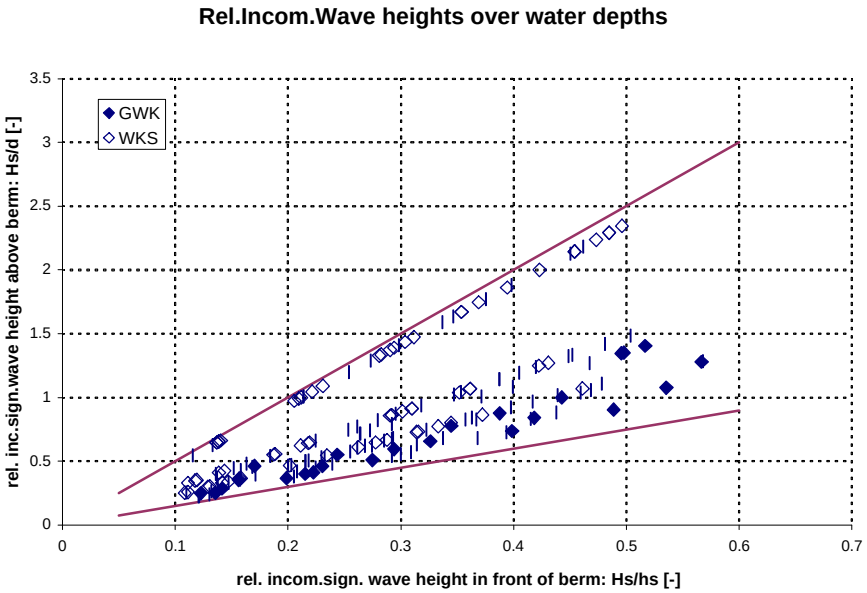

Figure 6-22: Relative incoming significant wave heights plotted for both water depths

Because all data can be plotted between these conditions, two data plots are shown (Figure 6-23 and Figure 6-24). These plots are calculated using the conditions for the relative incoming unreflected significant wave height proportional to the water depth above the berm. In these cases only sub-model A is shown (McCowan breaker function).

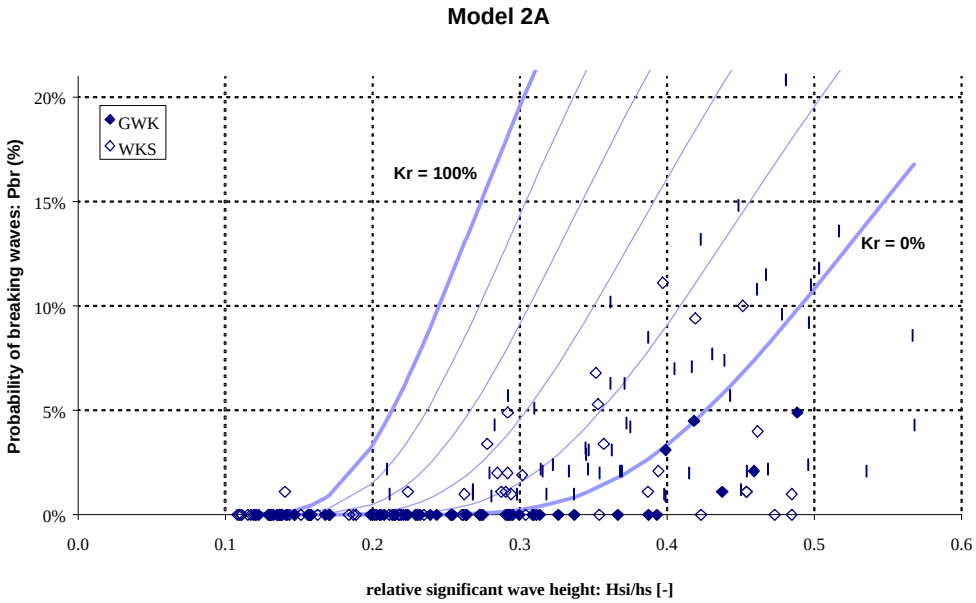

Figure 6-23: Data compared with truncated distribution model 2(A): relative low berms configurations

In case of assuming only relatively low berm height configurations (Figure 6-22) the line corresponding with a no-reflection crosses the data points. Calculating the probability of occurrence of breaking waves with this condition indicates that a reflection coefficient value around zero will result in the smallest deviations for the data sets.

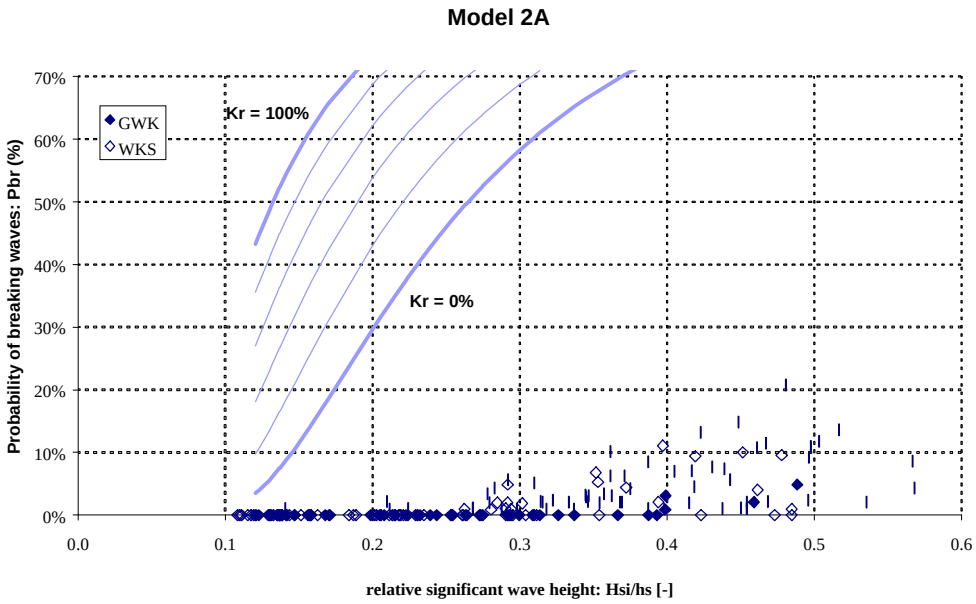

Figure 6-24: Data compared with truncated distribution model 2(A): relative high berms configurations

In case of assuming only relatively high berm height configurations (Figure 6-24) none of the data can be fitted with physically possible values of the reflection coefficient.

The following figure shows the full data set for the random reflection model with the McCowan breaker function, model 3A.

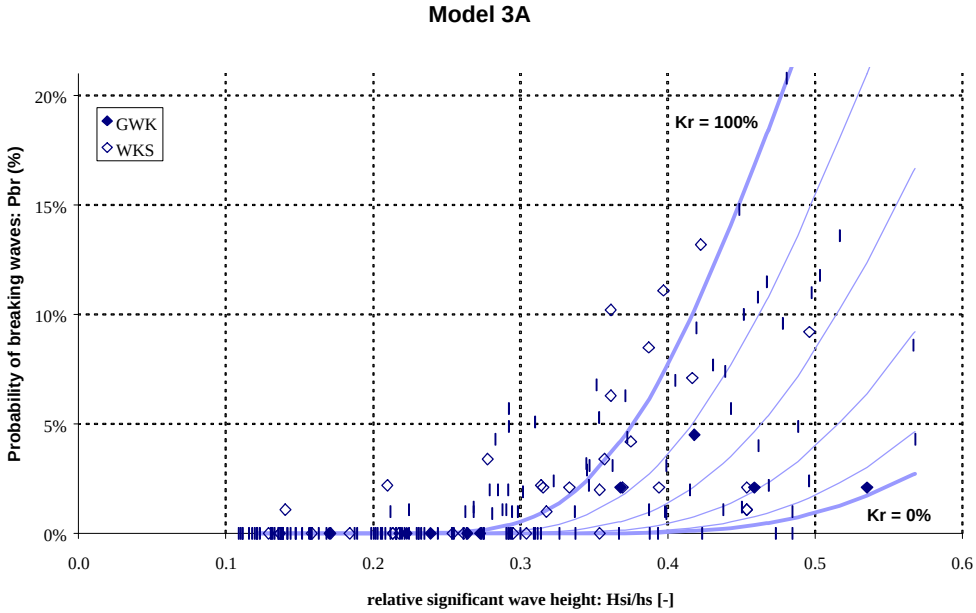

Figure 6-25: Data compared with random reflection model 3(A)

Model 1 and 3 show that the optimal reflection coefficients corresponding with the smallest variance of the error are within 0% (no reflection) and 100% (full reflection). Deriving optimal reflection coefficients with the method explained in section 6.5.3 is therefore possible.

Model 2 shows that the wave heights over the depth-ratios in front of the berm (H_s/d) are predicted much larger than the actual ratio's. This results in large error variances and should give no optimal reflection coefficient values in the possible range (0 to 1).

It can be seen that the probability of breaking waves does follow an exponential function of the relative significant wave height. If the measured probability of breaking waves is shown against the line of the more sophisticated random full reflection prediction model, it can be seen that for high probabilities this model gives an upper bound curve but for low probabilities this is less valid.

6.8 Calibration of models

In the following sections the data with the parameters are studied in two ways:

- Unsorted (combined and separated data sets)
- Sorted by the relative berm height (h_b/h_s)

Sorting the data by relative berm heights (h_b/h_s) results in seven groups with similar relative berm heights:

subset number	data set	relative berm height
A	GWK	0.460
B	GWK	0.503
C	GWK	0.557
D	GWK	0.632
E	WKS	0.569
F	WKS	0.788
G	WKS	0.661

Table 6-8: Relative berm heights for sorted data

6.8.1 Optimisations with unsorted data sets (combined and separated)

The following figures show the variance of the error between the observed probability of breaking waves (GWK and WKS data sets) and the probabilities of breaking waves calculated for different values of the reflection coefficient. The U-shaped variance-of-error functions dependent on the reflection coefficient are calculated for the situation when no berm influence is assumed (see U=0% in Figure 6-26). In this case the water depth in front of the berm h_s is used.

To clarify the function lines in the following figures an example is shown. Figure 6-26 shows an U-shaped variance of the error function (thick line). Only the depth in front of the berm is used (h_s) and gives this result for all models except model 2 (parameter U cannot be used when the two water depths are already used in case of model 2).

When this is also done for different values of the berm influence (see U=5%-15% in Figure 6-26) the minimum variances of the error can be connected (thick line with leftwards arrow).

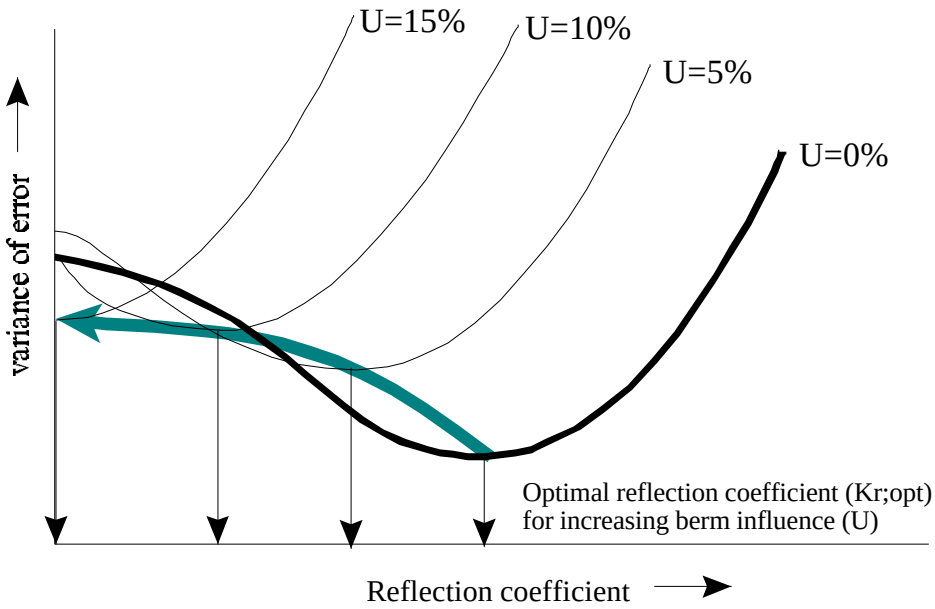

Figure 6-26: Example of optimal reflection coefficient ($K_{r;opt}$) for increasing berm influence (U)

When this is done with the full data set, the following figures demonstrate a wide u-shaped function (see Figure 6-27). This shape occurs for all different sub-models (A,B and C). In this figure various values for the berm influence parameter (U) are shown with which models 1 and 3 are calculated.

The figure shows a minimum of variance of the error when the free parameter, the reflection coefficient, equals the value 0.40 (see also Table 6-9). When the error is calculated for higher values for the reflection coefficient the error increases rapidly.

NOTE: In these figures the thick line shows the results when only h_s is used (except model 2) and the berm influence parameter U is equal to zero. An other thin line starting at the bottom of the U-shape function line and ending at the left of the figure (K_r=0) is added to the figure. This line, as explained in the previous paragraph, shows the connected minima of the errors (corresponding with the reflection coefficient optima) when the variable berm influence parameter U is used .

When the berm influence is implemented the line connecting the minima of the variance of the error shows an almost horizontal curve. This curve reaches often smaller minima and smaller corresponding reflection coefficients for increasing berm influence values.

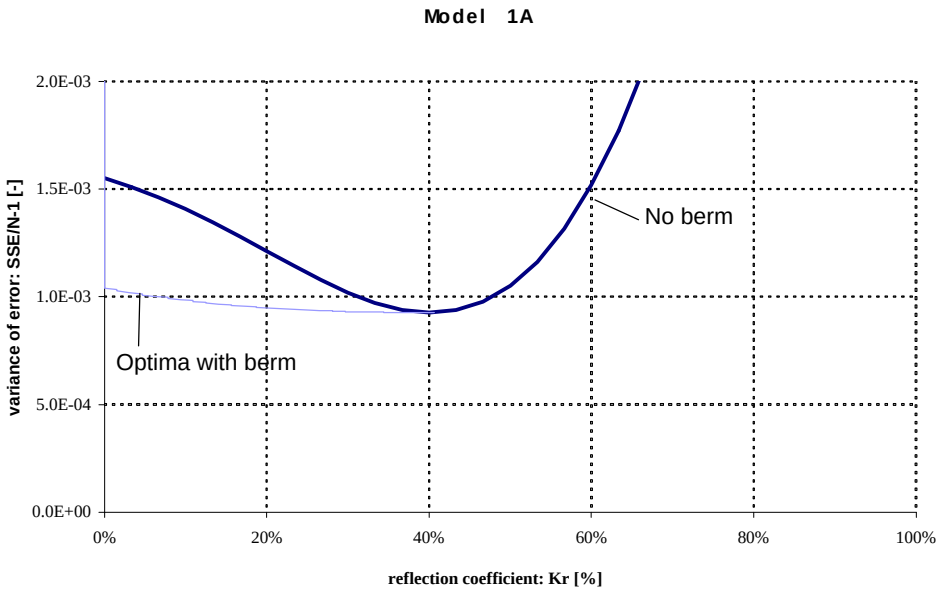

Figure 6-27: Model 1A with berminfluence; VAR(e)

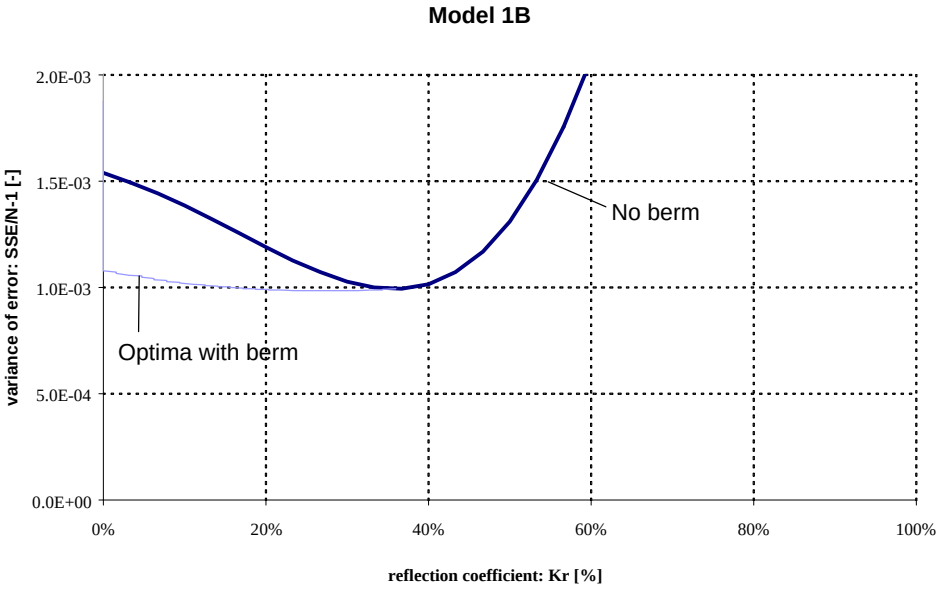

Figure 6-28: Model 1B with berminfluence; VAR(e)

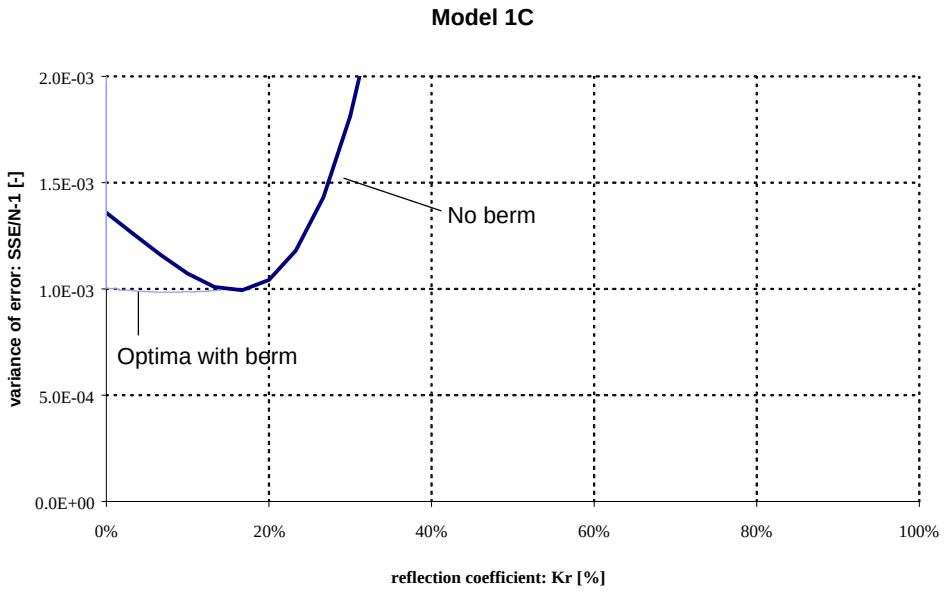

Figure 6-29: Model 1C with berminfluence; VAR(e)

The minima are plotted in the next two figures in case no berm influence (U=0) is taken into account (with only h_s as the water depth). They show the values for the reflection coefficients and the accompanying variance of the error. It can be seen that the optimal reflection coefficients are smaller when the wave steepness is taken into account (Miche (1B) and Oumeraci (1C) compared to McCowan (1A)). The corresponding variance of the error becomes larger in that case[6].

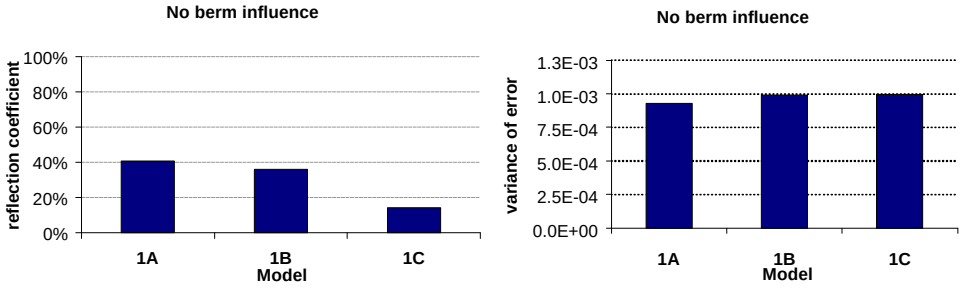

Figure 6-30: Model 1 without berm influence (optimal Kr)

We can also see that all three breaker criteria give similar variances of error, although the Miche and Oumeraci breaker functions result in somewhat larger errors. Both alternative breaker functions result in 6-7% larger variance of the error.

[6] Because an invalid Miche breaker function is used the values for the optimal reflection coefficients are also invalid. The smaller values for the Miche breaker function result in smaller values for the reflection coefficients as can be derived from equation (6.16). This does not influence the minima of the variance of the error.

If the berm influence (parameter U) is taken into account (using a varying water depth between h_s and d) the thin lines can be analysed (Figure 6-27, Figure 6-28 and Figure 6-29). The values of the optimal reflection coefficients corresponding with these new minima of the variance of the error are then plotted.

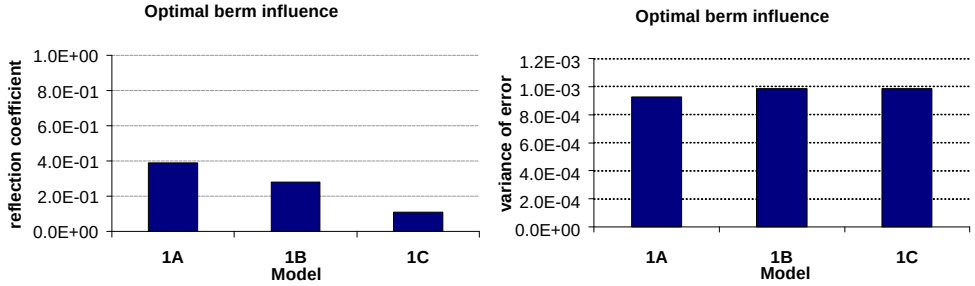

Figure 6-31: Model 1 with berm influence (optimal Kr)

Calculating optimal reflection coefficients in case the berm influence is taken into account gives similar results compared to no berm influence. Optimal values are often smaller. The minima of the variances decrease slightly for increasing values for the berm influence parameter and increase before the resulting reflection coefficient becomes negative (see Figure 6-27). The minimum variances of the error relative to the minimum variance for model 1A, in case of no berm, become:

Model	**berm infl.**	**$\Delta VAR_{MIN}(\varepsilon)$**	**U_{opt}**	**$K_{r;opt}$**
1A (McCowan)	Non	0%	0%	0.40625
	Optimal	-0.01%	1%	0.390625
1B (Miche)	Non	+7.14%	0%	0.359375
	Optimal	+6.26%	12%	0.28125
1C (Oumeraci)	Non	+7.19%	0%	0.140625
	Full	+6.48%	8%	0.109375

Table 6-9: Model 1 optimal reflection coefficient and Variance minima

Now the other models, truncated distribution model (2) and random reflection model (3) are calculated and the variance of the error as a function of the reflection coefficient is demonstrated. The following figure shows the results of model 2. This model uses both depths h_s and d. First the wave height distribution is truncated dependent on the depth in front of the berm (h_s) using Q_{br}. Then this new distribution is used to calculate the fraction of all incoming waves resulting in breaking waves above the berm with water depth d. This last probability is again defined as P_{br}. The berm influence parameter U is not used for this model to implement a water depth using both water depths, because they are already implemented separately.

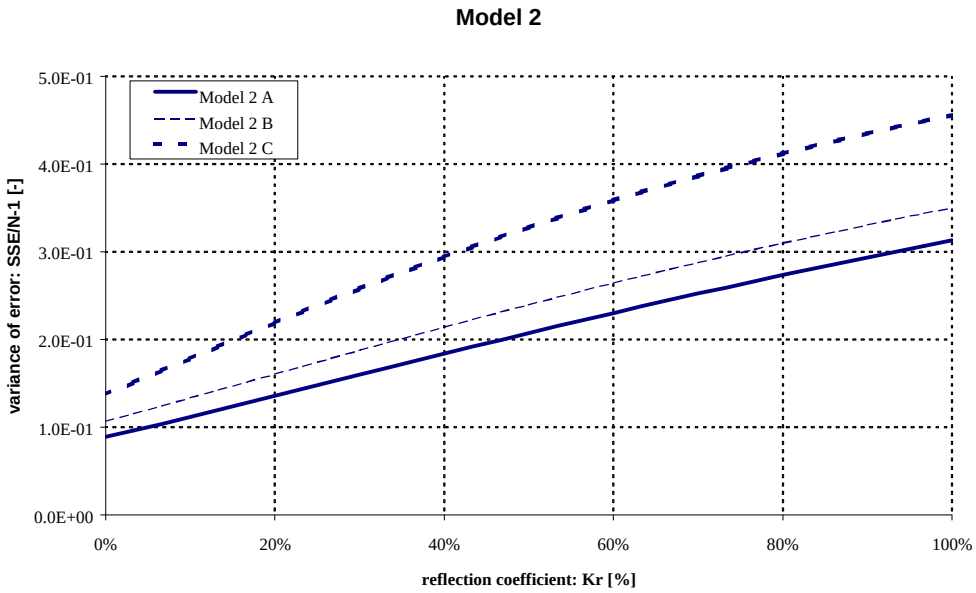

Figure 6-32: Model 2A,B and C; VAR(e)

Clearly the variance of the error is much larger than in case of model 1A. The variance of the error is 100 to 200 times larger (with increasing reflection coefficient).

Also it can be seen that the value for the reflection coefficient at which the variance of the error is minimum should be smaller than zero (and hence equals zero if an optimal possible value had to be chosen). Therefore it can be concluded that model 2 does not give good results and is denoted as non-applicable in the following sections.

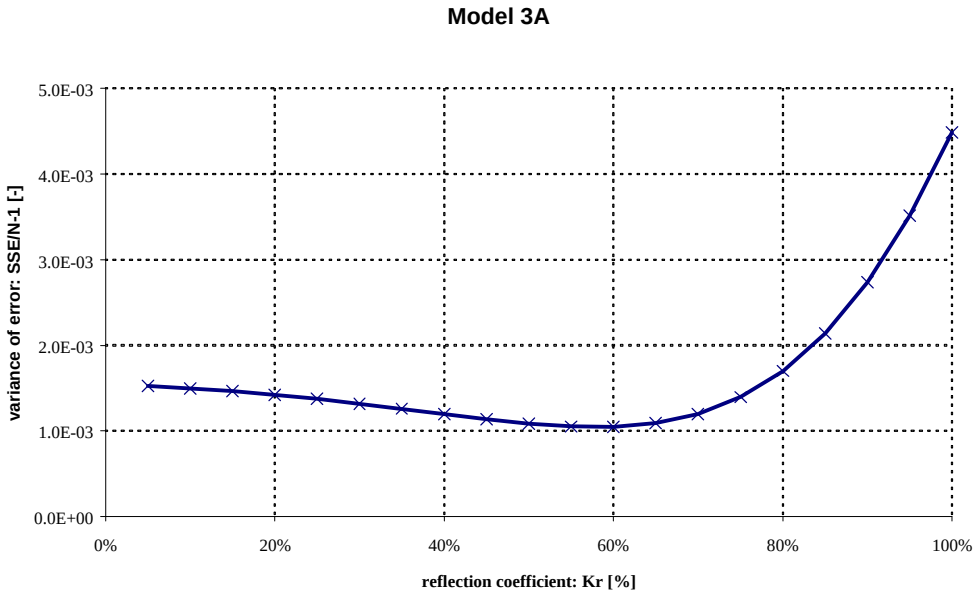

Figure 6-33: Model 3A; VAR(e)

This figure shows the result when model 3 (random reflection) has been calculated for the McCowan breaker function (3A). When results from this model (3A) are compared with

the results of model 1, the optimal reflection coefficient is larger and the the minimum variance of the error is larger.

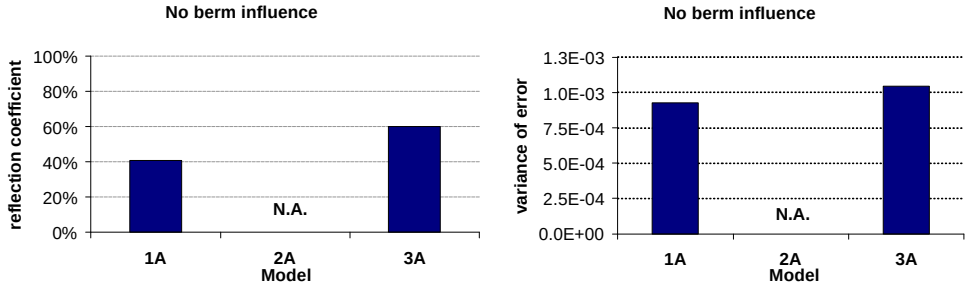

Figure 6-34: Model 1A,2A and 3A with no berm influence (optimal Kr)

Model	**$\Delta VAR_{MIN}(\varepsilon)$**	**$K_{r;opt}$**
1A	0.00%	0.406
2A	N.A.	N.A.
3A	12.95%	0.600

Table 6-10: Model 1,2 and 3 optimal reflection coefficient and variance minima

In the following figures the full data set is separated in the GWK and WKS data sets. First model 1A is shown.

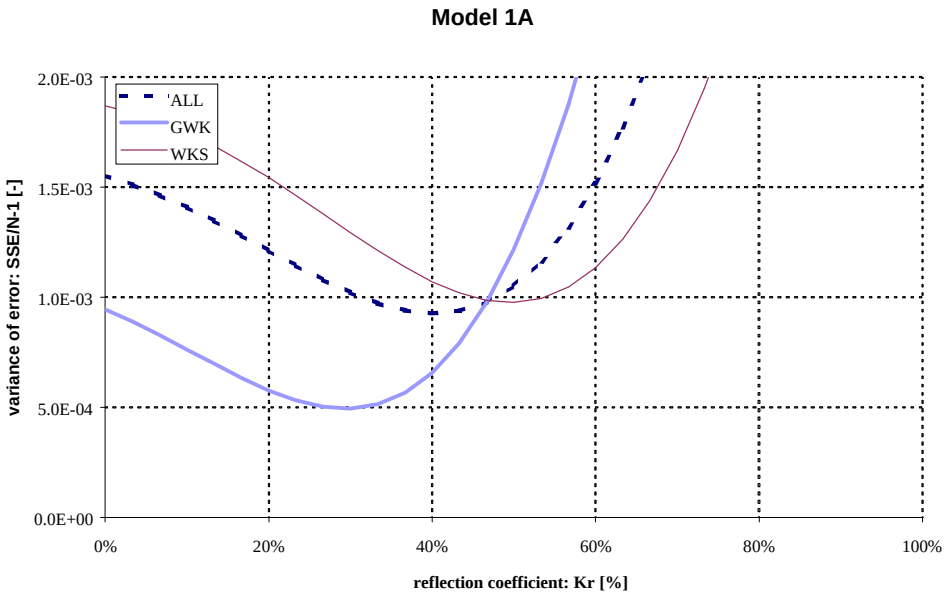

Figure 6-35: Model 1A with separated data set (GWK and WKS); VAR(e)

The variances with the GWK and WKS data sets calculated separately still demonstrate similar function shapes, although with altered minima and optimal reflection coefficient. As can be seen the GWK data set gives a smaller optimal reflection coefficient (30%), but also a smaller variance of error (-46.7%). The GWK data set conducted in the smaller wave flume results in higher variance of the error (+5.3%) and gives a larger optimal reflection coefficient (50%). When the models 1B and 1C are also calculated the following optimal values are obtained together with the variance of the error Figure 6-36).

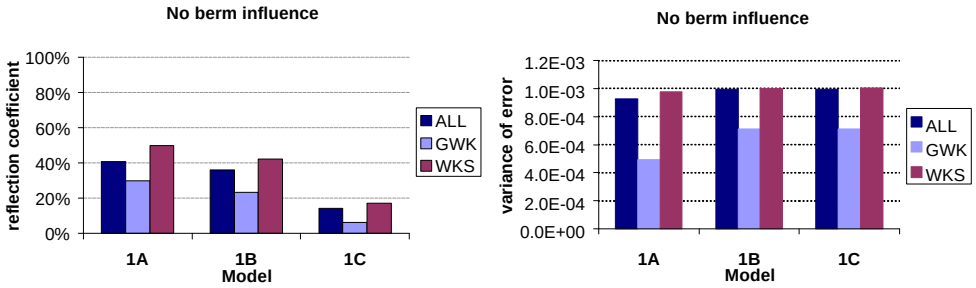

Figure 6-36: Model 1 without berm influence (optimal Kr;splittted)

In the following figures the models 1A, 1B and 1C (normal reflection model) are calculated with the berm influence taken into account. The thin lines represent the same results as shown in Figure 6-35. The additional thick lines represent the minima of the variance of the error corresponding with the reflection coefficient when the parameter U is used. The data sets GWK and WKS are shown separately for increasing berm influence. The minimum variances (shown as grey lines in Figure 6-37, equal to Figure 6-35) when no berm in taken into account correspond to the start of the lines showing the optimal variances of the error for increasing berm influence. For increasing berm influence the optimum variance of the error is constant for very small berm influences but converges for larger values.

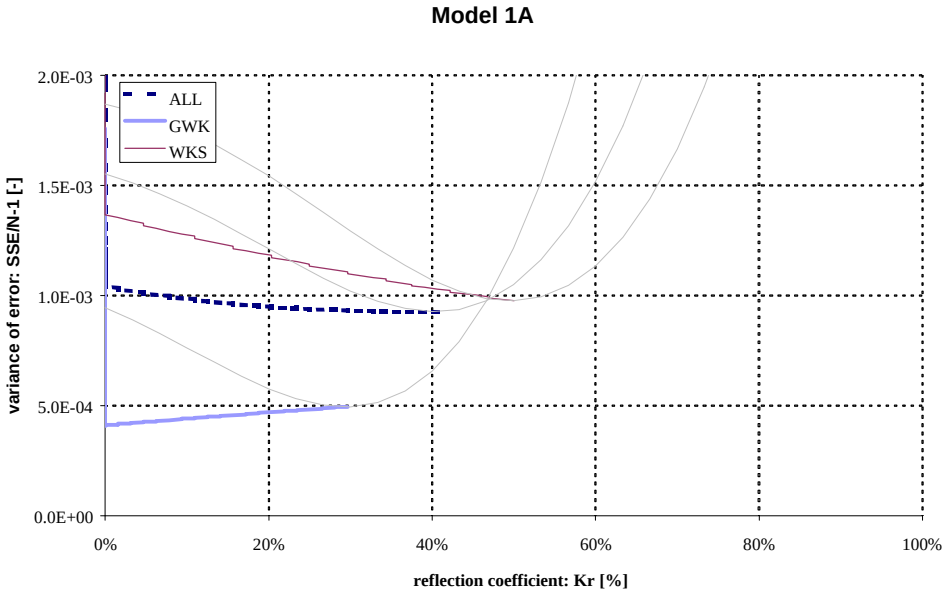

Figure 6-37: Model 1A with separated data sets with berm influence; VAR(e)

Figure 6-37 shows an increasing line for the smaller wave flume data (WKS) for increasing berm influences (and decreasing reflection coefficients). Also a decreasing line is shown for the larger wave flume data (GWK) for increasing berm influences (and also decreasing reflection coefficients).

When the variance of the error is plotted against the berm influence parameter U, Figure 6-38 shows that only the GWK data set gives smaller values when this berm influence is taken into account. No resulting optimal reflection coefficients are shown in this figure.

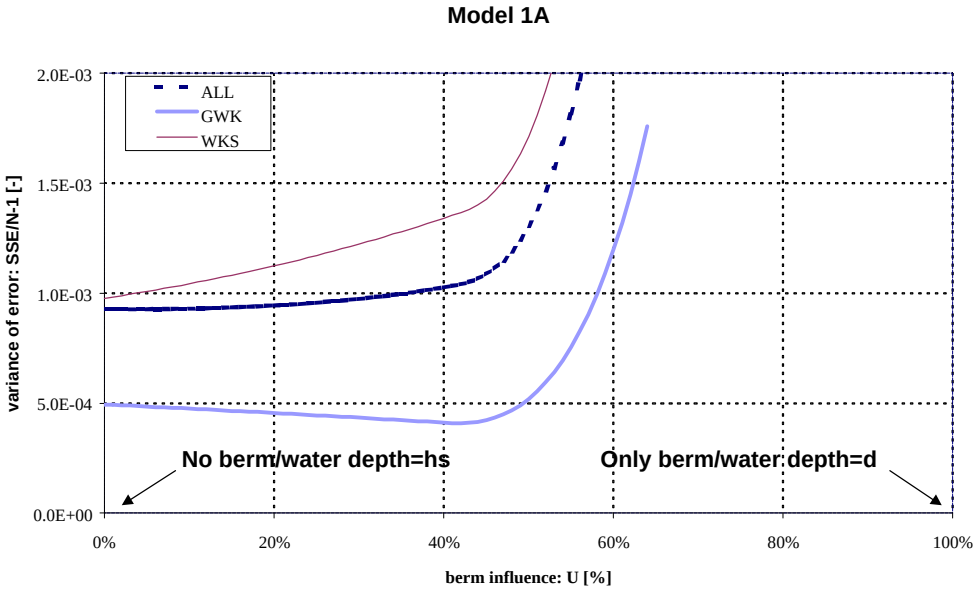

Figure 6-38: Model 1A (GWK and WKS); VAR(e) against berm influence

Also when calculated with the models 1B and 1C the smaller wave flume data (WKS) result in a bit larger (optimal) reflection coefficients and give similar variance of the error.

Also when calculated with the models 1B and 1C the results show a minimum value for the variance of the error for a negative reflection coefficient. Because this is impossible, derivation of an optimal berm influence value when splitting the dataset into the two data sets is considered to be non-applicable.

When the calculations have been performed for model 3A, the following figures and table show the results for the separated data set (into WKS and GWK data). No berm influence is taken into account and the relative increase of the variance of the error is also shown in Table 6-11.

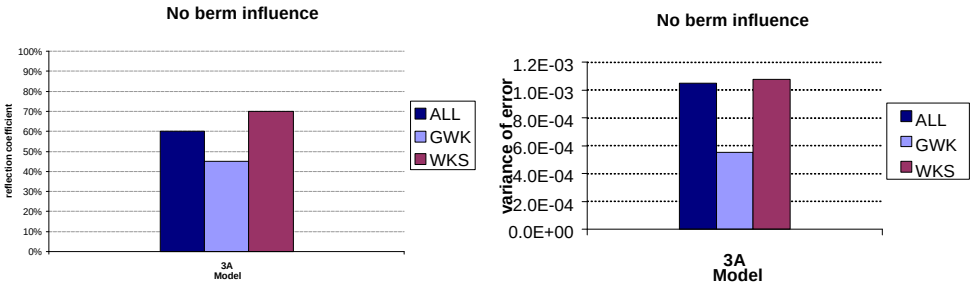

Figure 6-39: Model 3A without berm influence (optimal Kr; separated)

Data:	All		GWK		WKS	
Model:	K_r	$\Delta VAR_{MIN}(\varepsilon)$	K_r	$\Delta VAR_{MIN}(\varepsilon)$	K_r	$\Delta VAR_{MIN}(\varepsilon)$
1A	39.1%	0.00%	29.7%	-46.71%	50.0%	5.34%
2A	N.A.	N.A.	N.A.	N.A.	N.A.	N.A.
3A	60%	12.95%	45.0%	-40.16%	70.0%	16.37%

Table 6-11: Model 1,2 and 3 optimal reflection coefficient and variance minima (splitted)

6.8.2 Optimisations with sorted data sets (by relative berm height)

When the complete data set is sorted by relative berm height (h_b/h_s) seven data groups are obtained with (almost) equal relative berm heights (see Table 6-8). When these sub sets are analysed individually and the variance of the error is calculated as a function of the reflection coefficient, the following figure shows the results.

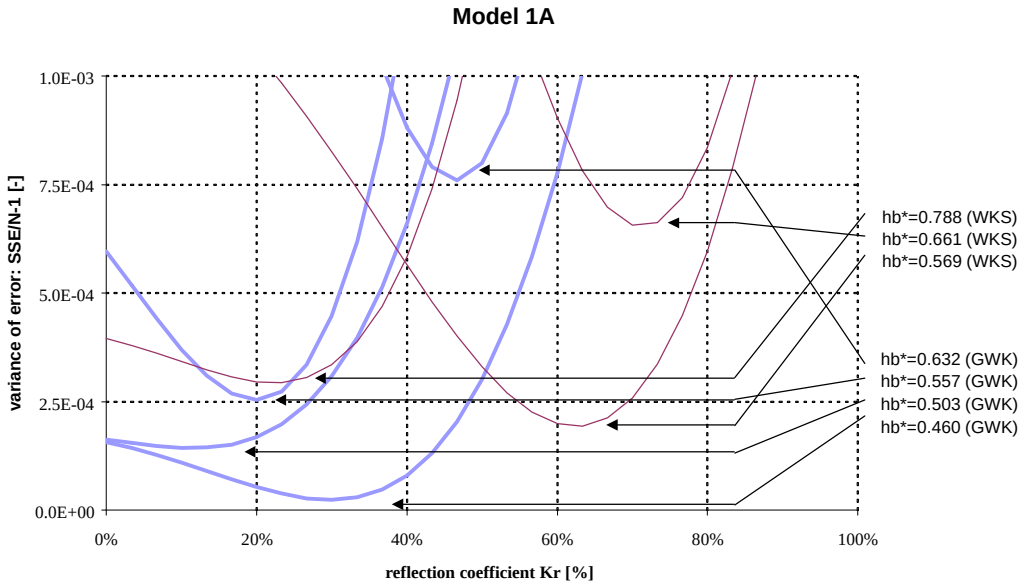

Figure 6-40: Model 1A (sorted); VAR(e)

As can be seen no systematic behaviour can be interpreted viewing these sub sets individually. When different values for the berm influence are used for calculating the optimal reflection coefficients, the following figure shows the connecting lines. All sub sets show almost straight function lines. This figure shows that for all sub sets, the optimal reflection coefficient decreases with an increasing berm influence.

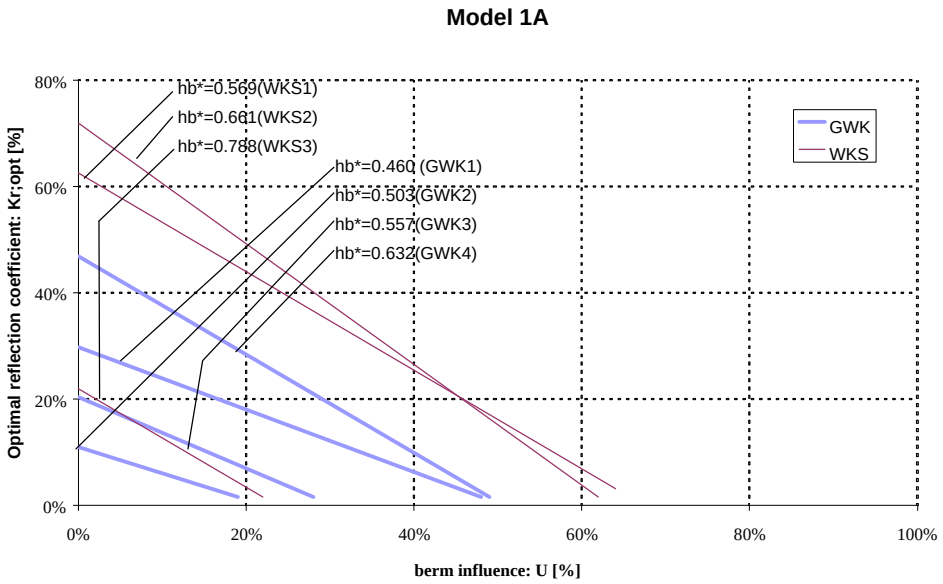

Figure 6-41: Model 1A (sorted); berm influence against reflection coefficient

When the berm influence is calculated for the sub sets, the following figure shows the lines connecting the minimal variances for different berm influence parameter values. Clearly altering the berm influence does not have any effect on the minimum variance of the error.

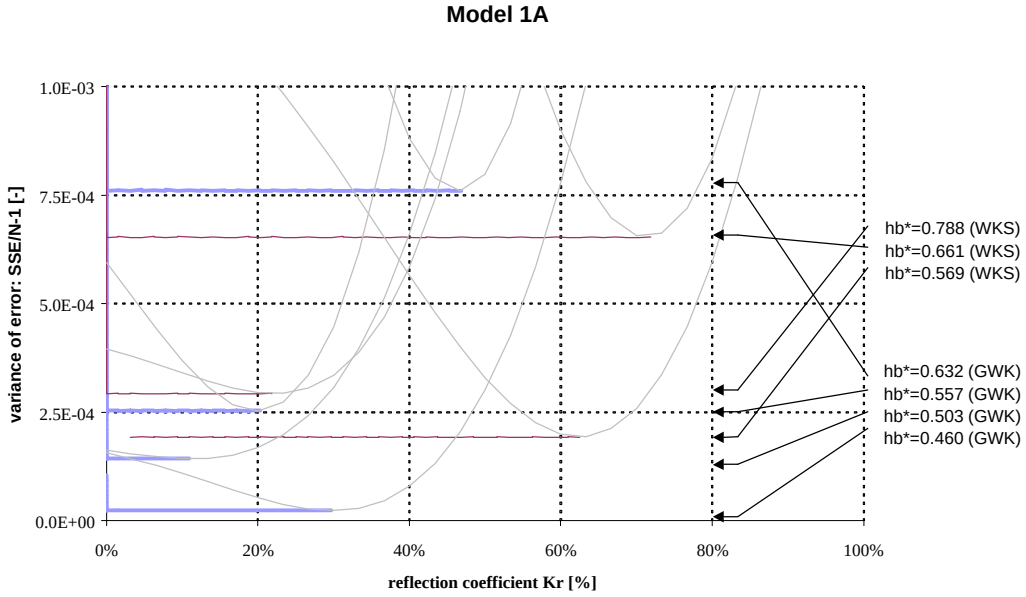

Figure 6-42: Model 1A (sorted); VAR(e) with berm influence

When the data is plotted against the berm influence instead of the reflection coefficient, Figure 6-43 demonstrates also no influence or dependency for berm influences smaller than 20%.

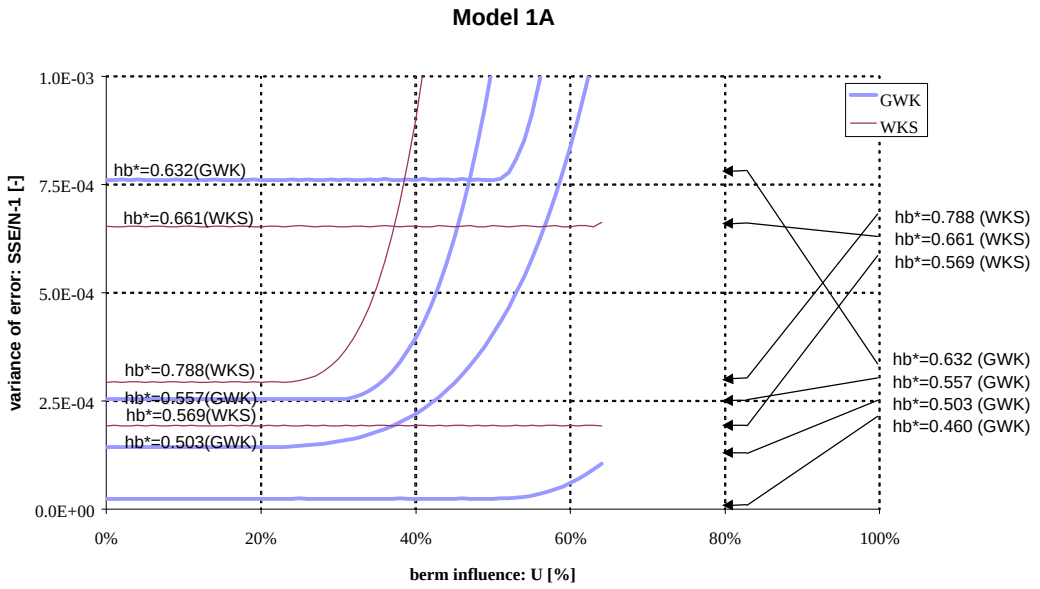

Figure 6-43: Model 1A (sorted); VAR(e) against berm influence

The point from which the variance of the error increases rapidly seems to be unpredictable. For the smallest sub set in each data set GWK or WKS the berm influence below which the variance of the error seem to be constant, decreases with increasing relative berm height.

If the berm influence parameter U is expressed with the relative berm length (B_{eq}/L_{hs}) this could clarify the horizontal shape, because the average berm length (B_{eq}) made relative with the wave length (L_{hs}) is smaller than 25%.

A possibility for the lines being horizontal and showing no dependence on the berm influence is maybe the size of the data sets. The four GWK (large scale wave flume) data subsets contain each approximately 16 tests. The three WKS (small scale wave flume) data subsets contain each approximately 40 tests. When a larger wave set size has been created more influence is to be expected from the implementation of the berm influence.

Now the calculated optimal reflection coefficient is plotted against the relative berm height. The first figure shows the varying (minimal) variance of the error also against the relative berm height. The lines, also calculated for the models 1B, 1C and 3A, demonstrate similar shapes. The large scale wave flume data set (GWK) shows an increasing variance of the error for increasing relative berm heights in contrast to the small scale wave flume data set (WKS) which shows a convex function shape. Apparently the scatter in the prediction models increases when configurations with higher berms are used to measure the probability of occurrence of breaking waves. The minimum variance of the error difference appears to be smaller for the highest berm height configuration (WKS with h_b/h_s=0.788) shown in the following figure.

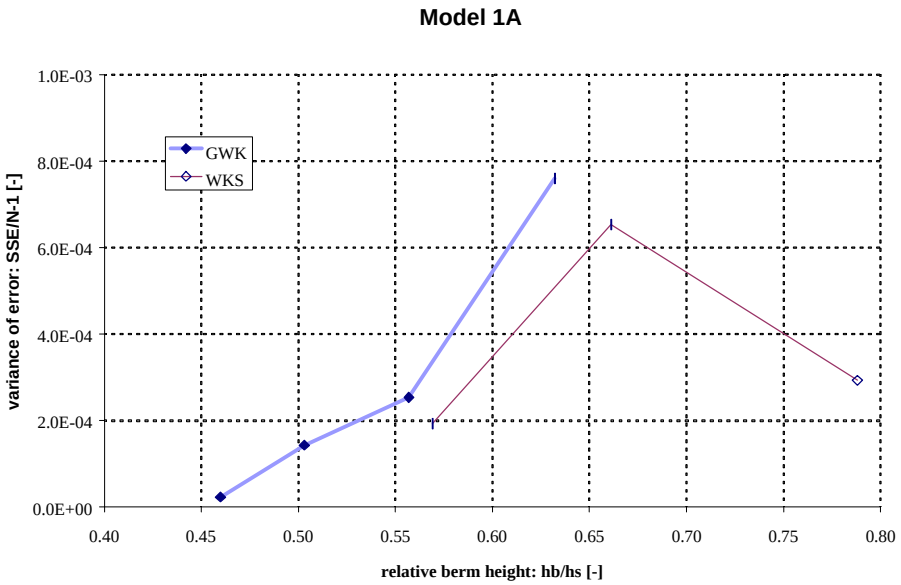

Figure 6-44: Model 1A (sorted); VAR(e) against relative berm height

It is expected that the models should give (almost) full reflection coefficient values (K_r = 100%) for configurations with no berm present. The wave is in that case not influenced by it, only by the depth h_s and the vertical wall.

For configurations with high relative berm heights the models should give very small reflection coefficients. This is the case when the berm height is equal to the depth h_s giving no vertical wall area for the waves to be reflected by it. This qualitative prediction of the behaviour of the reflection coefficient as a function of the relative berm height matches the following proposition made in the PROVERBS project. The reflection coefficient in the breaker criterion after Oumeraci is proposed for several configurations [Calabrese and Allsop, 1998]:

- $Kr = 0.95$ for simple vertical walls with a low berm and a high crest
- $Kr = 0.8 + 0.1R_c / H_{si}$ for low crest walls ($0.5 < R_c / H_{si} < 1.0$),
- $Kr = 0.5$ to 0.7 for composite walls, high berms and heavy breaking

These conditions include the crest of the wall (R_c) defined as the maximum elevation of the vertical wall above the still water level. The WKS data set (small wave flume, scale 1:15) does show a resemblance with the predicted function shape for the sorted data sets. The GWK data set demonstrates no resemblance whatsoever. It could be suggested that this data set shows an opposed function shape, meaning low reflection coefficients for small berm heights and higher reflection coefficients for high berm heights. This could be the result of the fact that the berm itself reflects the incoming waves.

The following figures show the reflection coefficient dependent as a function of the relative berm height.

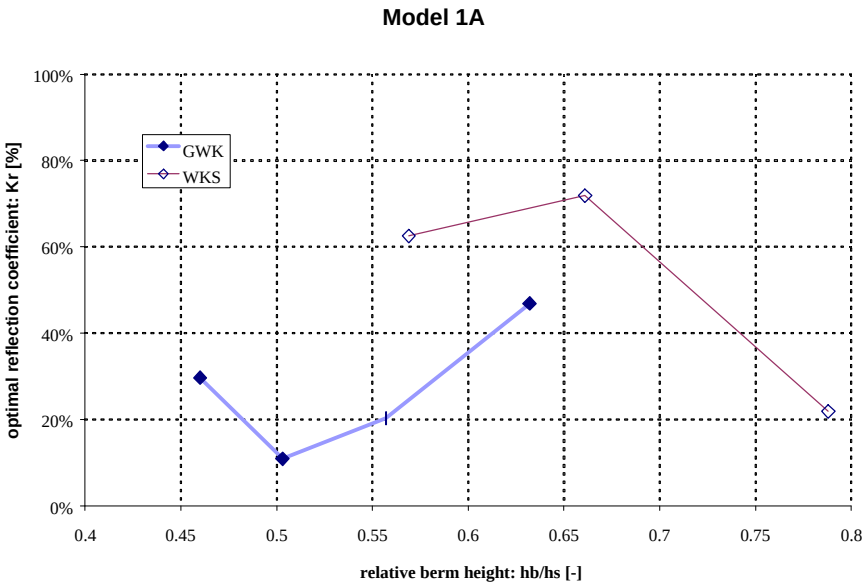

Figure 6-45: Model 1A (sorted); reflection coefficient against relative berm height

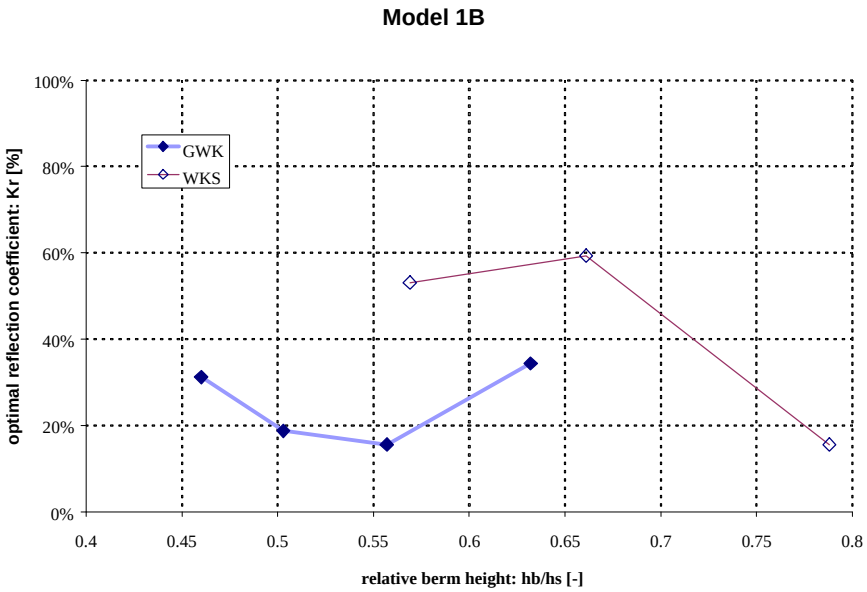

Figure 6-46: Model 1B (sorted); reflection coefficient against relative berm height

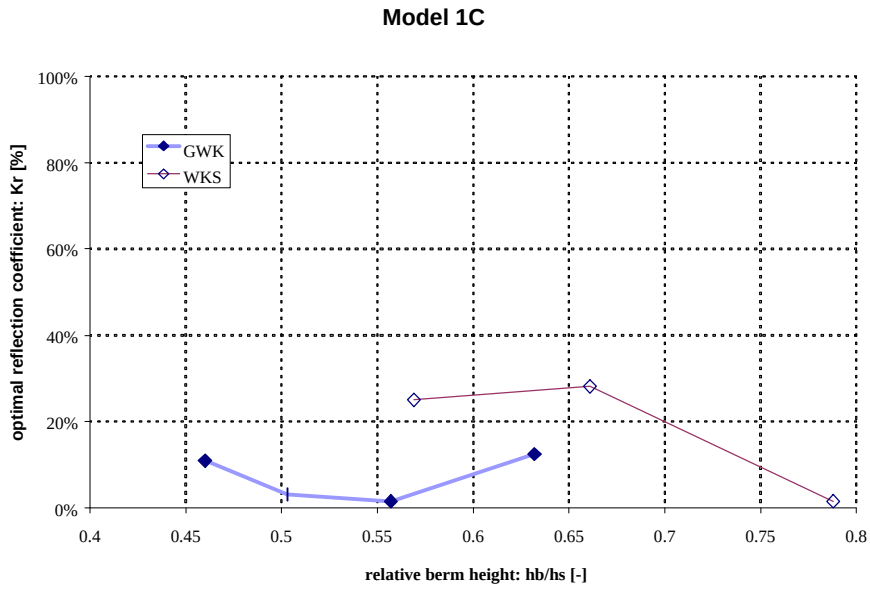

Figure 6-47: Model 1C (sorted); reflection coefficient against relative berm height

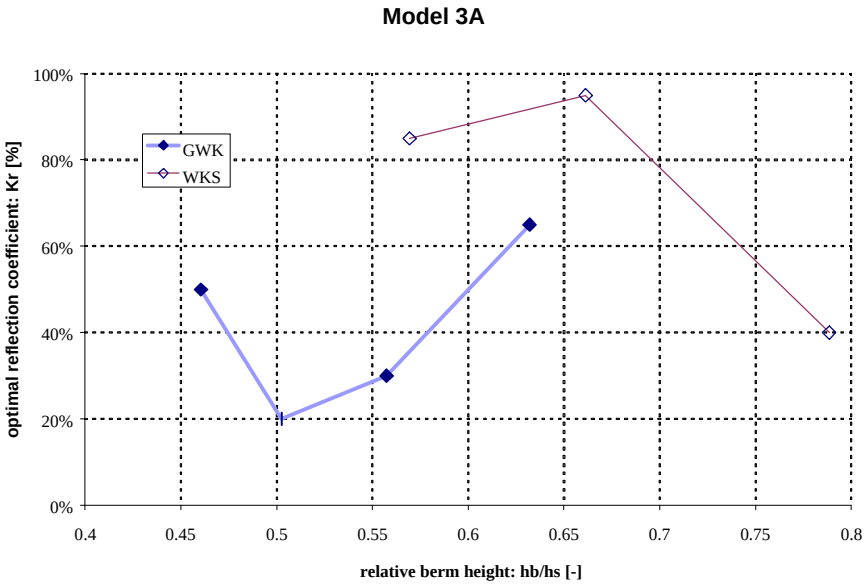

Figure 6-48: Model 3A (sorted); reflection coefficient against relative berm height

The following tables show the model results, similar to the results plotted in the previous figures. Both reflection coefficients are shown and their variance of model error.

Data set	h_b/h_s	Variance of error: var(ε) Model			
		1A	1B	1C	3A
GWK	0.460	0.024	0.019	0.019	0.025
GWK	0.503	0.143	0.105	0.105	0.149
GWK	0.557	0.254	0.403	0.404	0.285
GWK	0.632	0.760	2.392	2.392	0.861
WKS	0.569	0.193	0.146	0.148	0.302
WKS	0.661	0.653	1.051	1.050	0.903
WKS	0.788	0.293	0.342	0.343	0.295

Table 6-12: Variance of model error: var(e) for sorted sub sets

Data	h_b/h_s	Reflection coefficient: K_r Model			
		1A	1B	1C	3A
GWK	0.460	0.297	0.313	0.109	0.600
GWK	0.503	0.109	0.188	0.031	0.450
GWK	0.557	0.203	0.156	0.016	0.700
GWK	0.632	0.469	0.344	0.125	0.500
WKS	0.569	0.625	0.531	0.250	0.200
WKS	0.661	0.719	0.594	0.281	0.300
WKS	0.788	0.219	0.156	0.016	0.650

Table 6-13: Optimal reflection coefficient: K_r for sorted sub sets

All breaker functions show clearly similar function shapes. The large scale wave flume data set (GWK) demonstrates a concave function and the small scale wave flume data set (WKS) demonstrates a convex shape. Also the WKS data set shows every time larger reflection coefficients than the GWK data set.

No clear optimal reflection coefficient function can be derived when both data sets are used. It is therefore extremely difficult to extract a function consistent for different scales and configurations. The difference of the results is dependent on the different laboratories that performed these tests. The test results can therefore be characterised as suspicious.

7 CONCLUSIONS AND RECOMMENDATIONS

7.1 Introduction

In this chapter, the last chapter, the conclusions and the most important results of this study on probability of occurrence of breaking waves and wave impacts will be presented. Throughout the report conclusions and interim results have been presented by using the results of an extensive study of literature, own findings and the calculations which have been carried out by means of a least square error method used for three different models. These models have been used to study the probability of occurrence of different types of waves against a vertical wall structure and the effect of the presence of a berm on the probabilities.

In this chapter a summary of the most important conclusions and results can be found. Some of these conclusions end up in recommendations, which should -in my opinion- be taken into account when vertical walls are designed.

7.2 Conclusions

When the data sets were analysed a large dependency was found between the observed probability of occurrence of breaking waves (P_{br}) based on video analysis and the probability of occurrence of impact waves (P_{fh}) based on times series of forces. Sometimes the amount of observed wave impacts exceeded the amount of observed breaking waves ($P_{fh}>P_{br}$), which should be impossible.

Also the fact that the probability of impact waves is not a fraction of the probability of breaking waves, the definition of breaking waves used for the data set is not credible. The assumption that each breaking wave will give an impact is believed to be not true. Because the parameter used to define the probability of occurrence of breaking waves (P_{br}) is based on the breaking waves definition and is used throughout the study, the results are also not credible.

This dependency (almost all ratios of these probabilities are between 0.95 and 1.05, see Figure 6-7) is accepted in the rest of the study but should be envisaged when viewing the results.
Both data sets GWK and WKS can be sorted by relative berm height (h_b/h_s) and give only three resp. four data subsets. No relative berm height is equal for both data sets. Therefore no specific quantitative comparison of the results with this parameter can be performed, only a qualitatively comparison.

When the data was inspected with the PROVERBS Parameter Map, the parameter map conditions expressed with H_{si}/h_s and h_b/h_s showed disagreement with the data. Despite the fact that the two data sets GWK and WKS have been used to calibrate the PROVERBS parameter map, they give no perfect agreement with the impact conditions of the parameter map. For configurations for which the parameter map predicts impact loads, many observations (46%) show no impact loads at all (see Figure 6-13). For

configurations for which the parameter map predicts no impacts, impacts were observed (see Figure 6-13) in 6.3% of WKS tests (not for WKS tests).

When the models were compared with the data sets, the following conclusions have been drawn.

The method used for optimisation of the reflection coefficient gives satisfactory results. In case of model 1 and 3 (normal reflection model resp. random reflection model) physically possible reflection coefficients have been obtained. This is the case when the probability of occurrence of breaking waves (P_{br}) is plotted against the relative incoming unreflected significant wave height (H_{si}/h_s) as shown in Figure 6-21 and Figure 6-25. In case of model 2 negative values for the reflection coefficient have been obtained. Because this is physically impossible this model is not considered to be applicable.

When the different models are compared with each other, model 1 gives the smallest variances of the error calculated for the probability of occurrence of breaking waves. In this case no berm influence is taken into account and the resulting optimal reflection coefficient equals 40%. Model 3 shows a 13% larger variance of the error and a reflection coefficient of 60%.

In case of using different breaker index function, indicated as model A (with McCowan), model B (with Miche) and model C (with Oumeraci), the following conclusions are important. As explained at the introduction of the different breaker index functions used for the models, all three breaker index functions are specifically applicable to progressive waves, not standing waves. The correct Miche breaker function used for standing waves is shown but is not used throughout the calculations. Because this does not influence the variance of the error, used to compare the accuracy of the models, model 1A still does give the smallest variances in the error and it is still proposed that this model is the most appropriate to predict the probability of breaking waves. Using the incorrect breaker functions however changes the reflection coefficient. Because in the following equation which summarises the breaker equation for individual non breaking waves: $H_i(1+K_r)<\gamma h$ the breaker indices should be smaller, the optimal reflection coefficients should also be smaller. Because this applies to all models, the numeric results should not be fully trusted, but their behaviour is assumed to be less influences by it. Qualitative conclusions can still be drawn.

When the different sub-models are compared with each other, models 1B and 1C give approximately 7% larger variances of the error compared to model 1A. The resulting optimal reflection coefficients for the models 1B and 1C are 36% resp. 14% smaller compared to the optimal reflection coefficient of model 1A (40%).

When both data sets are viewed separately, the large scale wave flume data set (GWK) gives smaller optimal reflection coefficients and up to 46% smaller corresponding variances of the error compared to the full data set (GWK and WKS). The small scale wave flume data set (WKS) gives larger optimal reflection coefficients and larger corresponding variances of the error (compared to the full data set).

When the berm influence parameter is added to calculated the optimal reflection coefficient a systematically behaviour can be observed. For the large scale wave flume data set (GWK), in case of a berm influence equal to approximately 40%, an optimal but negative reflection coefficient has been found. For the small scale wave flume data set (WKS) the variance of the error increases for increasing berm influences and therefore

gives an optimal reflection coefficient equal to the one found for no berm influence (40%, see Figure 6-38). It can be concluded that implementing a berm influence parameter does not give satisfactory results for finding an optimal reflection coefficient with smaller variance of the error.

When the data sets are sorted by relative berm heights, the variance of the error demonstrates a very complex behaviour. For smaller relative berm heights the models 1B and 1C show smaller variances of the error, while for larger relative berm heights, the variance becomes larger. Only for model 3A, the variances of the error are approximately equal to those of model 1A, in case of the large scale wave flume data set (GWK). In case of the small scale wave flume data set (WKS), all variances of the error for model 3A are larger. The results are shown in Table 6-13.

The behaviour of the reflection coefficient in case of the large scale wave flume data set (GWK) shows no agreement with the premature predicted reflection coefficient when it is expressed with the relative berm height. In case of the small scale wave flume data (WKS) better agreement can be seen.

The following global conclusions have been drawn:

- The normal reflection model (model 1) gives the smallest variances in the error of the probabilities of the occurrence of breaking waves.
- The use of a berm influence parameter does not result in significant increase of the accuracy of any model developed in this project for the full data set.
- Including breaker functions dependent on the wave steepness or on the reflection coefficient does not result in an increase of the accuracy compared to model 1A.
- Although the large wave flume data set (GWK) consists of less data compared to the small wave flume data set (WKS), the resulting variances of the error are much smaller.
- For the WKS data set the model results show resemblance with the qualitative predictions, stating almost large reflection coefficients for relative small berm heights and small reflection coefficients for relative higher berm heights.
- The number of berm configurations, performed tests and scales used to construct the data sets is very small.
- The probability of occurrence breaking waves used in the data set is not clearly defined.
- The results of the calculations performed with these tests can be used for qualitative interpretation.
- No accurate breaker model used to predict the probability of occurrence of breaking waves and impact waves could be developed.

7.3 Recommendations

- The normal reflection model (1A) developed in this study can be used as an envelope curve when the probability of occurrence of wave impacts is to be calculated. Because of the large scatter around the model results a derived upper bound probability value should be used only in the early stage of the design process. The results should be compared with results from physical model scales.
- To investigate the influence of the model scales more data sets should be used or more tests should be performed to compare the different model scales and to analyse the influence of the scale on the probability of wave impacts.
- To develop a function for the probability of occurrence of wave impacts or breaking waves, a large number of configurations should be used to construct the necessary data set.
- Berm length and the slope of the front of the berm have to be investigated to increase the understanding about the influence of the berm dimensions on the wave breaking conditions.
- A further study taking into account the PROVERBS conclusions and calibrated parameters could be an extension of this study.
- The shape of breaking waves as a function of the geometric and hydraulic parameters could be investigated. This could result in a better model for calculating the probability of occurrences of breaking waves and wave impacts.
- Data set measurements can be compared to numerical or analytical simulation models. In these simulation models the upper limit for breaking waves could be investigated.
- Also models including turbulence could be developed and analysed with the use of more complex berm geometry. Although development of these models is still an important field of research at present, it could be available in the near future.

REFERENCES

Allsop, N.W.H.,et al'Wave forces on vertical and composite breakwaters.', Wallingford, United Kingdom,1996

d'Angremond K, Bezuijen K.G.,"Waterbouwkunde", Lecture notes F30, Subfaculty of Civil Engineering, Hydraulic Engineering, Delft University of Technology, The Netherlands, Delft 1993

d'Angremond K, Velden E.T.J.M. Pluim-Van der, "Introduction to Coastal Engineering", lecture notes CT4300, Subfaculty of Civil Engineering, Hydraulic Engineering, Delft University of Technology, The Netherlands, Delft, 2000

Battjes J.A., "Surf similarity", Proc. of 14th Int. Conf. on Coastal Eng., 1974

Battjes J.A., Janssen J.P.F.M., "Energy loss and set-up due to breaking of random waves", Proc. of 16th Int Conf. on Coastal Eng., 1978

Battjes J.A., Stive M.J.F., "Calibration and verification of a dissipation model for random breaking waves", Journ. of Geophys. Res. 90 (C5), 1985

Battjes J.A., "Surf-zone dynamics", Ann. Rev. Fluid. Mechanics, 1988

Battjes J.A., "Windgolven", lecture notes, Subfaculty of Civil Engineering, Hydraulic Engineering, Delft University of Technology, The Netherlands, Delft, 1992a

Battjes J.A., Beji S., "Breaking waves over a shoal", Proc of 23th Int. Conf. on Coastal Eng, 1992b

Battjes J.A., :Shallow water wave modelling", Proc. of international symposium: waves - physical and numerical modelling, 1994

Battjes J.A., "Korte golven", lecture notes, Subfaculty of Civil Engineering, Hydraulic Engineering, Delft University of Technology, The Netherlands, Delft 1998

Battjes J.A., Groenendijk H.W., "Wave height distribution on shallow foreshores", Coastal Eng, 40, 2000

Beji S, Battjes J.A., "Experimental investigation of wave propagation over a bar", Coastal Eng., 19, 1992

Bezuijen K.G.,"Waterbouwkunde", Lecture notes F30, Subfaculty of Civil Engineering, Hydraulic Engineering, Delft University of Technology, The Netherlands, Delft 1993

Boussinesq J., "Théorie des ondes et des remous qui se propagent le continu dans ce canal des vitesses sensiblement pareille de la surface au fond", J. Math. Pures Appl., Vol.17, pp55-108, 1872

Bruining J.W., "Wave forces on vertical breakwaters,. Reliability of design formula", 1994, TUDelft

Bruun P., "Port Engineering, Harbor Planning, Breakwaters, and Marine Terminals, Vol I, 4th edition", Housten 1989, GPC

CERC,' Shore Protection Manual, Fourth edition', U.S.Government Printing Office, Washington, D.C., U.S.A, 1984

Chuang S.L., “Experients on Slamming of Wedge-shaped Bodies”, Journal of Ship Research, September 1967

Cooker J. and Peregrine D.H. ,”Wave breaking and wave impact pressures. In:Development in Coastal Engineering”, Univ.of Bristol, 1991

Dantzig D.v., Extrapolation of the frequency curve of the loads at high tide at Hook of Holland by means of selected storms.”, Delta Rapport, 1960

Delft Hydraulics, Golfklappen op de schuif in de Oosterschelde-Caisson, verslag M1335, deel 1, band 1, Delft 1977

Delft Hydraulics, 'Golfklappen; een literatuuroverzicht en schaaleffecten in modelonderzoek, Stormvloedkering Oosterschelde, M1335, deel III', Delft Hydraulics, Delft, 1979

Delft Hydraulics, 'Dynamisch gedrag van waterbouwkundige constructies by stroming en golfklappen; deel B: Constructies in golven, concept 21', Delft Hydraulics, 1994

Dieterman H.A., 'Algemene mechanica II', deel II, inleiding mechanica van constructies, Lecture notes, Delft University of Technology, Delft, 1994

Goda Y., "The fourth order approximation to the pressure of standing waves, Coastal Engineering in Japan Vol 10", 1967

Goda Y., "Wave forces on structures", JSCE Hydraulic Eng. Series 67-10 (in Japanese), 1967

Goda Y., "Dynamic response of upright breakwaters to impulsive breaking wave forces, Coastal Engineering, Vol. 22, 1994, Elsevier Science, Amsterdam

Hattori M., Arami A. ,”Impact Breaking Wave Pressures on Vetical Walls”, 23rd International Conference on Coastal Engineering, Venice 1992

Hattori, M. et al, 'Wave impact pressure on vertical walls under breaking waves of varous type", Coastal Engineering 22, Elsevier science B.V., Amsterdam, 1994

Hull P., Müller G., Allsop N.W.H.,”A vertical distribution of wave impact pressures for design purposes", Research Report, MAST III, PROVERBS-Project: Probabilistic Design Tools for Vertical Breakwaters, Belfast, Northern Ireland, 16 pp., 1998

de Jong R.J et al..”Vibrations of Gates and Beams, Symposium on Hydraulic Aspects of Coastal Structures”, Rotterdam, August 1980

Kamel A.M., “Shock Pressures on Coastal Structures, ASCE Journal of the Waterways, Harbours and Coastal Eng. Div.”., Vol 96, No WW3, August 1970

Kaminsky G.M., Kraus N.C.,”Evaluation of depth-limited wave breaking criteria”, Ocean Wave Measurement and Analysis, Proc. of 2nd int. symp., 1993

Klatter H.E., Jannsen H., Dijkman M.,Wave impacts on the Eastern scheldt Barrier Evaluation of 5 years Field Measurements”, Coastal Engineering, Ch254, 1994

Klatter H.E., Konter J.L.M., Jongeling T.H.G. ,”Monitoring Hydraulic Loads on the Eastern Scheldt Storm Surge Barrier”, 22th international Conference on Coastal Engineering, Delft 1990

Kobayashi N., “Waves Forces on Inclined and Vertical Wall structures”, ASCE (American Society of Civil Engineers), New York 1995

Kolkman P.A. & T.H.G.Jongeling, “Dynamisch gedrag van waterbouwkundige constructies Deel B; Constructies in Golven”, 1996, TAW (Technische Adviescommissie

voor de Waterkeringen), RWS (Rijkswaterstaat) - DWW (Dienst Weg- en Waterbouwkunde)

Kortenhaus A, Oumeraci H.,"Wave uplift loading for impact breakers - tentative formulae and suggestions for the development of final formulae", Proceedings 2nd Task 1 Workshop, MAST III, PROVERBS-Project: Probabilistic Design Tools for Vertical Breakwaters, Edinburgh, U.K., Annex 1.0.3, 14 pp.; 2 Annexes. 1997

Korteweg D.J. & de Vries G., "On the change of Form of Long Waves Advancing in a rectangular Channel, and on a New Type of Long Stationary Waves", Philos. Mag., 5th Serie, Vol. 39, pp 422-443, 1895

Kuijper H.K.T. et al, "Constructieve Waterbouw", lecture notes, Subfaculty of Civil Engineering, Hydraulic Engineering, Delft University of Technology, The Netherlands, Delft 1999

Ligteringen, H. et al, "Wave impact forces, consequences for gate design," Symposium on Hydraulic Aspects of Coastal Structures", Rotterdam, August 1980

Longuet-Higgens M.S., Stewart R.W., "Radiation stress and mass transport in gravity waves, with application to surf-beats", Fluid. Mech.,13, p481-504, 1962

Marle J.G.A., "The breaker criterion for the mouth of the Oosterschelde", Rijkswaterstaat DDWT-79.031 (in Dutch)

McConnell, K., "Derivation, validation and use of parameter map". Research Report, MAST III, PROVERBS-Project: Probabilistic Design Tools for Vertical Breakwaters, Belfast, Northern Ireland, 16 pp., 1998

Miche R.,"Mouvements ondulatoires des mers en profondeur constante ou décroissante", Annales des Ponts et Chaussées, 1944

Minikin, "Wind, waves and maritime structures, 1963 Griffin London

Nelson R.C.,"Depth limited wave heights in very flat regions", Coastal Engineering, 23, 1994

Nelson R.C.,"Height limits in top down and bottom up wave environments", Coastal Engineering, 32, 1997

Novak P.,Èábelca "Models in Hydraulic Engineering - physical principles and design applications", Pitmax, London 1981

Novak P, Moffat A.I.B., Nalluri C, & Narayanan R., "Hydraulic Structures", Unwin Hyman, London, 1990

Oumeraci H., "Review and analysis of vertical breakwater failures -lessons learned, Coastal Engineering Vol. 22, 1994, Elsevier Science, Amsterdam

Oumeraci H., "Multi-disciplinary research experience in Europe on vertical breakwaters", Proceedings of the international workshop on Wave Barriers in Deep Waters, January 10-14, pp 267-278. Port and Harbour research Institute, Ministery of Transport, Ngase, Yokosuka, Japan, 1994(b)

Oumeraci H., "European Multi-Disciplinary Research Experience on Vertical Breakwaters: The MSC-Project", Mast II, 1997

Peregrine D.H., "Equations for water waves and the approximations behind them", in "Waves and Beaches", edited by R.E. Meyer, Academic Press, pp 95-121, 1972

Ramkema, C., 'A model law for wave impacts on coastal structures, 16th International Conferende on Coastal Engineering, 1978

Rijkswaterstaat, “Design plan Oosterschelde Storm-surge Barrier, Overall design and design philosophy”, Ministry of Transport, Public Works and Water Management, Road and Hydraulic Engineering Division, Balkema, Netherlands, 1994

Schiereck G.J.,"Introduction to Bed, Bank and Shore Protection, lecture notes", 1998, TUDelft

Smith E.R., Kraus N.C.,”Laboratory study of wave-breaking over bars and artificial reefs”, Journ. of Waterway, Port, Ocean and Coastal Eng., vol 117

Stokes G.G., "On the theory of Oscillatory Waves", Trans. Cambridge Phil. Soc., Vol 8, pp 441-455, 1847

Takahashi S., "Design of Vertical Breakwaters, Reference Document No. 34, Port and Harbour Research Institute, 1996, Tokyo

Technische Adviescommissie van de Water, “Leidraad Waterkerende Kunstwerken en Bijzondere Constructies”, 1997, TAW (Technische Adviescommissie voor de Waterkeringen), RWS (Rijkswaterstaat) - DWW (Dienst Weg- en Waterbouwkunde)

Technische Adviescommissie van de Water, “Basisrapport Waterkerende Kunstwerken en Bijzondere Constructies”, 1997, TAW (Technische Adviescommissie voor de Waterkeringen), RWS (Rijkswaterstaat) - DWW (Dienst Weg- en Waterbouwkunde)

University of Bristol, “Nonlinear Water Waves Workshop”, 1991

Vincent C.L., Smith J.,Davis J.,”Parameterization of wave height distribution”, Journ. of Geophys. Res., 88 (C10), 1994

Voortman H.G., “Economic optimal design of vertical breakwaters”, In: Edge, B.L. (Ed), Proceedings ICCE, 1999

Vrijling J.K., van Gelder P.H.A.M.”On the distribution of the maximum wave height in front of reflecting structures”, Subfaculty of Civil Engineering, Hydraulic Engineering, Delft University of Technology, The Netherlands, Delft 2000

Vrijling J.K. “Probabilistisch ontwerpen in de waterbouwkunde”, Lecture notes F30, Subfaculty of Civil Engineering, Hydraulic Engineering, Delft University of Technology, The Netherlands, Delft 2000

Weydert M, Lipiatou E, Goni R, Fragakis C, Bohle-Carbonell M, Barthel K.G., “Marine Sciences and Technologies, Project reports Volume 1”, Office for Official Publications, Commission of the European Communities, Brussel 1995,

ANNEX A: DATA SET GWK AND WKS

Data set used for calculating linear regression lines

GWK

Hsi/hs	hb/hs	Pbr	Hsi	hs	d	hb	Beq	Lhs
0.121	0.46	0	0.267	2.215	1.195	1.02	2.85	12.2
0.199	0.46	0	0.44	2.215	1.195	1.02	2.85	14.5
0.275	0.46	0	0.609	2.215	1.195	1.02	2.85	12.7
0.121	0.46	0	0.268	2.215	1.195	1.02	2.85	14.3
0.205	0.46	0	0.454	2.215	1.195	1.02	2.85	14.9
0.292	0.46	0	0.646	2.215	1.195	1.02	2.85	15.2
0.368	0.46	2.1	0.815	2.215	1.195	1.02	2.85	15.9
0.135	0.46	0	0.3	2.215	1.195	1.02	2.85	19.6
0.215	0.46	0	0.477	2.215	1.195	1.02	2.85	20
0.393	0.46	0	0.871	2.215	1.195	1.02	2.85	18.6
0.3	0.46	0	0.664	2.215	1.195	1.02	2.85	18.9
0.13	0.46	0	0.288	2.215	1.195	1.02	2.85	24
0.223	0.46	0	0.493	2.215	1.195	1.02	2.85	24.1
0.309	0.46	0	0.684	2.215	1.195	1.02	2.85	22.5
0.399	0.46	0.9	0.883	2.215	1.195	1.02	2.85	23.2
0.488	0.46	4.9	1.082	2.215	1.195	1.02	2.85	23.2
0.415	0.502	2	0.842	2.03	1.01	1.02	2.85	19.3
0.326	0.502	0	0.662	2.03	1.01	1.02	2.85	18.7
0.231	0.502	0	0.468	2.03	1.01	1.02	2.85	18.6
0.137	0.502	0	0.279	2.03	1.01	1.02	2.85	18.6
0.132	0.502	0	0.267	2.03	1.01	1.02	2.85	14.3
0.224	0.502	0	0.455	2.03	1.01	1.02	2.85	14.2
0.314	0.502	0	0.637	2.03	1.01	1.02	2.85	15
0.418	0.502	4.5	0.849	2.03	1.01	1.02	2.85	15.6
0.535	0.502	2.1	1.087	2.03	1.01	1.02	2.85	22.9
0.438	0.505	1.1	0.884	2.02	1	1.02	2.85	23.4
0.337	0.505	0	0.681	2.02	1	1.02	2.85	22.3
0.239	0.505	0	0.483	2.02	1	1.02	2.85	22.6
0.142	0.505	0	0.286	2.02	1	1.02	2.85	23
0.123	0.505	0	0.248	2.02	1	1.02	2.85	12.3
0.208	0.505	0	0.42	2.02	1	1.02	2.85	12
0.294	0.505	0	0.594	2.02	1	1.02	2.85	12.2
0.443	0.557	5.7	0.81	1.83	0.81	1.02	2.85	14
0.345	0.557	2.9	0.631	1.83	0.81	1.02	2.85	14
0.244	0.557	0	0.446	1.83	0.81	1.02	2.85	13.7
0.147	0.557	0	0.269	1.83	0.81	1.02	2.85	13.7
0.137	0.557	0	0.251	1.83	0.81	1.02	2.85	11.4
0.232	0.557	0	0.425	1.83	0.81	1.02	2.85	11.6
0.156	0.557	0	0.286	1.83	0.81	1.02	2.85	18
0.255	0.557	0	0.466	1.83	0.81	1.02	2.85	18.1
0.387	0.557	0	0.709	1.83	0.81	1.02	2.85	14.1
0.459	0.557	2.1	0.84	1.83	0.81	1.02	2.85	18
0.568	0.557	4.3	1.039	1.83	0.81	1.02	2.85	13.6
0.468	0.557	2.2	0.857	1.83	0.81	1.02	2.85	21.3
0.567	0.557	8.6	1.037	1.83	0.81	1.02	2.85	20.7
0.367	0.557	0	0.671	1.83	0.81	1.02	2.85	20.8
0.274	0.557	0	0.502	1.83	0.81	1.02	2.85	22.4
0.157	0.557	0	0.288	1.83	0.81	1.02	2.85	20.8

WKS

Hsi/hs	hb/hs	Pbr	Hsi	hs	d	hb	Beq	Lhs
0.517	0.632	14	0.834	1.614	0.594	1.02	2.85	19.6
0.399	0.632	3.1	0.644	1.614	0.594	1.02	2.85	19.8
0.292	0.632	0	0.471	1.614	0.594	1.02	2.85	18.7
0.168	0.632	0	0.271	1.614	0.594	1.02	2.85	19.9
0.17	0.632	0	0.275	1.614	0.594	1.02	2.85	16.1
0.273	0.632	0	0.44	1.614	0.594	1.02	2.85	17.1
0.496	0.632	2.4	0.8	1.614	0.594	1.02	2.85	9.3
0.498	0.632	11	0.803	1.614	0.594	1.02	2.85	17.3
0.467	0.632	12	0.754	1.614	0.594	1.02	2.85	14.4
0.371	0.632	6.3	0.599	1.614	0.594	1.02	2.85	13.3
0.263	0.632	0	0.425	1.614	0.594	1.02	2.85	13.8
0.158	0.632	0	0.255	1.614	0.594	1.02	2.85	13.7
0.137	0.632	0	0.221	1.614	0.594	1.02	2.85	11.4
0.264	0.632	0	0.426	1.614	0.594	1.02	2.85	11.2
0.108	0.569	0	0.078	0.72	0.31	0.41	1.33	2.6
0.157	0.569	0	0.113	0.72	0.31	0.41	1.33	2.9
0.2	0.569	0	0.144	0.72	0.31	0.41	1.33	3
0.235	0.569	0	0.169	0.72	0.31	0.41	1.33	3
0.261	0.569	0	0.188	0.72	0.31	0.41	1.33	3.3
0.285	0.569	2	0.205	0.72	0.31	0.41	1.33	3.2
0.111	0.569	0	0.08	0.72	0.31	0.41	1.33	2.9
0.158	0.569	0	0.114	0.72	0.31	0.41	1.33	3.1
0.215	0.569	0	0.155	0.72	0.31	0.41	1.33	3.4
0.262	0.569	1	0.189	0.72	0.31	0.41	1.33	3.6
0.292	0.569	2	0.21	0.72	0.31	0.41	1.33	4.3
0.315	0.569	2.1	0.227	0.72	0.31	0.41	1.33	3.9
0.11	0.569	0	0.079	0.72	0.31	0.41	1.33	3.4
0.171	0.569	0	0.123	0.72	0.31	0.41	1.33	3.7
0.229	0.569	0	0.165	0.72	0.31	0.41	1.33	3.9
0.278	0.569	3.4	0.2	0.72	0.31	0.41	1.33	3.9
0.314	0.569	2.2	0.226	0.72	0.31	0.41	1.33	4
0.357	0.569	3.4	0.257	0.72	0.31	0.41	1.33	4.4
0.131	0.569	0	0.094	0.72	0.31	0.41	1.33	4.4
0.201	0.569	0	0.145	0.72	0.31	0.41	1.33	4.5
0.268	0.569	1.2	0.193	0.72	0.31	0.41	1.33	4.6
0.322	0.569	2.4	0.232	0.72	0.31	0.41	1.33	5.2
0.372	0.569	4.4	0.268	0.72	0.31	0.41	1.33	4.8
0.417	0.569	7.1	0.3	0.72	0.31	0.41	1.33	5.1
0.129	0.569	0	0.093	0.72	0.31	0.41	1.33	5.2
0.203	0.569	0	0.146	0.72	0.31	0.41	1.33	5.1
0.268	0.569	1	0.193	0.72	0.31	0.41	1.33	5.1
0.333	0.569	2.1	0.24	0.72	0.31	0.41	1.33	4.7
0.142	0.569	0	0.102	0.72	0.31	0.41	1.33	6.2
0.215	0.569	0	0.155	0.72	0.31	0.41	1.33	6.2
0.293	0.569	0	0.211	0.72	0.31	0.41	1.33	6.2
0.362	0.569	3.1	0.261	0.72	0.31	0.41	1.33	6
0.147	0.569	0	0.106	0.72	0.31	0.41	1.33	7.1
0.218	0.569	0	0.157	0.72	0.31	0.41	1.33	6.9
0.287	0.569	1.1	0.207	0.72	0.31	0.41	1.33	6.1
0.344	0.569	3.2	0.248	0.72	0.31	0.41	1.33	6.7
0.439	0.569	7.4	0.316	0.72	0.31	0.41	1.33	6.2
0.478	0.569	9.6	0.344	0.72	0.31	0.41	1.33	7.2
0.397	0.569	11	0.286	0.72	0.31	0.41	1.33	5.4
0.461	0.569	11	0.332	0.72	0.31	0.41	1.33	5.3
0.111	0.661	0	0.069	0.62	0.21	0.41	1.33	2.7
0.163	0.661	0	0.101	0.62	0.21	0.41	1.33	2.9
0.218	0.661	0	0.135	0.62	0.21	0.41	1.33	2.8
0.261	0.661	0	0.162	0.62	0.21	0.41	1.33	3.3
0.295	0.661	0	0.183	0.62	0.21	0.41	1.33	3.3
0.318	0.661	1	0.197	0.62	0.21	0.41	1.33	3.3
0.118	0.661	0	0.073	0.62	0.21	0.41	1.33	3.3
0.184	0.661	0	0.114	0.62	0.21	0.41	1.33	3.2
0.253	0.661	0	0.157	0.62	0.21	0.41	1.33	3.2
0.31	0.661	0	0.192	0.62	0.21	0.41	1.33	3.7
0.347	0.661	3.1	0.215	0.62	0.21	0.41	1.33	3.6
0.387	0.661	1.1	0.24	0.62	0.21	0.41	1.33	3.5
0.119	0.661	0	0.074	0.62	0.21	0.41	1.33	3.2
0.187	0.661	0	0.116	0.62	0.21	0.41	1.33	3
0.302	0.661	1.9	0.187	0.62	0.21	0.41	1.33	4.1
0.31	0.661	5.1	0.192	0.62	0.21	0.41	1.33	3.7
0.361	0.661	6.3	0.224	0.62	0.21	0.41	1.33	3.8
0.405	0.661	7	0.251	0.62	0.21	0.41	1.33	4
0.139	0.661	0	0.086	0.62	0.21	0.41	1.33	4
0.211	0.661	0	0.131	0.62	0.21	0.41	1.33	4
0.29	0.661	0	0.18	0.62	0.21	0.41	1.33	4.3

0.352	0.661	6.8	0.218	0.62	0.21	0.41	1.33	4.6
0.419	0.661	9.4	0.26	0.62	0.21	0.41	1.33	4.8
0.452	0.661	10	0.28	0.62	0.21	0.41	1.33	4.7
0.135	0.661	0	0.084	0.62	0.21	0.41	1.33	4.8
0.189	0.661	0	0.117	0.62	0.21	0.41	1.33	4.2
0.292	0.661	5.7	0.181	0.62	0.21	0.41	1.33	4.6
0.387	0.661	8.5	0.24	0.62	0.21	0.41	1.33	4.7
0.431	0.661	7.7	0.267	0.62	0.21	0.41	1.33	4.7
0.481	0.661	21	0.298	0.62	0.21	0.41	1.33	5
0.144	0.661	0	0.089	0.62	0.21	0.41	1.33	5.7
0.219	0.661	0	0.136	0.62	0.21	0.41	1.33	5.6
0.292	0.661	4.9	0.181	0.62	0.21	0.41	1.33	5.3
0.361	0.661	10	0.224	0.62	0.21	0.41	1.33	5.6
0.448	0.661	15	0.278	0.62	0.21	0.41	1.33	5.9
0.152	0.661	0	0.094	0.62	0.21	0.41	1.33	5.8
0.224	0.661	1.1	0.139	0.62	0.21	0.41	1.33	5.6
0.279	0.661	2	0.173	0.62	0.21	0.41	1.33	5.8
0.353	0.661	5.3	0.219	0.62	0.21	0.41	1.33	5.7
0.423	0.661	13	0.262	0.62	0.21	0.41	1.33	6
0.503	0.661	12	0.312	0.62	0.21	0.41	1.33	6.3
0.115	0.788	0	0.06	0.52	0.11	0.41	1.33	2.5
0.254	0.788	0	0.132	0.52	0.11	0.41	1.33	2.6
0.231	0.788	0	0.12	0.52	0.11	0.41	1.33	2.8
0.273	0.788	0	0.142	0.52	0.11	0.41	1.33	3
0.304	0.788	0	0.158	0.52	0.11	0.41	1.33	3
0.346	0.788	2.2	0.18	0.52	0.11	0.41	1.33	3.1
0.137	0.788	0	0.071	0.52	0.11	0.41	1.33	3
0.21	0.788	2.2	0.109	0.52	0.11	0.41	1.33	2.9
0.281	0.788	0.9	0.146	0.52	0.11	0.41	1.33	3.3
0.337	0.788	1	0.175	0.52	0.11	0.41	1.33	3.5
0.394	0.788	2.1	0.205	0.52	0.11	0.41	1.33	3.6
0.423	0.788	0	0.22	0.52	0.11	0.41	1.33	3.7
0.138	0.788	0	0.072	0.52	0.11	0.41	1.33	3.1
0.221	0.788	0	0.115	0.52	0.11	0.41	1.33	3
0.298	0.788	1	0.155	0.52	0.11	0.41	1.33	3.3
0.369	0.788	2.1	0.192	0.52	0.11	0.41	1.33	3.7
0.454	0.788	1.1	0.236	0.52	0.11	0.41	1.33	3.7
0.454	0.788	1.1	0.236	0.52	0.11	0.41	1.33	3.6
0.133	0.788	0	0.069	0.52	0.11	0.41	1.33	3.6
0.212	0.788	1	0.11	0.52	0.11	0.41	1.33	3.4
0.29	0.788	1.1	0.151	0.52	0.11	0.41	1.33	4
0.354	0.788	0	0.184	0.52	0.11	0.41	1.33	4.2
0.473	0.788	0	0.246	0.52	0.11	0.41	1.33	4.6
0.45	0.788	1.2	0.234	0.52	0.11	0.41	1.33	3.9
0.137	0.788	0	0.071	0.52	0.11	0.41	1.33	4.2
0.213	0.788	0	0.111	0.52	0.11	0.41	1.33	4.2
0.312	0.788	0	0.162	0.52	0.11	0.41	1.33	4.1
0.398	0.788	1	0.207	0.52	0.11	0.41	1.33	4.2
0.485	0.788	0	0.252	0.52	0.11	0.41	1.33	4.4
0.485	0.788	1	0.252	0.52	0.11	0.41	1.33	4.5
0.138	0.788	0	0.072	0.52	0.11	0.41	1.33	5.2
0.213	0.788	0	0.111	0.52	0.11	0.41	1.33	5.1
0.294	0.788	1	0.153	0.52	0.11	0.41	1.33	5
0.354	0.788	2	0.184	0.52	0.11	0.41	1.33	5.2
0.462	0.788	4	0.24	0.52	0.11	0.41	1.33	5.2
0.496	0.788	9.2	0.258	0.52	0.11	0.41	1.33	5.4
0.14	0.788	1.1	0.073	0.52	0.11	0.41	1.33	4.9
0.206	0.788	0	0.107	0.52	0.11	0.41	1.33	5.1
0.283	0.788	4.3	0.147	0.52	0.11	0.41	1.33	5.3
0.375	0.788	4.2	0.195	0.52	0.11	0.41	1.33	5.5
0.454	0.788	2.1	0.236	0.52	0.11	0.41	1.33	5

ANNEX B: RANDOM WAVE REFLECTION

```
{berekent rnd-set met dKr=1/20 en
dHsi/h=1/1000}
{ P(Hs/h)|rnd uitrekenen, ook P-1(Pbr) }

const list:array[0..9,1..2] of integer =

((1,184),(1,62),(63,184),(1,16),(17,32),(
33,48),(49,62),(63,102),(103,143),(144,1
84));
     lezenf =
'u:\vanos\magchiel\afstud~1\model\rndr
ef~1\lr_dat';
{     lezenf2 =
'u:\vanos\magchiel\afstud~1\model\linea
r~1\rnd_set2.txt';}
{     schrijvenf =
'u:\vanos\magchiel\afstud~1\model\linea
r~1\lr_res';}
var data:array[1..184,1..9] of real;
{    rndset:array[0..1000,1..2] of real;}

const maxray = 4000;
     fin = 20;     {H/Hs}
     maxset = 1000; {Hs/h}
     endf = 1;  {Hs/h}
     maxKr = 20;


var raydistr:array[0..maxray] of real;
   Prnd_set:array[0..maxset] of real;

procedure readdata;
var f:text;
   x,y:integer;
   s,s2:string;
   code:integer;
   r:real;
begin
  assign(f,lezenf+'.txt');
  reset(f);
  readln(f,s);
  readln(f,s);
        {  1      2       3       4     5    6
7    8       9}

writeln('Hsi/hs':8,'hb/hs':8,'Pbr':8,'Hsi':8,'
hs':8,'d':8,'hb':8,'Beq':8,'Lhs:8');
  for y:=1 to 184 do
  begin
   readln(f,s);s:=s+#9;
   for x:=1 to 9 do
   begin
     s2:=copy(s,1,pos(#9,s)-1);
     val(s2,r,code);
     data[y,x]:=r;
     delete(s,1,pos(#9,s));
   end;
  end;
  close(f);
  for y:=1 to 184 do
  begin
   write(y:3);
   for x:=1 to 9 do write(data[y,x]:8:4);
   writeln;
  end;
end;

procedure buildray;
var x:integer;
   r:real;
begin
  for x:=0 to maxray do
  begin
   r:=fin*x/maxray;      {H/Hs}
   raydistr[x]:=4*r*exp(-2*sqr(r));
  end;
end;

function Prnd_calc(g,Kr,x:real):real;
var
d,HbHs,H1_Hs,H2_Hs,Ht_Hs,f1,f2:real;
   Frnd:real;
   i,i2,i3:integer;
begin
  Frnd:=0;
  HbHs:=g/x;
  {for i:=0 to maxset do prnd_set[i]:=0;}

  d:=HbHs/maxray;
```

```
  for i2:=1 to maxray do
  begin
    H1_Hs:=HbHs*(i2-0.5)/maxray;
{0...HbHs}
    H2_Hs:=(HbHs-H1_Hs)/Kr;
{HbHs/Kr .. 0/Kr}
    Ht_Hs:=H1_Hs+H2_Hs*Kr;
     if H1_Hs>40 then H1_Hs:=40;
     if H2_Hs>40 then H2_Hs:=40;

    f1:=4*H1_Hs*exp(-2*sqr(H1_Hs));
    F2:=1-exp(-2*sqr(H2_Hs));
    Frnd:=Frnd + f1*d *F2;
  end;
  Prnd_calc:=1-Frnd;
end;

procedure schrijf;
var f:text;
    i:integer;
begin
  assign(f,'rnd_set.txt');
  rewrite(f);
  for i:=0 to maxset do
  begin

writeln(f,(endf*i/maxset):10:4,prnd_set[
i]:10:5);
  end;
  close(f);
end;

function P(x:real):real;
var i:integer;
    r:real;
    x1,x2,p1,p2:real;
begin
  i:=round(x*maxset+0.5);if i<1 then
i:=1 else if i>maxset then i:=maxset;
  r:=x*maxset-i+1;if r<0 then r:=0 else if
r>1 then r:=1;
  p1:=Prnd_set[i];
  p2:=Prnd_set[i+1];
  P:=p1+(p2-p1)*r;
end;

procedure schrijf2;
var f:text;
    i,Kr_:integer;
    Kr,g,Pbr,b,x,Pbrrnd:real;
begin
  assign(f,'c:\rnd2pbr2.txt');
  rewrite(f);
  g:=0.78;


write(f,'i:':15,'Hs/hs':15,'hb/hs':15,'Pbr;i':
15);
  for i:=1 to maxKr do
write(f,i/maxkr:12:9,'':3);writeln(f);

{}writeln('i:':12,'Hs/hs':12,'hb/hs':12,'Pbr
;i':12,'Kr=0..1':12);

  for i:=1 to 184 do
  begin
    Pbr:=data[i,3]/100;
    b:=data[i,2];
    x:=data[i,1];

write(f,i:12,x:12:9,'':3,b:12:9,'':3,Pbr:12:
9,'':3);
    {write(i:12,x:12:9,b:12:9,Pbr:12:9);}
    for Kr_:=1 to maxKr do
    begin
      Kr:=Kr_/maxKr;
      Pbrrnd:=Prnd_calc(g,Kr,x);
{prnd_set (0..maxset=1000) }
      write(f,Pbrrnd:12:9,'':3);
      write('.');
    end;
    writeln(f);
    writeln;
  end;
  close(f);
end;

begin
  buildray;
  readdata;

  schrijf2;

  readln;
end.
```